Vol. 59 NOVEMBER, 1955 No. 11

THE JOURNAL OF PHYSICAL CHEMISTRY

(Registered in U. S. Patent Office)

SYMPOSIUM ON BOND MOMENTS, KANSAS CITY, MO., MARCH 24, 1954

Charles P. Smyth: Bond Moment and Type 1121
D. F. Eggers, Jr., I. C. Hisatsune and L. Van Alten: Bond Moments, their Reliability and Additivity: Sulfur Dioxide and Acetylene 1124
Gordon M. Barrow: The Intensities of Infrared Hydroxyl Bands 1129
D. F. Hornig and D. C. McKean: Bond Moments and Molecular Structure 1133

A. Packter: Studies on the Crystal Growth of Soluble Metal Salts. I. The Effect of "Protecting Agents" on the Interface Reaction 1140
H. Tracy Hall: The Melting Point of Germanium as a Function of Pressure to 180,000 Atmospheres 1144
Mei Chio Chen, Carl J. Christensen and Henry Eyring: Kinetics of Oxidation of Pyrolytic Carbon 1146
Ole Lamm: The Dynamics of the Diffusion of Fluids in Relation to the Choice of Components 1149
R. Greene-Kelly: Lithium Absorption by Kaolin Minerals 1151
L. J. E. Hofer, E. Sterling and J. T. McCartney: Structure of Carbon Deposited from Carbon Monoxide on Iron, Cobalt and Nickel 1153
W. A. Pliskin and R. P. Eischens: The Effect of Using the Pressed Salt Technique to Obtain the Spectrum of Chemisorbed Ammonia 1156
Alvin S. Gordon and R. H. Knipe: The Explosive Reaction of Carbon Monoxide and Oxygen at the Second Explosion Limit in Quartz Vessels 1160
W. R. Krigbaum and D. K. Carpenter: The Configuration of Polymer Molecules: Polystyrene in Cyclohexane 1166
David L. Camin and Frederick D. Rossini: Physical Properties of Fourteen API Research Hydrocarbons, C_9 to C_{15} 1173
Note: **James M. Schreyer and C. F. Baes, Jr.:** The Solubility of $UO_2HPO_4 \cdot 4H_2O$ in Perchloric Acid Solutions 1179
Note: **John P. Ryan and Joseph Wm. Shepard:** Structure of Stearatic Acid Monolayers in the Region Le-G 1181
Note: **Elton M. Baker:** The Ternary System *n*-Propyl Alcohol–Toluene–Water at 25° 1182
Communication to the Editor: **A. Klinkenberg:** A Molecular Dynamic Theory of Chromatography 1184

NOT FOR LENDING

THE JOURNAL OF PHYSICAL CHEMISTRY

(Registered in U. S. Patent Office)

W. Albert Noyes, Jr., Editor

Allen D. Bliss — Assistant Editors — Arthur C. Bond

Editorial Board

R. P. Bell
E. J. Bowen
R. E. Connick
R. W. Dodson
Paul M. Doty
G. D. Halsey, Jr.
J. W. Kennedy
S. C. Lind
H. W. Melville
W. O. Milligan
E. A. Moelwyn-Hughes

Published monthly by the American Chemical Society at 20th and Northampton Sts., Easton, Pa.

Entered as second-class matter at the Post Office at Easton, Pennsylvania.

The *Journal of Physical Chemistry* is devoted to the publication of selected symposia in the broad field of physical chemistry and to other contributed papers.

Manuscripts originating in the British Isles, Europe and Africa should be sent to F. C. Tompkins, The Faraday Society, 6 Gray's Inn Square, London W. C. 1, England.

Manuscripts originating elsewhere should be sent to W. Albert Noyes, Jr., Department of Chemistry, University of Rochester, Rochester 3, N. Y.

Correspondence regarding accepted copy, proofs and reprints should be directed to Assistant Editor, Allen D. Bliss, Department of Chemistry, Simmons College, 300 The Fenway, Boston 15, Mass.

Business Office: Alden H. Emery, Executive Secretary, American Chemical Society, 1155 Sixteenth St., N. W., Washington 6, D. C.

Advertising Office: Reinhold Publishing Corporation, 430 Park Avenue, New York 22, N. Y.

Articles must be submitted in duplicate, typed and double spaced. They should have at the beginning a brief Abstract, in no case exceeding 300 words. Original drawings should accompany the manuscript. Lettering at the sides of graphs (black on white or blue) may be pencilled in, and will be typeset. Figures and tables should be held to a minimum consistent with adequate presentation of information. Photographs will not be printed on glossy paper except by special arrangement. All footnotes and references to the literature should be numbered consecutively and placed in the manuscript at the proper places. Initials of authors referred to in citations should be given. Nomenclature should conform to that used in *Chemical Abstracts*, mathematical characters marked for italic, Greek letters carefully made or annotated, and subscripts and superscripts clearly shown. Articles should be written as briefly as possible consistent with clarity and should avoid historical background unnecessary for specialists.

Symposium papers should be sent in all cases to Secretaries of Divisions sponsoring the symposium, who will be responsible for their transmittal to the Editor. The Secretary of the Division by agreement with the Editor will specify a time after which symposium papers cannot be accepted. The Editor reserves the right to refuse to publish symposium articles, for valid scientific reasons. Each symposium paper may not exceed four printed pages (about sixteen double spaced typewritten pages) in length except by prior arrangement with the Editor.

Remittances and orders for subscriptions and for single copies, notices of changes of address and new professional connections, and claims for missing numbers should be sent to the American Chemical Society, 1155 Sixteenth St., N. W., Washington 6, D. C. Changes of address for the *Journal of Physical Chemistry* must be received on or before the 30th of the preceding month.

Claims for missing numbers will not be allowed (1) if received more than sixty days from date of issue (because of delivery hazards, no claims can be honored from subscribers in Central Europe, Asia, or Pacific Islands other than Hawaii), (2) if loss was due to failure of notice of change of address to be received before the date specified in the preceding paragraph, or (3) if the reason for the claim is "missing from files."

Subscription Rates (1955): members of American Chemical Society, $8.00 for 1 year, $15.00 for 2 years, $22.00 for 3 years; to non-members, $10.00 for 1 year, $18.00 for 2 years, $26.00 for 3 years. Postage free to countries in the Pan American Union; Canada, $0.40; all other countries, $1.20. $12.50 per volume, foreign postage $1.20, Canadian postage $0.40; special rates for A.C.S. members supplied on request. Single copies, current volume, $1.00; foreign postage, $0.15; Canadian postage $0.05. Back issue rates (starting with Vol. 56): $15.00 per volume, foreign postage $1.20, Canadian, $0.40; $1.50 per issue, foreign postage $0.15, Canadian postage $0.05.

The American Chemical Society and the Editors of the *Journal of Physical Chemistry* assume no responsibility for the statements and opinions advanced by contributors to This Journal.

The American Chemical Society also publishes *Journal of the American Chemical Society*, *Chemical Abstracts*, *Industrial and Engineering Chemistry*, *Chemical and Engineering News*, *Analytical Chemistry*, and *Journal of Agricultural and Food Chemistry*. Rates on request.

PHOTOCOPY

THE JOURNAL OF
PHYSICAL CHEMISTRY

(Registered in U. S. Patent Office) (Copyright, 1955, by the American Chemical Society)

VOLUME 59 NOVEMBER 17, 1955 NUMBER 11

BOND MOMENT AND TYPE[1]

BY CHARLES P. SMYTH

Department of Chemistry, Princeton University, Princeton, New Jersey

Received May 18, 1955

A bond moment is a measure of the asymmetry of charge distribution in the bond and its immediate vicinity and is affected by the environment of the molecular section in question. The moment values, 0–2.0 × 10^{-18}, for typical covalent single bonds lie, for the most part, between zero and about 0.2 of the values which they would have if they were pure, undistorted ionic bonds, and those of coördinate single bonds, 3–4.5 × 10^{-18}, lie between 0.35 and 0.65 of the undistorted ionic bond values. The lower limits, 2–4 × 10^{-18}, established for bonds between metallic and acidic elements in organometallic compounds indicate polarities roughly intermediate between those of typically covalent and those of typically ionic bonds. The moments found for salt molecules, 6–20 × 10^{-18}, are lowered by inductive distortion of the electronic shells below those calculated for the undistorted ionic structures. The covalent single bond moments tend to increase roughly with increase in the electronegativity difference between the bonded atoms. The moments of single coördinate bonds and of double and triple bonds, which may contain resonance contributions from coördinate bond structures, are largely independent of the electronegativity differences between the atoms, often being opposite in direction to the electronegativity difference.

The electric dipole moment of a molecule is sometimes treated as the resultant of moments associated with all of the bonds in the molecule, the contributions of some one or two bonds usually predominating. In the case of a diatomic molecule, such as that of hydrogen chloride, the moment is associated with the one bond in the molecule, although it is dependent on the charge distribution of the entire molecule. If the hydrogen chloride molecule is arbitrarily described as consisting of a symmetrical chloride ion with a proton at a distance 1.28 Å., the moment calculated for the structure is (4.80 × 10^{-10}) × (1.28 × 10^{-8}) = 6.14 × 10^{-18}, a value differing greatly from the observed 1.08 × 10^{-18}. The large difference can be explained in terms of an induced shift of electronic charge toward the proton with consequent shortening of the molecular dipole, the calculated shift being of the right magnitude to account for the large discrepancy.[2,3] Pauling[4] has described the molecule in terms of resonance as a linear combination of a covalent structure H–Cl, to which a zero moment is arbitrarily assigned, and the undistorted ionic structure H^+Cl^- of moment 6.14 × 10^{-18}. The hydrogen–chlorine bond is then described as possessing a fractional amount of ionic character, $x = 1.08 \times 10^{-18}/6.14 \times 10^{-18}$. However, it has been calculated[5] that the dipole moment of the covalent bond is of the order of −1, the hydrogen being negative, if the bond is a pure p bond, but may be increased to as much as +2 by s-p hybridization. On this basis, the covalent structure could have almost any reasonable dipole moment and a calculation of amount of ionic character based upon the assumption of zero moment for the covalent structure would seem to be meaningless. The moment evidently depends not only upon the positions of the proton, the chlorine nucleus, and the electrons of the bond, but also upon those of the chlorine electrons not involved in the bond.[6]

According to Mulliken,[7–9] the moment of a bond A–B may be represented as the sum of four moments, which may be written in summary fashion as

Total moment = Primary + Overlap + Hybridization + Core

(1) This research has been supported in part by the Office of Naval Research. Reproduction, translation, publication, use or disposal in whole or in part by or for the United States Government is permitted.

(2) C. P. Smyth, *Phil. Mag.*, **47**, 530 (1924).

(3) C. P. Smyth, "Dielectric Constant and Molecular Structure," The Chemical Catalog Company, Inc., New York, N. Y., 1931, p. 64.

(4) L. Pauling, "The Nature of the Chemical Bond," 2nd Ed., Cornell University Press, Ithaca, N. Y., 1940, Chap. II.

(5) D. Z. Robinson, *J. Chem. Phys.*, **17**, 1022 (1949); see also C. A. Coulson, "Valence," Oxford University Press, Oxford, 1952, p. 208.

(6) C. P. Smyth, *Trans. Faraday Soc.*, **30**, 752 (1934).

(7) R. S. Mulliken, *J. chim. phys.*, **46**, 497 (1949).

(8) R. S. Mulliken, *J. Am. Chem. Soc.*, **72**, 4493 (1950).

(9) W. Gordy, W. V. Smith and R. F. Trambarulo, "Microwave Spectroscopy," John Wiley and Sons, Inc., New York, N. Y., 1953, Chap. 7.

The primary moment arises from the difference in the fractional parts of the bonding electron cloud in the atomic orbitals ψ_A and ψ_B. If the overlap cloud is divided equally between atoms A and B, it arises from the difference between the electronegativities of A and B, which gives the bond its ionic character. The overlap moment is due to the fractional parts of the electron cloud occupying the orbital overlap region. The hybridization moment is due to the displacement of the centers of gravity of the electronic clouds in ψ_A and ψ_B from the nuclei of A and B. The core moment arises from polarization of the core A^+B^+ by the primary moment. It is obvious from this that the total moment of A–B should not, normally, be a measure of the electronegativity difference between A and B. There is, nevertheless, sufficient parallelism between many bond moment values and the electronegativity differences to have some qualitative, if not quantitative significance.[10]

In an unsymmetrical polyatomic molecule containing only one kind of bond, such as PCl_3, the bond moment can be calculated by simple geometry from the molecular moment and the bond angle. Where the molecular moment is the resultant of two or more moments of different value, one bond moment cannot be calculated without knowledge of the others. The carbon bond moments are dependent upon the small and apparently variable value of the H–C bond moment, for which 0.4×10^{-18} with the negative end toward the carbon has been somewhat arbitrarily used in calculating values for the other carbon bonds (Table I). The moments of the bonds between hydrogen and other elements show an almost linear dependence upon the electronegativity and, indeed, are almost numerically equal to the electronegativity differences in several cases. However, wide discrepancies often occur for other elements as is apparent in Table I, which gives the electronegativity value below or beside a number of elements and, in line with an element at the left, the moment of the bond between that element and the element given at the top of each column.

TABLE I

BOND MOMENTS ($\times 10^{18}$) AND ELECTRONEGATIVITIES

Electronegativity	I 2.4	S 2.5	Br 2.8	N 3.0	Cl 3.0	O 3.5	F 4.0
Sb 1.8	0.8		1.9		2.6		
As 2.0	0.78		1.27		1.64		2.03
P 2.1	0		0.36		0.81		
H 2.1	0.38	0.68	0.78	1.31	1.08	1.51	1.94
C 2.5	1.19	0.9	1.38	0.22	1.46	0.74	1.41
K 2.8					10.6		7.3
Cs 0.7					10.5		7.9

Among the methyl halides, the atomic moment of the carbon in CH_3I is small because the four hybridized orbitals are almost equally filled, there being only a small difference between the electronegativities of carbon and iodine. It is suggested[9] that, in CH_3F and CH_3Cl, the ionic character of the forms $H_3C^+X^-$ and $H_3^+C^-X$ causes the electron density in the C orbitals directed toward the hydrogens to be greater than that in the orbital directed toward the halogen, giving a dipole with positive pole toward the halogen and, therefore, opposing the primary moment. This opposing carbon moment increases with the ionic character and thus tends to equalize the methyl halide moments, which show smaller differences in the apparent C–X moments (Table I) than would be expected from the electronegativity differences between the halogens. The extremely small moment, 0.17, of the N–F bond is much smaller than would be expected from the difference between the electronegativities of the two elements in Table I, probably because of the partial cancellation of the primary moments of the $N^+F_3^-$ structures by the hybridization moment of the unshared electron pair of the nitrogen.[9]

The so-called moment of the C–Cl bond in a molecule involves not only effects like those just discussed, but also the effects of the forces exerted by the rest of the molecule. This emphasizes the fact that a bond moment is merely a measure of the electrical asymmetry of a certain section of a molecule and is affected by the environment of the section. If the immediate environment of the section in molecules of different compounds is the same, the bond moment remains constant; if it is different, the electrical asymmetry of the section and its moment change more or less. In terms of resonance the rest of the molecule may be such as to alter the relative amounts of the contributions of the different structures or introduce new contributing structures, thus altering the bond moment.

The effects of environment and resonance are illustrated by the moments of the methyl chloride, chloroform and chlorobenzene molecules, which, geometrically, should be identical and equal to the H–C moment plus the C–Cl moment. Actually, the values are: CH_3Cl, 1.87; $CHCl_3$, 1.02; C_6H_5-Cl, 1.70. The three effective C–Cl moments in the chloroform molecule are reduced by mutual inductive effects[11] and the chlorobenzene moment is reduced by resonance involving contributions from structures with positively charged chlorine.[12,13]

The effects of induced shifts of charge are very pronounced in the moments of the alkali metal halide molecules in the vapor state. In terms of the resonance picture of these molecules, the lowering of the moment below that calculated for the undistorted ionic structure was attributed to partial covalent character of the bond.[4] However, from a consideration of quadrupole coupling data, Townes and Dailey[14] have assigned a maximum of 4% covalent character to the bond in the sodium chloride molecule and 3% to that in sodium bromide and have concluded that the alkali halides should be considered as almost purely ionic with a large amount of polarization reducing the moment. Rittner[15] has calculated the moments of alkali halide molecules by means of the equation

(10) C. P. Smyth, THIS JOURNAL, **41**, 209 (1937); *J. Am. Chem. Soc.*, **60**, 183 (1938).

(11) C. P. Smyth and K. B. McAlpine, *J. Chem. Phys.*, **1**, 190 (1933).

(12) L. E. Sutton, *Proc. Roy. Soc. (London)*, **A133**, 668 (1931); *Trans. Faraday Soc.*, **30**, 789 (1934).

(13) C. P. Smyth, *J. Am. Chem. Soc.*, **63**, 57 (1941).

(14) C. H. Townes and B. P. Dailey, *J. Chem. Phys.*, **17**, 782 (1949).

(15) E. S. Rittner, *ibid.*, **19**, 1030 (1951).

$$\mu = ea - \frac{a^4e(\alpha_1 + \alpha_2) + 4ae\alpha_1\alpha_2}{a^6 - 4\alpha_1\alpha_2}$$

in which e is the electronic charge; a, the equilibrium separation of the ion centers; α_1 and α_2, the polarizabilities of the two ions; and the second term on the right is the total induced moment opposing the moment ea of the undistorted ionic structure. The calculated moment values differ from the observed by an average amount, $\pm 6.5\%$, no greater than the considerable uncertainties of the latter. It would appear, therefore, that the alkali halide molecules are almost pure ionic structures with their moments reduced about 20–35%, and occasionally as much as 50%, by mutual induction.

TABLE II

MOMENTS ($\times 10^{18}$) OF COÖRDINATE SINGLE BONDS AND DOUBLE AND TRIPLE BONDS

Coördinate Single				Double	
N–O	4.3	Se–O	3.1	C=C	0.0
P–O	2.7	Te–O	2.3	C=O	2.3
P–S	3.1	N–B	3.9	C=S	2.6
P–Se	3.2	P–B	4.4	Triple	
As–O	4.2	O–B	3.6	C≡C	0.0
Sb–S	4.5	S–B	3.8	C≡N	3.5
S–O	2.8	S–C	(5.0)	N≡C	3.0

Double and triple bond moments usually have resonance contributions from semi-polar bond structures, such as $A^+ - B^-$, or $A^+ = B^-$, which seem to depend little upon the electronegativities of the bonded atoms. Sidgwick[16] called attention to the fact that the moments of double and triple bonds between atoms of different elements were more than two and three times the values for the single bonds. The cyanide moment is ten times that of the single carbon–nitrogen bond and the double bonds between carbon and oxygen and carbon and sulfur have moments about three times those of the single bonds. Although the C≡N bond is primarily C:::N, contribution from a form $^+C::\ddot{N}^-$ would raise the moment, presumably, being responsible for the high value observed. It is a semi-polar bond acting in the opposite direction in the isocyanide N→C which gives it a large moment opposite in direction to that of the C≡N bond.[17] These two triple bond moments, one with the carbon positive and the nitrogen negative and the other with the carbon negative and the nitrogen positive, show that, although electronegativity may be a factor in determining the multiple bond moments, it need not be the controlling factor.

The bond moments for the so-called coördinate single bonds are formally represented by a single structure, $A^+ - B^-$, without resonance from other polar structures. Although there seems to be evidence[18] in favor of the double bond character of these bonds, it is clear that the NO bond, which is observed in the amine oxides, cannot be double since all of the available orbitals are used in forming the single bonds. In the bonds involving boron, which are observed in addition compounds with boron trifluorides and boron trichloride, there can also be no double bond character since the 2s and 2p orbitals of the boron are completely filled in the formation of single bonds and, as in the nitrogen and oxygen atoms, no d orbitals are available. The NO bond moment is about $^2/_3$ what it should be if the bond were a pure, undistorted, single coordinate bond, the boron bonds are about $^1/_2$ of what they should be, and the PO and PS bonds about $^1/_3$ of what they should be. There is no sharp break between the bonds that cannot be double and those that can. Indeed, the necessarily single SB bond has only 0.42 of the moment that it should have if it were a pure, undistorted coördinated bond, while the SO bond, thought by Phillips, Hunter and Sutton[18] to be double, has 0.40 of the moment that it should have if it were a pure, undistorted coördinate bond.

In a structure A^+–B^-, the induced shift of charge should lower the moment below that calculated for the undisorted structure. The lowering should be less, the smaller and, consequently, the less polarizable the bonded atoms. The lowering is least for the bond between the small and difficultly polarizable nitrogen and oxygen atoms and greatest for the bond between the larger and more polarizable phosphorus and sulfur atoms. Next after the NO bond, the bonds between the small nitrogen and boron and oxygen and boron atoms are least lowered. However, the difference between the PB and OB bond lowerings is negligibly small, as is also that between the PO and PS lowerings. The general trend of these so-called coördinate bond moments is consistent with a structure, A^+–B^-, in which distortion lowers the moment, but the relative amounts of the lowering are not explained by the atomic polarizabilities alone. Neither the coördinate bond nor the double bond alone provides a generally satisfactory description of all of these bonds. It is natural to suggest a certain amount of resonance between the two structures where this is possible, but it is clearly impossible for the bonds between two atoms of the first short period of the periodic system. The additional factors included in the discussion of the moments in Table I are, presumably, responsible for the apparent discrepancies.

TABLE III

TYPICAL BOND MOMENTS

Bond	Obsd. moment ($\times 10^{18}$)	Fraction of undistorted ion pair moment
Covalent		
Single, A–B	0– 2.0	0 –0.2
Organometallic, M–X	>2– 4	>0.2 – .35
Double, A=B	0–2.5	
Triple, A≡B	0–3.5	
Coördinate, A^+–B^-	3–4.5	0.35– .65
Ionic, A^+B^-	6–20	0.65– .8

The approximate ranges of moment values for the different bond types are summarized in Table III and, for the single bonds, compared with the moments of the corresponding, undistorted ion pairs. The ranges given are only approximate, as illustrated by the fact that, while most of the co-

(16) N. V. Sidgwick, "The Covalent Link in Chemistry," Cornell University Press, Ithaca, N. Y., 1933, p. 153.

(17) N. V. Sidgwick, *Chem. Revs.*, **9**, 77 (1931).

(18) G. M. Phillips, J. S. Hunter and L. E. Sutton, *J. Chem. Soc.*, 146 (1945).

valent single bond moments lie within the ranges given, the H–F moment is 0.44 of that for an undistorted H^+F^- pair, that is, about half-way between a typical covalent and a typical ionic bond. The bonds between metals and acidic elements in organometallic molecules are listed separately under covalent single bonds because their ionic characters tend to be greater than those of the typical single bonds. The double and triple bond moments are usually zero when the two bonded atoms are the same, and near the upper limits when they are different because of contributions from the structures A^+–B^- and A^+=B^-. Values much above 10 for ionic bonds are found not for a single pair of charged atoms, but, rather, for a pair of polyatomic ions.[19]

(19) J. A. Geddes and C. A. Kraus, *Trans. Faraday Soc.*, **32**, 585 (1936).

BOND MOMENTS, THEIR RELIABILITY AND ADDITIVITY: SULFUR DIOXIDE AND ACETYLENE

BY D. F. EGGERS, JR., I. C. HISATSUNE AND L. VAN ALTEN

Department of Chemistry, University of Washington, Seattle, Washington

Received May 18, 1955

Absolute infrared intensity measurements are reported for all active fundamentals of sulfur dioxide and the isotopic acetylenes, C_2H_2, C_2D_2 and C_2HD in the gas phase with high pressures of nitrogen added. Samples were checked for thoroughness of mixing and freedom from adsorption on the cell walls. Interpreting the intensities as arising from a bond moment and its derivative with respect to bond length, values of these parameters are computed from the experimental data. In sulfur dioxide the bond moment disagrees with the value from static dipole moment measurements. Two possible values are obtained for the derivative, with no clear-cut choice apparent. In acetylene, isotopic substitution gives, within experimental error, the same bond moment and derivative. The three acetylenes furnish checks of isotopic intensity sum rules of Crawford and of Decius. These rules are found to hold within the experimental error.

Introduction

The dipole moment of a molecule, determined by measurements of dielectric constant or of the microwave spectrum, is one parameter for the entire molecule in question. By comparison of many chemically-related molecules, values have been assigned to the individual bonds in a molecule, such that the vector sum of the bond moments is equal to the observed molecular dipole. Measurement of the infrared absorption intensities for all fundamental bands of a single molecule permits calculation of the change of dipole moment during vibration. If we assume that this oscillating total dipole is given as the vector sum of contributions from individual bonds, and if the molecule has sufficient symmetry, we may calculate the contribution from each bond. Even early measurements[1] have shown, however, that the contribution from the stretching of a bond may be quite different from its bending. Therefore, it is customary to represent the latter by the bond moment, μ, and the former by the derivative of μ with respect to bond distance, $\partial\mu/\partial r$. Even this assignment of two parameters to each type of bond in the molecule gives rise to some difficulties: ethylene[2] and ethane[3] give bond moments which vary widely from one vibration to another even in the same molecule.

In view of these difficulties, it was thought advisable to investigate molecules which are symmetric and small enough to furnish checks between different vibrational bands. These two compounds show certain additional features of interest: sulfur dioxide is heavier than most of the molecules investigated thus far, and is believed to be a resonance hybrid of two principal structures; the isotopic acetylenes furnish a check on the effect of isotopic substitution. The fundamental vibrational bands of most molecular species are also well separated, so that uncertainty from overlapping of bands is reduced.

(1) R. Rollefson and R. Havens, *Phys. Rev.*, **57**, 710 (1940).

(2) A. M. Thorndike, A. J. Wells and E. B. Wilson, Jr., *J. Chem. Phys.*, **15**, 157 (1947).

(3) A. M. Thorndike, *ibid.*, **15**, 868 (1947).

Experimental

All measurements were carried out in the gas phase using the method of Wilson and Wells.[4] Pressures of 100 and 300 p.s.i. gage of nitrogen were used in the measurements on sulfur dioxide, and 300 p.s.i. gage in those on the acetylenes. Large systematic errors may be introduced in this method by the incomplete mixing of the two gases in the absorption cell, and adsorption of one of the gases on the walls of the cell.[5] The first difficulty was investigated by placing a number of loose Teflon chips in the absorption cell, introducing the gases, measuring the spectrum, shaking the cell vigorously and then remeasuring the spectrum. No change in the spectrum was noted, indicating that introduction of the inert broadening gas second gives essentially complete mixing. The second difficulty was investigated by mass-spectrometric analysis of several mixtures after the infrared spectrum had been measured; in every case, no difference was found between compositions from pressures of the pure gases introduced and those from the mass spectrometer.

The absorption cell used in these measurements was patterned after that of Bartholomé.[6] The body of the cell was steel, and the potassium bromide windows, 50 mm. diameter by 20 mm. thick, were sealed with beeswax–rosin mixture. All spectral measurements were carried out on a ratio-recording double-beam instrument with automatic slit control similar to that described by Hornig, Hyde and Adcock.[7] The monochromator was a Perkin–Elmer model 83, and was converted to double-pass before C_2HD, the last in the series, was measured. Prisms of fused quartz, calcium fluoride, sodium chloride, potassium bromide and cesium bromide were used in appropriate regions for the measurements. In spectral regions showing interference from atmospheric water vapor or carbon dioxide, the entire housing of the instrument was flushed with dry nitrogen. Corrections were also made for stray light when necessary.

(4) E. B. Wilson, Jr., and A. J. Wells, *ibid.*, **14**, 578 (1946).

(5) S. S. Penner and D. Weber, *ibid.*, **19**, 807 (1951).

(6) E. Bartholomé, *Z. physik. Chem.*, **B23**, 131 (1933).

(7) D. F. Hornig, G. E. Hyde and W. A. Adcock, *J. Opt. Soc. Am.*, **40**, 497 (1950).

The spectra are replotted as logarithm of per cent. transmission *vs.* frequency, and the area between the absorption curve and the 100% line is measured with a polar planimeter[2]; these areas are denoted by $\mathfrak{B}$. If each value of $\mathfrak{B}$ is divided by pL, where p is the partial pressure of absorbing gas and L the thickness of the cell, one obtains B, the apparent band intensity. The extrapolation may be done either by measuring the limiting slope of a plot of $\mathfrak{B}$ *vs.* pL, as was done for SO_2, or by measuring the intercept of a plot of B *vs.* pL, as was done for the acetylenes.

The relationship between these measured intensities and the quantity of theoretical interest has been derived by Thorndike, Wells and Wilson[2]

$$A_i = (N\pi/3c)|\partial\mu/\partial Q_i|^2 \qquad (1)$$

Here A_i is the extrapolated experimental intensity of the ith fundamental in cycles per second per cm., N is the number of absorbing molecules per cc., c is the velocity of light, and $\partial\mu/\partial Q_i$ is the rate of change of total molecular dipole with the ith normal coördinate.

Sulfur Dioxide.—Mass-spectrometric analysis showed that the gas drawn directly from a cylinder of Dow refrigeration grade sulfur dioxide was amply pure, and it was used without further treatment. The measured values of $\mathfrak{B}$ were found to vary linearly with the partial pressure of sulfur dioxide, as shown in Figs. 1, 2 and 3. The total band intensities obtained are listed in Table I, along with the values of $\partial\mu/\partial Q_i$ calculated from them by eq. 1. The uncertainties in these measurements are difficult to assess since much personal judgment is involved in "smoothing out" the noise of a spectrum and in replotting it, nor have we found any published measurements to check ours. We estimate that the intensities are probably reliable to 10% and the values of $\partial\mu/\partial Q_i$ to 5% because of the square in eq. 1.

TABLE I

INTENSITIES OF SULFUR DIOXIDE

Band, cm.$^{-1}$	A_i (c.p.s. cm.$^{-1}$ × 10^{-11})	$\partial\mu/\partial Q_i$ (e.s.u. g.$^{-1/2}$)
ν_1 1151	226	± 49.1
ν_2 519	257	± 52.3
ν_3 1361	1606	±130.8

Acetylenes.—For the light molecule, C_2H_2, gas from a Matheson cylinder was passed through sodium bisulfite solution to remove acetone, then sodium hydroxide solution to remove sulfur dioxide, and finally a trap at −78° to remove water vapor. Mass-spectrometric analysis showed this sample to be sufficiently pure. The C_2D_2 was prepared by the action of D_2O on an excess of a special grade of calcium carbide; its mass spectrum showed about 0.7% C_2HD and a trace of C_2H_2 as the only impurities. The C_2HD was prepared by treating sodium acetylide with deuterium chloride at −78°. The excess deuterium chloride was removed by treating the reaction product with triethylamine to form the solid triethylamine deuterium chloride, and excess triethylamine was removed by fractional condensation. While it was hoped this procedure might give an isotopically pure sample of C_2HD, mass-spectrometric analysis showed it to consist of 15.1% C_2D_2, 66.1% C_2HD and 18.8% C_2H_2. This sample was richer in C_2HD than a sample in isotopic equilibrium, and was used in all the measurements on C_2HD. In regions of the spectrum where C_2HD bands were overlapped by bands of either C_2H_2 or C_2D_2, corrections were made for the contributions of the symmetrical molecules.

The sharp Q-branches of the perpendicular bands, ν_4 and ν_5, render quantitative measurement more difficult, and so a different graphical extrapolation was employed, as shown in Figs. 4 through 12. The final values of intensity are given in Table II, along with the values of $\partial\mu/\partial Q_i$ calculated by eq. 1. It is estimated that the values of band intensity are probably accurate to within 20% for ν_4 and ν_5 in all molecules, and to within 10% for ν_1 and ν_3; but ν_2, appearing very weakly and only in C_2HD, may be in error by 50%. These error estimates then give percentage errors approximately one-half as large in $\partial\mu/\partial Q_i$. Intensities are given in Table II for C_2H_2 by other workers; infrared dispersion was employed by Kelly, Rollefson and Schurin[8] and should give results of greater precision on this molecule; Callomon, McKean and Thompson[9] employed infrared intensity, as in the present work.

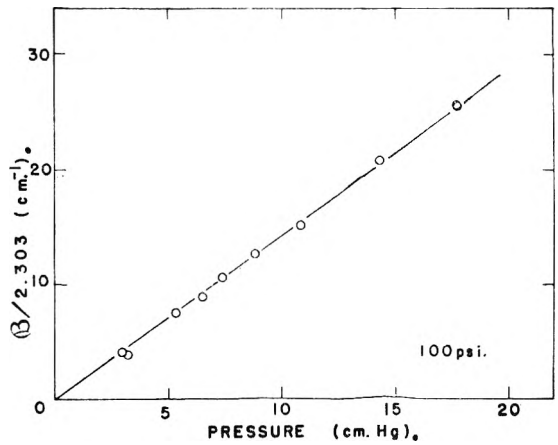

Fig. 1.—Integrated intensity for sulfur dioxide, ν_1.

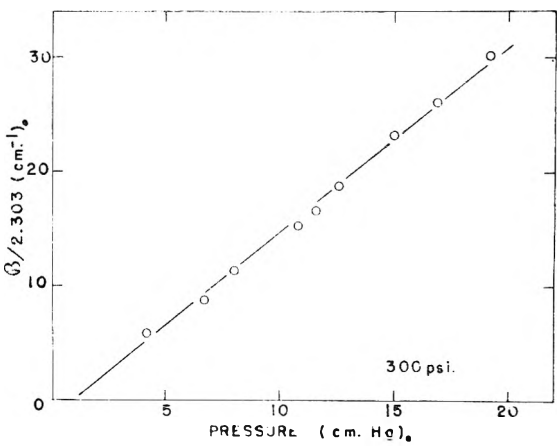

Fig. 2.—Integrated intensity for sulfur dioxide, ν_2.

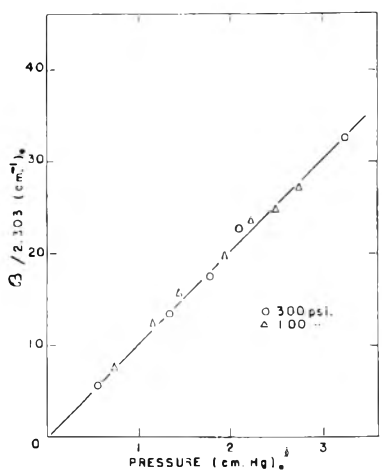

Fig. 3.—Integrated intensity for sulfur dioxide, ν_3.

Calculations

To interpret these measurements in terms of the individual bonds in the molecule, it is necessary to know the detailed motions of the atoms in the different vibrations. Normal coördinate calculations were, therefore, carried out for all molecules

(8) R. L. Kelly, R. Rollefson and B. S. Schurin, *J. Chem. Phys.*, **19**, 1595 (1951).

(9) H. J. Callomon, D. C. McKean and H. W. Thompson, *Proc. Roy. Soc.* (*London*), **A208**, 332 (1951).

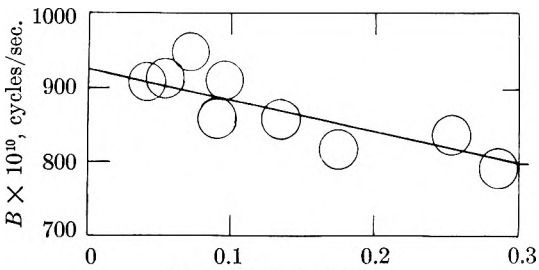

Fig. 4.—Intensity extrapolation for C_2H_2, ν_-.

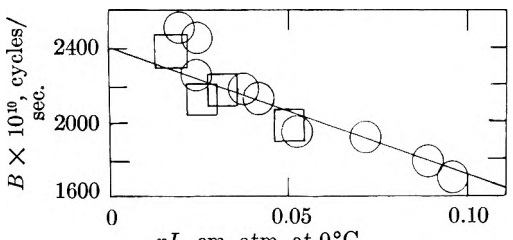

Fig. 5.—Intensity extrapolation for C_2H_2, ν_5. The squares represent measurements after conversion to double-pass.

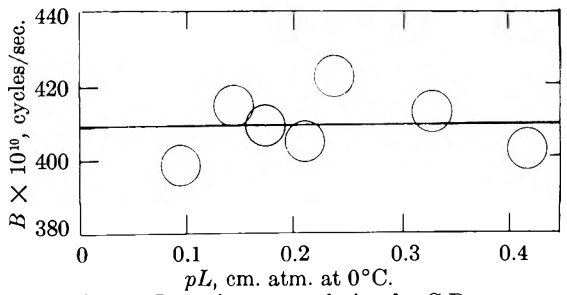

Fig. 6.—Intensity extrapolation for C_2D_2, ν_3.

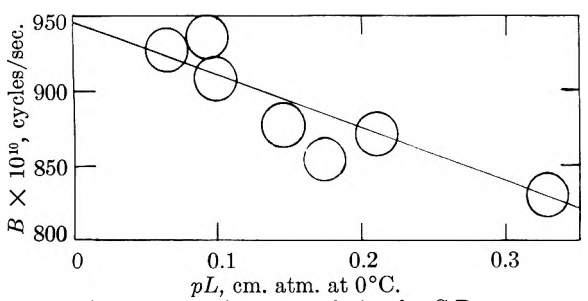

Fig. 7.—Intensity extrapolation for C_2D_2, ν_5.

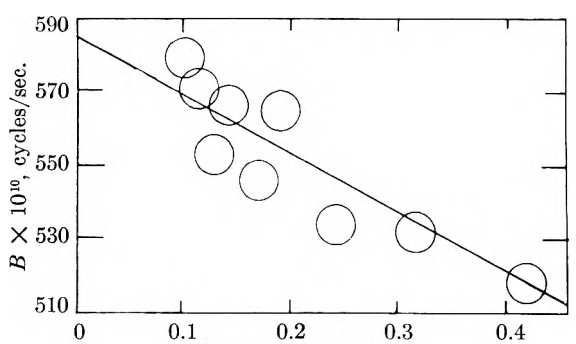

Fig. 8.—Intensity extrapolation for C_2HD, ν_1.

by the methods of Wilson.[10] The various partial derivatives of importance are related by the expression

(10) E. B. Wilson, Jr., *J. Chem. Phys.*, **7**, 1047 (1939); **9**, 76 (1941).

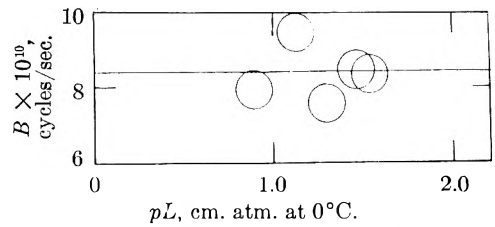

Fig. 9.—Intensity extrapolation for C_2HD, ν_2.

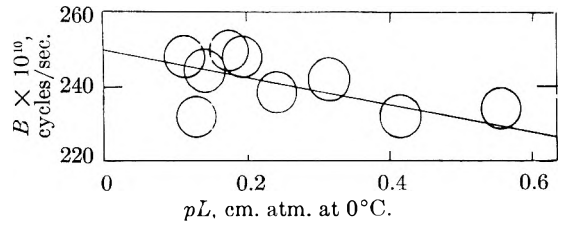

Fig. 10.—Intensity extrapolation for C_2HD, ν_3.

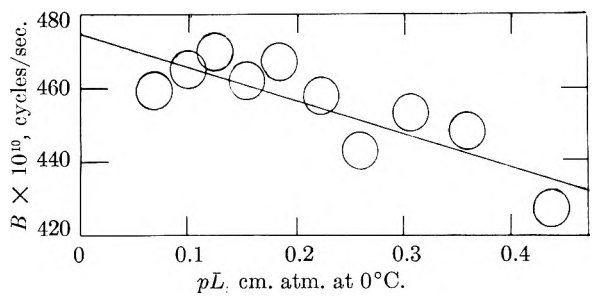

Fig. 11.—Intensity extrapolation for C_2HD, ν_4.

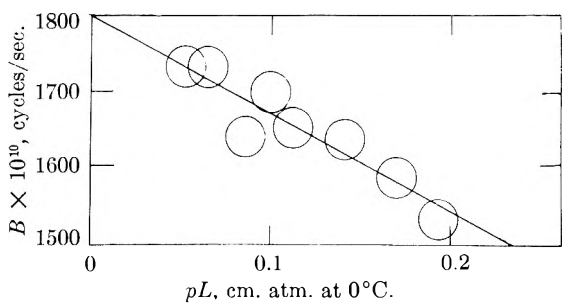

Fig. 12.—Intensity extrapolation for C_2HD, ν_5.

$$\frac{\partial\mu}{\partial S_i} = \frac{\partial Q_1}{\partial S_i}\frac{\partial\mu}{\partial Q_1} + \frac{\partial Q_2}{\partial S_i}\frac{\partial\mu}{\partial Q_2} \qquad (2)$$

where the S_i are the symmetry coördinates. The partial derivatives $\partial Q_i/\partial S_j$ are determined by the normal coördinate calculation, and the $\partial\mu/\partial Q_i$ are determined from the measured intensities. The last step is then to calculate μ and $\partial\mu/\partial r$ for the different kinds of bonds by using the known molec-

TABLE II

INTENSITIES OF ACETYLENES

(Units are identical with Table I)

	C_2H_2		C_2D_2		C_2HD	
Band	A_i	$\partial\mu/\partial Q_i$	A_i	$\partial\mu/\partial Q_i$	A_i	$\partial\mu/\partial Q_i$
ν_1	...	...	..	...	327	±58.8
ν_2	...	...	..	...	8.4	± 9.4
ν_3	925	± 98.8	408	±65.6	250	±51.4
	976[a]	835[b]				
ν_4	...	...	..	...	261	±37.1
ν_5	2400	±112.5	945	±70.4	1116	±76.7
	2410.8[a]	2410.8[b]				

[a] See reference 8. [b] See reference 9.

ular geometry and the assumptions stated in the introduction.

Sulfur Dioxide.—The normal coördinate problem in sulfur dioxide is indeterminate, in that we must calculate four force constants, but have only three observed frequencies, which give us three equations.[11] One solution of this dilemma, extensively used to furnish a unique set if not the correct one, has been to plot possible values for three of these constants as a function of the fourth.[12] The resulting curves are ellipses and, by drawing tangents, one obtains values for all four force constants. The most general quadratic force field may be written

$$2V = k_r(\Delta r_1^2 + \Delta r_2^2) + k_{\theta} r^2 \Delta\theta^2 + 2k_{rr}\Delta r_1 \Delta r_2 + 2k_{r\theta}(\Delta r_1 + \Delta r_2) r\Delta\theta \quad (3)$$

where Δr_1 and Δr_2 are changes in S–O bond distances, $\Delta\theta$ is the change in O–S–O angle, and r is the equilibrium bond length. The set of force constants labelled "ellipse" in Table III was taken from the work of Shelton, Nielsen and Fletcher.[11] Some time later, new work on the microwave spectrum of sulfur dioxide, coupled with new measurements on the infrared spectrum of isotopic sulfur dioxide, became available to us.[13] This work gives a complete determination of all four force constants, and these are listed "microwave" in Table III.

TABLE III

FORCE CONSTANTS FOR SULFUR DIOXIDE, $\times 10^{-5}$ DYNES CM.$^{-1}$

	k_r	k_θ	k_{rr}	$k_{r\theta}$
Ellipse	10.75	1.10	0.461	1.41
Microwave	10.006	0.7933	0.0236	0.189

We shall choose to define the symmetry coördinates by the following relations

$$S_1 = 2^{-1/2}(\Delta r_1 + \Delta r_2)$$
$$S_2 = r\Delta\theta$$
$$S_3 = 2^{-1/2}(\Delta r_1 - \Delta r_2) \quad (4)$$

The various force constants of Table III then give the following normal coördinates: for the ellipse constants

$$Q_1 = 0.481 \times 10^{-11} S_1 + 0.0859 \times 10^{-11} S_2$$
$$Q_2 = -0.00318 \times 10^{-11} S_1 + 0.275 \times 10^{-11} S_2 \quad (5)$$

and for the microwave constants

$$Q_1 = 0.457 \times 10^{-11} S_1 + 0.00706 \times 10^{-11} S_2$$
$$Q_2 = -0.153 \times 10^{-11} S_1 + 0.289 \times 10^{-11} S_2 \quad (6)$$

while for either set

$$Q_3 = 0.390 \times 10^{-11} S_3 \quad (7)$$

Since S_1 and S_2 are both totally symmetric, $\partial\mu/\partial S_1$ and $\partial\mu/\partial S_2$ are related by two simultaneous equations like eq. 2 to $\partial\mu/\partial Q_1$ and $\partial\mu/\partial Q_2$. Our uncertainty in the algebraic sign of the $\partial\mu/\partial Q_i$ gives several different solutions for the $\partial\mu/\partial S_i$, all of which are listed in Table IV. Since $\partial\mu/\partial S_3$ is related to only $\partial\mu/\partial Q_3$, there is only one possible magnitude for $\partial\mu/\partial S_3$. Finally, the molecular geometry,[14] taken as $\theta = 119.53°$ for the O–S–O angle and 1.432 Å. for the S–O distance, gives

$$\frac{\partial\mu}{\partial r} = \frac{2^{-1/2}}{\cos(\theta/2)} \frac{\partial\mu}{\partial S_1}$$
$$\mu = -\frac{r}{2\sin(\theta/2)} \frac{\partial\mu}{\partial S_2}$$
$$\frac{\partial u}{\partial r} = \frac{2^{-1/2}}{\sin(\theta/2)} \frac{\partial u}{\partial S_3} \quad (8)$$

The values of μ and $\partial\mu/\partial r$ for the S–O bond calculated from these expressions are also listed in Table IV.

TABLE IV

MOMENTS CALCULATED FOR SULFUR DIOXIDE

(Values of μ(S–O) are debyes; all others are e.s.u. $\times 10^{10}$.)

Moment	Relative signs of $\partial\mu/\partial Q_i$ and $\partial\mu/\partial Q_2$	Ellipse	Microwave
$\partial\mu/\partial S_1$	same	±2.34	±1.443
$\partial\mu/\partial S_1$	different	±2.38	±3.04
$\partial\mu/\partial S_2$	same	±1.861	±2.21
$\partial\mu/\partial S_2$	different	∓1.019	∓2.11
$\partial\mu/\partial S_3$	...	±5.11	±5.11
$\partial\mu/\partial r$(S–O)	same	±3.30	±2.03
(from ν_1 and ν_2)	different	±3.35	±4.27
μ(S–O)	same	∓1.53	∓1.27
(from ν_1 and ν_2)	different	±0.83	±1.21
$\partial\mu/\partial r$(S–O)	...		
(from ν_3)		±4.17	±4.17

Acetylenes.—In principle, the six quadratic force constants are completely determined by the three isotopic species. In practice, zeroth-order frequencies are known most reliably for C_2D_2,[15] and we have based our potential function largely on these. Calculation of zeroth-order frequencies for the other molecules with this potential function gives values which are quite close to the probable observed zeroth-order frequencies for these molecules. The expression for the complete quadratic force field is

$$2V = k_{CH}(\Delta r_1^2 + \Delta r_2^2) + k_{CC}\Delta r_3^2 + 2k'(\Delta r_1 + \Delta r_2)\Delta r_3 + 2k''\Delta r_1\Delta r_2 + d_1 d_2[k_\delta(\Delta\alpha_1^2 + \Delta\alpha_2^2 + \Delta\beta_1^2 + \Delta\beta_2^2) + 2k_\delta'(\Delta\alpha_1\Delta\alpha_2 + \Delta\beta_1\Delta\beta_2)] \quad (9)$$

The various symbols have the following meanings: Δr_1 and Δr_2 are changes in C–H distances, Δr_3 is the change in C≡C distance, d_1 and d_2 are the equilibrium C–H and C≡C distances, $\Delta\alpha_1$ and $\Delta\alpha_2$ are changes in H–C–C angle in a plane passing through the molecular axis, $\Delta\beta_1$ and $\Delta\beta_2$ are changes in H–C–C angle in a plane also passing through the molecular axis but perpendicular to the first plane. The following values were used for the force constants in all calculations; units are dynes cm.$^{-1}$ $\times 10^{-5}$.

$k_{CH} = 6.37$ $\quad k_{CC} = 16.4$ $\quad k' = -0.03$
$k'' = 0$ $\quad k_\delta = 0.201$ $\quad k_\delta' = 0.072$

For the symmetrical molecules, the symmetry coördinates are defined by the relations

$$S_1 = 2^{-1/2}(\Delta r_1 + \Delta r_2)$$
$$S_2 = \Delta r_3$$
$$S_3 = 2^{-1/2}(\Delta r_1 - \Delta r_2)$$
$$S_{4a} = 2^{-1/2}(\Delta\alpha_1 - \Delta\alpha_2)$$
$$S_{5a} = 2^{-1/2}(\Delta\alpha_1 + \Delta\alpha_2) \quad (10)$$

(11) R. D. Shelton, A. H. Nielsen and W. H. Fletcher, *J. Chem. Phys.*, **21**, 2178 (1953).

(12) Reference 11, see footnote 12.

(13) S. R. Polo and M. K. Wilson, *J. Chem. Phys.*, **22**, 900 (1954); D. Kivelson, *ibid.*, **22**, 904 (1954).

(14) In reference 11, see footnotes 1–3.

(15) A. H. Nielsen, private communication.

For the unsymmetrical molecule, the symmetry coördinates are simply the various internal coördinates; *i.e.*, with hydrogen numbered one, deuterium two

$$S_1 = \Delta r_1 \quad S_2 = \Delta r_2 \quad S_3 = \Delta r_3$$
$$S_{4a} = \Delta\alpha_1 \quad S_{5a} = \Delta\alpha_2 \qquad (11)$$

These force constants then give the normal coördinates for infrared-active vibrations as follows; for C_2H_2

$$Q_3 = 1.242 \times 10^{-12} S_3, \; Q_{5a} = 1.317 \times 10^{-20} S_{5a}$$

for C_2D_2

$$Q_3 = 1.692 \times 10^{-12} S_3, \quad Q_{5a} = 1.794 \times 10^{-20} S_{5a}$$

and for C_2HD

$$Q_1 = 1.198 \times 10^{-12} S_1 + 0.0668 \times 10^{-12} S_2 - 0.411 \times 10^{-12} S_3$$
$$Q_2 = 0.351 \times 10^{-12} S_1 + 1.052 \times 10^{-12} S_2 + 3.112 \times 10^{-12} S_3$$
$$Q_3 = 0.231 \times 10^{-12} S_1 - 1.408 \times 10^{-12} S_2 + 1.162 \times 10^{-12} S_3$$
$$Q_{4a} = 0.084 \times 10^{-20} S_{4a} - 1.445 \times 10^{-20} S_{5a}$$
$$Q_{5a} = 1.212 \times 10^{-20} S_{4a} + 0.495 \times 10^{-20} S_{5a} \qquad (12)$$

Expressions similar to (2) permit calculation of the various $\partial\mu/\partial S_i$; these are listed in Table V. Since only S_3 and S_5 give rise to infrared absorption in the symmetrical molecules, we have finally that

$$\partial\mu/\partial r = 2^{-1/2}\partial\mu/\partial S_3, \; \mu = \partial\mu/\partial\alpha = 2^{-1/2}\partial\mu/\partial S_{5a} \qquad (13)$$

in C_2H_2 and C_2D_2. In these two molecules, then, there is just one magnitude for the values of $\partial\mu/\partial r$ and μ, in contrast to sulfur dioxide. In the C_2HD molecule, the internal coördinates were themselves taken as the symmetry coördinates; therefore, the relationships now become

$$\partial\mu/\partial r = \mp\partial\mu/\partial S_1 = \pm\partial\mu/\partial S_2$$
$$\mu = \partial\mu/\partial\alpha_1 = \partial\mu/\partial\alpha_2$$
$$\partial\mu/\partial S_3 = 0 \qquad (14)$$

By assuming that the moment and its derivative are not greatly changed by the isotopic substitution, we may determine the relative signs of the various $\partial\mu/\partial Q_i$ for the unsymmetrical molecule. These were found to be $(\mp \pm \mp)$ for the first three, and $(\mp \pm)$ for the last two. With these choices of signs, values for the moment and its derivative were calculated for C_2HD as well. All these values are listed in Table V. The non-zero value for $\partial\mu/\partial S_3$ is probably caused by the large experimental uncertainty in the intensity of the very weak band, ν_2.

TABLE V

MOMENTS CALCULATED FOR ACETYLENES

(Units are the same as in Table IV.)

Moment	C_2H_2	C_2D_2	C_2HD
$\partial\mu/\partial S_1$	...	...	∓ 0.790
$\partial\mu/\partial S_2$	...	...	$\pm$ .783
$\partial\mu/\partial S_3$	± 1.228	± 1.110	$\mp$ .062
$\partial\mu/\partial S_{4a}$	...	...	$\pm$ .899
$\partial\mu/\partial S_{5a}$	± 1.482	± 1.263	$\pm$ .916
$\partial\mu/\partial r$	± 0.868	± 0.785	$\pm$ .790(CH)
			$\pm$ .783(CD)
μ	± 1.048	± 0.893	$\pm$ .899(CH)
			$\pm$ .916(CD)

Discussion

The better values of μ and $\partial\mu/\partial r$ in sulfur dioxide are found using the microwave force field; however, it is interesting to note how rapidly the moment and its derivative change with a small change in the force field. The same calculations were repeated with observed frequencies instead of zero frequencies, and the results were changed very little. This suggests caution in the calculation of bond moments using very simplified force fields.

Whether the signs of $\partial\mu/\partial Q_1$ and $\partial\mu/\partial Q_2$ are really the same or different, we find the S–O bond moment from infrared intensities does not agree within the experimental error with the molecular moment, 1.59 Debye, derived from the microwave spectrum.[16] One might choose the signs of $\partial\mu/\partial Q_1$ and $\partial\mu/\partial Q_2$ different because of the agreement between the value of $\partial\mu/\partial r$ here and from the ν_3 band. However, Benedict[17] finds that the $\partial\mu/\partial r$ values in carbon dioxide are quite different for symmetrical and for anti-symmetrical vibrations. Similarly, McKean[18] finds quite different values for $\partial\mu/\partial r$ of the C–F bond in fluoroform from symmetric and antisymmetric stretching.

In the acetylenes, we note that μ and $\partial\mu/\partial r$ are independent of isotopic substitution; all three molecules give values agreeing within experimental error. Even further, the values are consistent within the same molecule, independent of the relative amplitudes or directions of vibration. This result is quite surprising, in view of the discrepancies noted in carbon dioxide and in fluoroform. It may be associated with the presence of unshared electron pairs and the fact that one can draw a number of resonance structures for these latter two molecules. In acetylene, on the other hand, there are neither unshared pairs of electrons nor other resonating structures.

Two rules have recently been proposed[19,20] relating the infrared intensities of isotopic molecular species. These rules are of particular importance in molecules for which a complete normal coördinate treatment is not possible. It is of interest, then, to check these rules in small, symmetrical molecules before using them as aids in the analysis of larger molecules.

Crawford's rule may be expressed for the acetylenes as

$$\sum_a I_a(C_2H_2)/\nu_a^2(C_2H_2) = \sum_a I_a(C_2D_2)/\nu_a^2(C_2D_2) = \sum_a I_a(C_2HD)/\nu_a^2(C_2HD) \qquad (15)$$

where I_a is the measured intensity of the ath band and ν_a is its observed frequency. The sum is taken individually over the parallel bands and over the perpendicular bands, giving two relations. Using the data of Table II, we obtain, for the parallel bands

$$8.58 \times 10^5 = 6.86 \times 10^5 = 6.93 \times 10^5$$

and for the perpendicular bands

(16) G. F. Crable and W. V. Smith, *J. Chem. Phys.*, **19**, 502 (1951).
(17) W. S. Benedict, private communication.
(18) D. C. McKean, private communication.
(19) B. L. Crawford, Jr., *J. Chem. Phys.*, **20**, 977 (1952).
(20) J. C. Decius, *ibid.*, **20**, 1039 (1952).

$$4.50 \times 10^7 = 3.21 \times 10^7 = 3.36 \times 10^7$$

These sums are consistent within the range of experimental error stated earlier.

Decius' rule may be expressed for the acetylenes as

$$\sum_a I_a(C_2H_2) + \sum_a I_a(C_2D_2) = 2\sum_a I_a(C_2HD) \quad (16)$$

Here again, the sum is taken individually over the parallel and the perpendicular bands. The data of Table II give, for the parallel bands

$$1323 \times 10^{10} = 1171 \times 10^{10}$$

and for the perpendicular bands

$$3350 \times 10^{10} = 2754 \times 10^{10}$$

These sums are also consistent within the range of experimental error.

Acknowledgment.—It is a pleasure to acknowledge the help of others toward completion of this work. We should like to mention especially correspondence with Professor A. H. Nielsen concerning C_2D_2 and SO_2, communication of the microwave work by Professor E. B. Wilson, Jr., preparation of the C_2D_2 by Mr. T. Flanagan, and suggestions on the preparation of C_2HD by Professor D. M. Ritter.

THE INTENSITIES OF INFRARED HYDROXYL BANDS

BY GORDON M. BARROW

Department of Chemistry, Northwestern University, Evanston, Illinois

Received May 18, 1955

Measurements are reported of the infrared absorption intensities of the OH band of a number of alcohols in carbon tetrachloride, ether and triethylamine. The intensities are greater for the more acidic alcohols and for the more basic solvent. This behavior is that expected if the stretching vibration of the OH bond is considered to be the beginning of the ionization of the OH group. Such a view leads to a quantitatively satisfactory explanation of the observed intensities in terms of a variable amount of ionic character of the OH bond.

The intensity of an infrared absorption band of a vibrating molecule is dependent on the variation of the molecular dipole moment, and, therefore, on the variation of the electronic configuration of the molecule, as the atoms move according to the normal coördinate which describes the vibration. The study of the intensities of vibrational absorption bands, therefore, leads to an understanding of the effect of distortions of the nuclear positions on the electronic structure of the molecule.

For conjugated systems this dependence is implied by the usual valence-bond structures introduced for a complete description of the electronic distribution in the molecule and the intensities of infrared absorption bands due to vibrations of groups involved in resonance, confirm the idea of an easily variable electronic configuration.[1,2] For saturated or non-conjugated molecules there is no completely satisfactory approach to understanding the molecular dipole moment in terms of the electronic configuration of the molecule. The interpretation of the dipole moment in terms of the amount of ionic character of a bond[3] has been a very useful concept. Recently, however, calculations have shown[4-8] that when an atom of the molecule has electrons in non-bonding orbitals the dipole moment of the molecule depends to a considerable extent on the hybridization of these orbitals.

Neither the dependence of the per cent. ionic character nor the dependence of the amount of hybridization on the bond length of a bond to an atom with non-bonding electrons is known. The intensity of an infrared absorption band of a vibration involving such an atom may, therefore, be viewed in terms of the variation of percentage of ionic character with bond stretching. On the other hand, the intensity may be interpreted in terms of a change in hybridization resulting from bond stretching and the subsequent decrease in overlap of the bonding orbital.

This investigation of the intensities of the OH stretching bands of a series of alcohols in different solvents was undertaken to obtain an understanding of the importance of such factors in determining the dipole moment dependence on atomic positions in non-conjugated systems. This set of compounds is particularly suitable since a large body of chemical evidence gives some *a priori* understanding of the charge distribution in the OH bond and the variation of this distribution with the nature of the associated molecules.

Experimental

All spectra were obtained with a Beckman Model IR-2T instrument equipped with a lithium fluoride monochromator. With this instrument the slit width varies to compensate for solvent and atmospheric absorption and the slit widths given below are therefore average values. To permit band area measurements the spectra were recorded at either 0.1 or 0.05 μ per inch of chart paper.

The series of alcohols was studied in carbon tetrachloride, ether and triethylamine solutions with a few measurements also being made in *n*-butyl chloride and benzene. In carbon tetrachloride, concentrations varied from about 0.002 to 0.01 molar and a 2.06 cm. cell was used. The average slit width was 0.023 mm. For the ether and triethylamine results the concentrations of about 0.01 to 0.1 were suitable in a 0.1 cm. cell and the slit widths were about 0.03 and 0.1 mm. No evidence of hydrogen bonding in the carbon tetrachloride solutions or of bonding other than to the solvent molecules in the other solutions was observed. Carbon tetrachloride dried over drierite, absolute ether and freshly distilled triethylamine were used.

(1) D. Z. Robinson, *J. Chem. Phys.*, **19**, 88 (1951).

(2) G. M. Barrow, *ibid.*, **21**, 2008 (1953).

(3) L. Pauling, "The Nature of the Chemical Bond," Cornell University Press, Ithaca N. Y., 1945.

(4) D. Z. Robinson, *J. Chem. Phys.*, **18**, 1316 (1950).

(5) J. E. Lennard-Jones and J. A. Pople, *Proc. Roy. Soc. (London)*, **A202**, 166 (1950).

(6) J. A. Pople, *ibid.*, **A202**, 323 (1950).

(7) C. A. Coulson, *ibid.*, **A207**, 63 (1951).

(8) A. B. F. Duncan and J. A. Pople, *Trans. Faraday Soc.*, **49**, 217 (1953).

The absolute intensities were determined by graphical integration on a plot of log I_0/I *versus* the frequency, ν (cm.$^{-1}$). Only for the sharp band of the alcohols in carbon tetrachloride did the integrated intensity vary regularly with log $(I_0/I)_{max.}$ and in these cases the true absolute intensity was obtained by a linear extrapolation of the apparent intensity to zero absorption on a plot of apparent intensity *versus* log $(I_0/I)_{max.}$.[9] For the hydrogen bonded bands no significant dependence of the integrated intensity on concentration was noticed and the absolute intensity was taken as the average of the observed intensities. For all solutions the final intensities, as listed together with the frequency of the band maxima, in Table I, are the result of an extrapolation or an average of at least four separate determinations. For the strong hydrogen bonds existing in the triethylamine solutions the broad OH band overlaps the CH band of the solvent and the intensity was obtained either from an estimate of the concealed portion of the band or, as was necessary for 2-ethoxy- and 2-chloroethanol, by doubling the intensity of the high frequency half of the band. Figure 1 shows the band shapes obtained for *n*-butyl alcohol in the three solvents for the same values of the product of concentration and path length. The intensities are considered to be internally reliable to better than 10% and only for the carbon tetrachloride solutions where the narrow band makes an extrapolation to zero absorption necessary is the absolute uncertainty possibly greater.

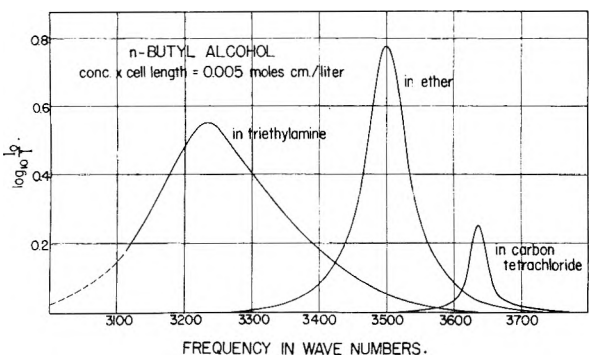

Fig. 1.—Comparison of the OH absorption bands of *n*-butyl alcohol in different solvents.

Discussion

The data of Table I show an immediate correlation of the intensities in ether and triethylamine with the strength of the hydrogen bond as measured by the shift in the frequency of the OH band maximum. Furthermore the order of the alcohols in terms of these intensities corresponds to the order in terms of the acidities given by chemical and physical evidence.[10] In view of this correlation it seems necessary to consider that stretching of the OH bond of alcohols in hydrogen bonding solvents corresponds to incipient ionization with the hydrogen atom becoming more positively charged. That is, on the assumption that at the equilibrium bond length the hydrogen atom is the more positive end of the OH bond, $d\mu/dr$ is positive for these alcohols. Here r is the OH bond length and μ the dipole moment of the dimer composed of the alcohol and the bonded solvent molecule.

For the free alcohols, *i.e.*, in carbon tetrachloride solution, the sign of $d\mu/dr$ cannot at once be predicted. Indeed, the deduction of the signs of $d\mu/dr$ and the bond dipole moments from infrared intensities has not as yet proven very successful and the procedure of choosing a particular set of signs for the bond polar properties in order to obtain reasonable numerical values for these properties does not appear to lead to unambiguous choices.[11,12] However, since the intensities of the OH bands in carbon tetrachloride solutions show a fair parallelism, except for methyl alcohol, to the intensities in ether and triethylamine, evidence seems to exist for assigning to the free alcohol, as well as to the bonded case, a positive value for $d\mu/dr$. It appears unlikely that an inversion of the sign of $d\mu/dr$ would still lead to this ordering of the intensities.

TABLE I

INTENSITIES AND FREQUENCY SHIFTS OF THE OH BAND OF ALCOHOLS IN CARBON TETRACHLORIDE, ETHER AND TRIETHYLAMINE

Alcohol	Frequencies (cm.$^{-1}$). CCl$_4$	Ether	Triethylamine	Intensity (l. mole^{-1} cm.$^{-1}$) $\times 10^{-4}$ In CCl$_4$	In ether	In triethylamine
t-Butyl	3614	116	337	0.42	2.6	4.6
Isopropyl	3620	122	374	.48	3.0	4.8
sec-Butyl	3623	123	375	.58	3.2	5.3
Ethyl	3634	133	393	.62	3.8	6.1
n-Butyl	3636	135	400	.72	3.8	6.7
Methyl	3644	136	401	.53	3.9	6.2
2-Ethoxyethanol	(3630)	143	424	..	3.5	7.1
2-Chloroethanol	(3630)	177	479	..	4.6	8.2
Phenol	3609	276		1.2	8.5	..

It has been assumed that no appreciable interaction between the hydroxyl group and the carbon tetrachloride solvent molecules exists. Although there is some frequency decrease in the OH band in going from the vapor to carbon tetrachloride solution it appears that this can be attributed to the dielectric constant of the medium rather than to specific interaction.[13] It is concluded therefore, that the intensities in carbon tetrachloride solution are applicable to the free molecules at least to such an extent that a reversal of the sign of $d\mu/dr$ is unlikely.

Further evidence that $d\mu/dr$ for the OH bond of the alcohols are positive is the fact that the measurements of the intensities of the butyl alcohols and phenol in benzene and *n*-butyl chloride, where weak hydrogen bonding occurs, show in all cases an increase in intensity over the results in carbon tetrachloride. The reverse would be expected if the contributions from the hydrogen bonding were added to an initially negative value of $d\mu/dr$.

It is of interest also to consider in more detail the intensities of the hydrogen bonded bands. These have previously been recognized as having a high intensity and the present data show that this intensity is greater the more acidic is the alcohol and the more basic the bonding agent. If the effect of the solvent molecules on the molecular pair joined by the hydrogen bond is ignored a value of $d\mu/dr$ can be calculated. Although the nature of the surrounding medium will certainly affect the intensity of the infrared band it appears from the measurements of Whiffen[14] on the 760 cm.$^{-1}$ band of chloro-

(9) D. A. Ramsay, *J. Am. Chem. Soc.*, **74**, 72 (1952).

(10) J. Hine and M. Hine, *ibid.*, **74**, 5268 (1952).

(11) P. N. Schatz and D. F. Hornig, *J. Chem. Phys.*, **21**, 1516 (1953).

(12) G. M. Barrow and D. C. McKean, *Proc. Roy. Soc. (London)*, **A213**, 27 (1952).

(13) L. H. Jones and R. M. Badger, *J. Am. Chem. Soc.*, **73**, 3132 (1951).

(14) D. H. Whiffen, *Trans. Farad. Soc.*, **49**, 878 (1953).

form that this effect may not be large since for very different solvents the integrated intensities varied at most 25% from the value for the vapor.

From the observed intensities, A, in l. mole^{-1} cm.$^{-1}$ the change in dipole moment, μ, with the normal coördinate, Q, describing the vibration is given by

$$\frac{d\mu}{dQ} = \pm \left(\frac{3c^2}{N}\frac{1000}{}A\right)^{1/2}$$

where c is the velocity of light and N is Avogadro's number. If the vibration is taken to be purely an OH bond stretching mode then the desired quantity $d\mu/dr$ is given by

$$\frac{d\mu}{dr} = \left(\frac{1}{m_H} + \frac{1}{m_0}\right)^{-1/2}\frac{d\mu}{dQ}$$

where m_H and m_0 are the masses of the hydrogen and oxygen atoms, respectively. Table II summarizes these data for the alcohols grouped according to the significant differences in intensity as tertiary and secondary alcohols, normal alcohols and phenol in carbon tetrachloride, ether and triethylamine.

TABLE II

THE CHANGE IN DIPOLE MOMENT WITH OH BOND STRETCHING (IN E.S.U./CM. $\times 10^{10}$)

	In CCl_4	In Ether	In Triethylamine
t- and *sec*-alc.	1.0	2.5	3.2
Normal alc.	1.2	2.9	4.4
Phenol	1.5	3.85	..

These data can be interpreted most easily by considering the dipole moment of the OH bond as arising, at least formally, from the ionic character of the bond. For the hydrogen bonded alcohol, stretching of the OH bond can now be considered as an approach to the limiting case of the ion-pair consisting of the alkoxide ion and the protonated ether or triethylamine. Since the dipole moment of such a system can be estimated this case can be more easily understood than for the stretching of a free bond where the mode of approach to the limiting form consisting of two uncharged species is not easily defined. A suitable approximation to the dipole moment of the ion-pair can be calculated by assuming the proton to be a normal bond length from the acceptor molecule and full positive and negative electric charges to be on the proton and the alkoxide oxygen. Any covalent character of the new OH or NH bond will tend to cancel out the effect of polarizability on the dipole moment of the system.

As in the treatment of molecular dipole moments[3] we assume that the OH bond can be described in terms of a covalent and ionic character, *i.e.*

$$\psi = \sqrt{a}\psi_{\text{covalent}} + \sqrt{b}\psi_{\text{ionic}}$$

and that the covalent character of the bond gives no dipole contribution while that of the ionic character has associated with it a dipole moment of er where e is the electronic charge. For a fixed system of charges the expected value of $d\mu/dr$ would then be the fraction of ionic character times the electronic charge. Such a view is unsatisfactory in that as the OH bond is stretched and ionization begins the ionic character of the bond rapidly increases. A suitable equation representing the expected behavior of the ratio of the amount of ionic character, b, to the amount of covalent character, a, is

$$\frac{b}{a} = Ae^{r_e/(1.7 - r)}$$

where, as indicated in Fig. 2, 1.7 is the limit in ångströms to which the OH bond is stretched to place the proton completely on the acceptor molecule, r_e

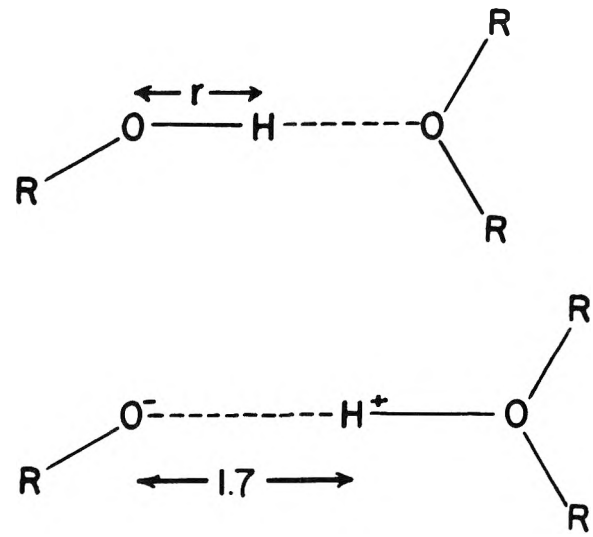

Fig. 2.—Model for interpretation of $d\mu/dr$ for a hydrogen bonded alcohol.

is the equilibrium OH bond length, and A is a factor dependent on the acidity of the alcohol and the basicity of the proton accepting molecule. The value of $d\mu/dr$ from the intensity measurements can now be related to the ionic character of the bond since, with $\mu_{\text{covalent}} = 0$ and $\mu_{\text{ionic}} = 4.8 \times 10^{-10}$ the calculated value for $d\mu/dr$ is

$$\frac{d\mu}{dr} = b(4.8 \times 10^{-10}) + 4.8 \times 10^{-10}\frac{db}{dr}$$

To fit the values of $d\mu/dr$ for the three groups of alcohols in ether values of A have been chosen and Fig. 3 shows the calculated dipole moment of the system as a function of the OH bond length. The O . . . O distance has been taken as 2.7 Å. and the equilibrium O–H distance as 1.0 Å., the small bond stretching with hydrogen bonding[15] being ignored, Fig. 4 shows the per cent. ionic character as a function of OH bond length corresponding to the cases of Fig. 3. The calculated equilibrium dipole moments are 0.95, 1.14 and 1.65 debye corresponding to ionic contributions of 20, 24 and 35% which are in satisfactory agreement with the ionic character of about 30% obtained from molecular dipole moments.

The variation in dipole moment of the alcohols in the different solvents and the variation of the OH bond dipoles of the different alcohols implied by the equation relating ionic character to bond length and the infrared intensities cannot readily be confronted with experimental evidence. However, Lüttke and Mecke[16] have shown that the dipole

(15) M. M. Davis and G. B. B. M. Sutherland, *J. Chem. Phys.*, **6**, 755 (1938).

(16) W. Lüttke and R. Mecke, *Z. Elektrochem.*, **53**, 241 (1949).

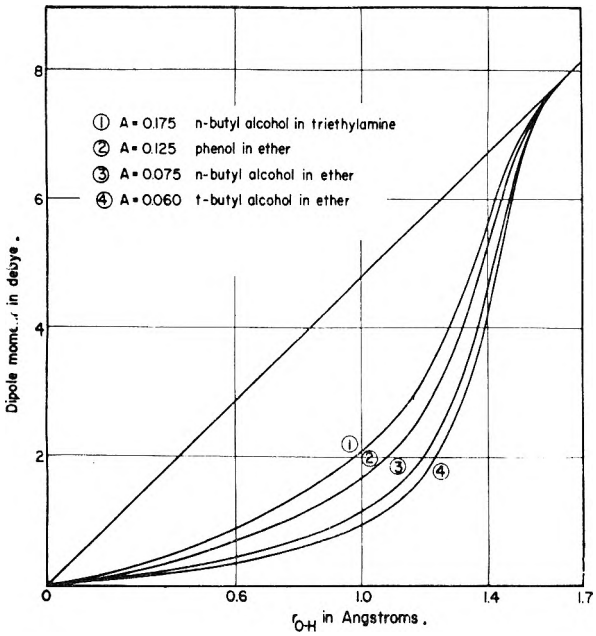

Fig. 3.—The OH bond dipole moment as a function of the OH distance. Values of A obtained to fit the observed $d\mu/dr$.

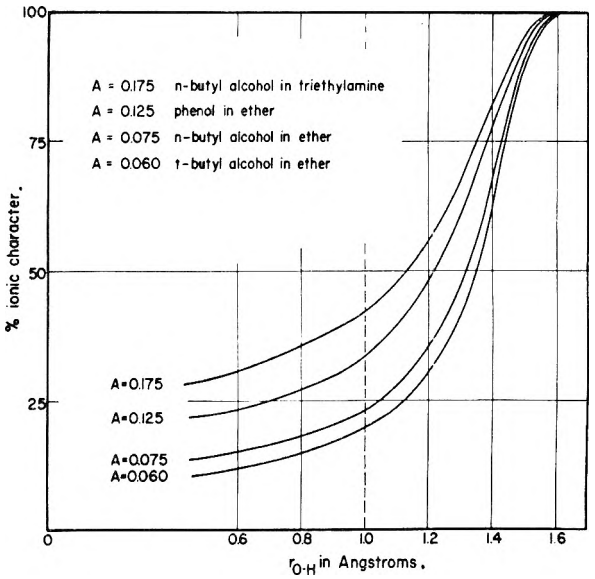

Fig. 4.—The ionic character of the OH bond for hydrogen bonded alcohols as a function of the OH distance.

moment of phenol varies from values of about 1.37 debye in non-polar solvents and 1.44 in polar solvents to 2.29 in ether. This suggests that the ionic character and the bond dipole moments at the equilibrium distance may be somewhat larger than those calculated here.

The interpretation of the $d\mu/dr$ values in terms of this empirical equation for the ionic contribution to the OH bond leads to some interesting observations. For increasingly acidic OH groups or more basic proton accepting molecules, if the equilibrium OH bond length remains about 1 Å., the intensity of the OH band should rise to a maximum value corresponding to $d\mu/dr$ equal to about 5 debye/Å. before going over to the completely ionic case with $d\mu/dr = 4.8$ debye/Å. Furthermore the largest contribution to the intensity comes from the term involving the change of ionic character with distance rather than from the term corresponding to the separation of the charges.

The above treatment seems to provide a consistent explanation for the polar properties of the hydrogen bonded OH group from considerations of the ionic character of the bond. The possibility that the observed effects are due at least in part to changes in the hybridization of the oxygen orbitals has not been ruled out. In view of the large effect of the hydrogen bonding on the intensity it appears that, since hydrogen bonding would be expected to play a more important role in the ionic character than in the oxygen atom hybridization, the most important contribution to the intensity of the hydrogen bonded OH band must be related to the ionic character of the bond. A corresponding conclusion, however, does not necessarily follow for the free alcohols.

The direction, as well as the magnitude, to be expected for $d\mu/dr$ on the basis of a variable amount of hybridization is not clearly established. However, applying the arguments used by Linnett[17] to interpret interaction force constants of H_2O it appears that stretching of the OH bond would lead to a change of hybridization which results in a decreased contribution of the non-bonding electrons to the dipole moment. This leads to an opposite direction for $d\mu/dr$ from that deduced above and suggests that even for the free alcohol the major contribution to $d\mu/dr$ must be considered as arising from the ionic character of the bond.

(17) D. F. Heath and J. W. Linnett, *Trans. Faraday Soc.*, **44**, 556 (1948).

BOND MOMENTS AND MOLECULAR STRUCTURE[1]

BY D. F. HORNIG AND D. C. MCKEAN

Metcalf Research Laboratory, Brown University, Providence, Rhode Island

Received May 18, 1955

This paper discusses the question of what information concerning molecular structure can be or has been obtained from the intensities of infrared vibration bands. The first part summarizes the assumptions involved and information required in relating the intensity of a fundamental vibration band to bond parameters μ and $\partial\mu/\partial r$. The need for accurate knowledge of the potential function is stressed. In the second part the available data on μ and $\partial\mu/\partial r$ are surveyed with a view to examining (a) their self-consistency and (b) the question as to whether "infrared" and "static" bond moments can be regarded as equal. It is seen that the only self-consistency lies in the order of magnitude of the values found. From the results from molecules containing CN groups it appears that infrared and static bond moments are not the same quantity. In the third part the possible influence of unshared pairs of electrons on bending vibration intensities is considered for the specific cases of NH_3 and HCN. It is shown that rehybridization or reorientation of these electrons may largely determine the bond moments found in these molecules. It is also suggested that the high CH moments found in C_2H_4 and C_2H_2 are due to movements of charge in the double or triple carbon–carbon bonds. Some general conclusions are summarized.

Enough experimental data have now been accumulated on infrared absorption intensities so that the time seems ripe to inquire into the validity of the conclusions which have been drawn from them about the structure of molecules. We should particularly like to examine the "effective bond moments" which have been derived and to ask what relation they bear to the conventional bond moments whose vector sum equals the static dipole moment of the molecule.

In order to do this it is first necessary to examine a typical problem to see exactly what is measured and under what conditions meaningful measurements can be obtained. When that is done the assumptions involved in the conventional interpretation of the results can be examined, particularly in those cases where they lead to internal inconsistencies, and new interpretations suggested.

The basic equation from which infrared intensity measurements proceed is

$$\int_{\text{band}} \alpha_\nu d\nu = \frac{N\pi}{3c^2}\left(\frac{\partial\vec{\mu}}{\partial Q}\right)^2 \qquad (1)$$

The left-hand side of this equation represents the integrated absorption coefficient over an entire vibration–rotation band. On the right-hand side N is the number of molecules per cc. of sample and $(\partial\vec{\mu}/\partial Q)$ represents the rate of change of the *vector* dipole moment when the molecule is deformed in the manner specified by the normal coördinate Q. This quantity, $\partial\vec{\mu}/\partial Q$, is what can be determined directly from the experiments. However, the measurement gives only the absolute magnitude of $(\partial\vec{\mu}/\partial Q)$, so the direction in which the dipole moment change is produced must be known on other grounds, and unless it is known no further analysis of the result is possible. This limits the method at present to symmetrical molecules, whose symmetry determines the direction of dipole moment change.

For example, the methyl chloride molecule, CH_3Cl, possesses a threefold axis of symmetry. As a consequence, three of its normal vibrations change the dipole moment along the axis of symmetry and three produce a component of dipole moment perpendicular to the symmetry axis. By measuring the intensity of the corresponding six infrared absorption bands, the six $(\partial\mu/\partial Q)$'s may be obtained.

This is not enough, however, since we do not as yet know what the form of the distortion specified by the normal coördinates, Q, is. Provided we know the potential energy of the molecule accurately in terms of all possible distortions, the usual theory of molecular vibrations[2] can tell us what motion was involved in each normal coördinate. For example, any of the normal coördinates in CH_3Cl which change the moment parallel to the axis can be represented as a superposition of three distinct symmetrical distortions which are illustrated in Fig. 1. These are a symmetrical C–H stretching motion (S_1), a symmetrical H–C–H bending is motion (S_2) and a C–Cl stretching motion (S_3); that is,

$$\begin{aligned} Q_1 &= L_{11}^{-1} S_1 + L_{12}^{-1} S_2 + L_{13}^{-1} S_3 \\ Q_2 &= L_{21}^{-1} S_1 + L_{22}^{-1} S_2 + L_{23}^{-1} S_3 \\ Q_3 &= L_{31}^{-1} S_1 + L_{32}^{-1} S_2 + L_{33}^{-1} S_3 \end{aligned} \qquad (2)$$

The coefficients, L_{ij}^{-1}, in these equations can be obtained from a knowledge of the masses of the atoms, the potential energy function of the molecule, and its geometry.[3] Assuming for the moment that they are known accurately, we can then get without any arbitrary assumptions, the change in the parallel component of the dipole moment of the molecule during an arbitrary symmetrical deformation, *e.g.*

$$\frac{\partial\mu_z}{\partial S_1} = L_{11}^{-1}\frac{\partial\mu_z}{\partial Q_1} + L_{21}^{-1}\frac{\partial\mu_z}{\partial Q_2} + L_{31}^{-1}\frac{\partial\mu_z}{\partial Q_3} \qquad (3)$$

In a similar way one may find the change in the perpendicular dipole moment produced by a distortion of suitable symmetry. In CH_3Cl these are an antisymmetric C–H stretch, a CH_3 deformation and the H_3–C–Cl bending motion.

This analysis is readily generalized and we come to the conclusion that the maximum information which can be derived from infrared intensity measurements without subsidiary assumptions is the change in each component of the dipole moment produced by distortions of the molecule which are of the same symmetry type as the dipole moment component.

This is important information about the structure of a molecule if it is not misused. Before

(1) Work supported by the Office of Naval Research.

(2) G. Herzberg, "Infrared and Raman Spectra of Polyatomic Molecules," D. Van Nostrand Co., Inc., New York, N. Y., 1945.

(3) E. B. Wilson, Jr., *J. Chem. Phys.*, **7**, 1047 (1939); **9**, 76 (1941).

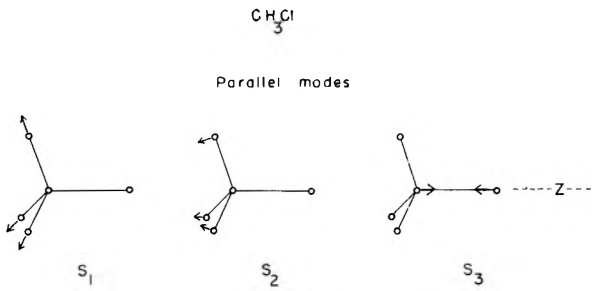

Fig. 1.—Symmetry internal coördinates for the A_1 class of CH_3Cl.

proceeding it is well to ask how well this information can actually be achieved. The difficulty of making accurate intensity measurements is well known and imposes an obvious limitation. We shall assume, nevertheless, that reasonable accuracy has been achieved. The results are then limited by the accuracy of our knowledge of the coefficients L_{ij}^{-1} which specify the form of the normal vibration. Unfortunately, these are frequently very hard to determine for the simple reason that most molecules have more force constants than frequencies so that the complete potential function cannot be determined. Furthermore, although it has been shown that the direct effect of anharmonicity is small,[4] it may have the serious effect of making it hard to find the correct harmonic force constants. The reason for this is that some force constants which have a considerable effect on the normal coördinates are extremely sensitive to the exact harmonic frequencies and in the presence of anharmonicity they are not usually known.

In this dilemma it is customary to fill the gap by such methods as (a) to carry over some of the force constants from other molecules (b) to assume that some of them can be neglected, or (c) to adopt a physical model of the molecular force field which will supply the missing constants. The result may be good or bad, depending on the sensitivity of the conclusion to the potential function. Unfortunately this may sometimes be a difficult stumbling block, as Eggers has already shown.[5] It is extremely important, therefore, that the effect of any assumptions about the force field be carefully analyzed, and in this most of what has been published is deficient. It should be emphasized that the absence of potential constants is not always serious; some conclusions may be very insensitive to the dubious constants while others may be so sensitive as to make the results meaningless with the best force constants when anharmonicity is ignored. We shall return to this point, with examples, a little later.

Even if all of the potential constants are known, one more great difficulty arises. In equation 3 or its generalization

$$\frac{\partial \vec{\mu}}{\partial S_i} = \sum_j L_{ji}^{-1} \left(\frac{\partial \vec{\mu}}{\partial Q_j} \right) \qquad (4)$$

the sign of each term is indeterminate. Consequently, 2^n different solutions are possible, yielding 2^{n-1} different absolute values for $\partial\mu/\partial S$. Here n is the number of normal vibrations of the symmetry type under discussion. It is plain then that until criteria for selecting the correct result are available, unambiguous conclusions can only be drawn when n is a small number. Here again, though, it is sometimes true that for some of the $\partial\mu/\partial S$'s all of the solutions will give nearly the same results. This arises in such cases as hydrogen vibrations when all terms but one are small.

Altogether, the problem of obtaining reliable results is a difficult one and it is hard to say how much of what has been published is reliable when all of these factors have been considered.

Bond Moments

In order to reduce the measured quantities, $\partial\mu/\partial S$, to quantities characteristic of individual bonds, it has been customary to make three further assumptions. These are: (1) When a bond is stretched by dr, a moment $(\partial\mu/\partial r)dr$ is produced in the direction of the bond. (2) When a bond is bent through an angle $d\theta$, a moment $\mu_0 d\theta$, where μ_0 is the "effective bond moment," is produced in the plane of bending and perpendicular to the direction of the bond. (3) When any one bond is bent or stretched, no moments are produced in other bonds. With these assumptions the total moment resulting from an arbitrary distortion is just the vector sum of the moments produced by each individual bond. These assumptions have been used, although often unwillingly and distrustfully, in all of the published work with which we are acquainted.

If these assumptions work they have the great virtue of reducing the data on many molecules to a common basis. If they are not only self-consistent but physically meaningful, the bond moments ought to be near to those derived from dipole moment measurements. Let us examine the results obtained using these assumptions with two questions in mind. (1) Are the results self-consistent? (2) If so, are the effective bond moments obtained equal to the static bond moments?

Results which have been obtained in compounds containing C–H, C–F, C–Cl and certain multiple bonds are listed in Tables I–IV. There is certainly a general consistency in the values given in that the variation in μ_0 and $\partial\mu/\partial r$ for any given bond type is much smaller than the differences between various kinds of bonds. Inspection of the data for C–H bonds shows that most of the values of $\partial\mu/\partial r$ are in the vicinity of 0.5 D but that there are a number of conspicuous exceptions such as C_2H_6, HCN, CH_3Cl on the high side and $CHCl_3$ on the low side. Similarly, the values of μ_0 cluster about 0.3 D with the exception of multiple bonded compounds. The value 1.0 D in HCN and C_2H_2 seems well established. Of course it is well known that there is a real variation in many of the characteristics, such as internuclear distances and force constants, of the C–H bond. The sign of $(\partial\mu/\partial r)_{CH}$ is indeterminate in all cases; that of μ_0 is indeterminate except in those cases designated by a negative sign in which it has been concluded that the H atom is at the positive end of the dipole. However, this conclusion was reached in all cases but one by assuming that Cl was at the negative end of the C–Cl

(4) The effect of higher order terms in the dipole moment expansion has been considered by B. L. Crawford and H. L. Dinsmore, *J. Chem. Phys.*, **18**, 983, 1682 (1950).

(5) D. F. Eggers, THIS JOURNAL, **59**, 1124 (1955).

dipole and it is not at all clear that this is a safe assumption. In the remaining case, HCN, it is based on the assumption that N is at the negative end of the C–N dipole but for reasons which will be elaborated later, this conclusion is not on unshakeable ground either.

TABLE I

CH BOND MOMENTS AND DERIVATIVES

Molecule	Symmetry type	μ in D	$\partial\mu/\partial r$ in D/Å.
CH_4[a]	∥ and ⊥	0.3	0.6
C_2H_6		0.3[b]	0.5[c]
		0.2 or 0.0[b,c]	1.7[c]
C_2H_4	out of plane	0.7[d]	...
	in plane ⊥ (to C=C)	0.3[d]	0.5[c]
	in plane ∥ (to C=C)	0.3[d]	0.8[c]
C_2H_2[e]	⊥	1.0	...
	∥	...	0.6
HCN[f]	⊥	−1.0	...
	∥	...	1.0
CH_3F[g]	⊥	−0.3[i]	0.8–0.4
	∥	0.4 or 0.0	2.2 or 1.4
CH_3Cl[g]	⊥	−0.4[i]	0.8–0.2
	∥	0.4 or 0.2	1.4
CH_2F_2[h]	⊥	−0.2[i]	1.0 or 0.6
	∥	−0.2[i]	0.0?
CH_2Cl_2[h]	⊥	−0.4[i]	0.0
	∥	−0.4[i]	0.5
CHF_3[h]	⊥	−0.2[i]	...
	∥	...	1.2 or 0.2
$CHCl_3$[h]	⊥	−0.3[i]	...
	∥	...	≤0.1
cis-$C_2H_2Cl_2$[i]	out of plane	−0.8[i]	...

[a] R. Rollefson and R. Havens, *Phys. Rev.*, 57, 710 (1940). [b] A. M. Thorndike, *J. Chem. Phys.*, 15, 868 (1947). [c] D. C. McKean and H. W. Thompson (unpublished work on C_2H_6 and C_2H_4). [d] B. L. Crawford (Discussion, this symposium). [e] R. L. Kelly, R. Rollefson and B. S. Schurin, *J. Chem. Phys.*, 19, 1595 (1951). [f] See ref. 10. [g] See ref. 6. [h] See ref. 7. [i] D. C. McKean (unpublished work). [j] Combined use of infrared and molecular dipole moment data.

TABLE II

VALUES OF μ AND $\partial\mu/\partial r$ IN CF AND SIMILAR BONDS

Molecule	Symmetry Type	μ in D	$\partial\mu/\partial r$ in D/Å.
CH_3F[a]	⊥	+1.5[d]	...
	∥	...	4.0
CH_2F_2[b]	⊥	+1.5[d]	−6.3
	∥	+1.5[d]	+5.0 or −2.9
CHF_3[b]	⊥	+1.5[d]	+4.3 or +5.1
	∥	+0.4 or 2.0	+11.8 or +6.6
CF_4[c]	⊥ and ∥	1.1 or 2.4	+4.8 or +3.4
SiF_4[c]	⊥ and ∥	2.3 or 3.3	−7.5 or +3.7
SF_6[c]	⊥ and ∥	2.6	3.8

[a] See ref. 6. [b] See ref. 7. [c] See ref. 8. [d] Obtained by combined use of infrared and molecular dipole moment data.

The real difficulty which shows up in Table I is the systematic disagreements in both $\partial\mu/\partial r$ and μ_0 when they are calculated from vibrations of different symmetry type in the same molecule. This may be due in part to inadequate potential functions or experimental uncertainties but this is unlikely to account for all of the cases and it appears that the phenomenon is quite genuine.

TABLE III

VALUES OF μ AND $\partial\mu/\partial r$ FOR C–Cl AND C–Br BONDS

Molecule	Symmetry type	μ in D	$\partial\mu/\partial r$ in D/Å.
CH_3Cl[a]	⊥	+1.5[e]	...
	∥	...	2.3
CH_2Cl_2[b]	⊥	+1.0[e]	−4.2
	∥	+1.0[e]	−1.6
$CHCl_3$[b]	⊥	+0.7[e]	−3.5
	∥	?	2.1 or 1.0
cis-$C_2H_2Cl_2$[c]	out of plane	+0.4[e]	...
ClCN[d]	⊥	−1.4[e]	...
	∥	...	1.6–2.1
CH_3Br[a]	⊥	+1.4[e]	...
	∥	...	1.6–2.0
BrCN[d]	⊥	−1.3[e]	...
	∥	...	0.5–0.8

[a] See ref. 6. [b] See ref. 7. [c] See Table I, ref. *i*. [d] R. W. Hendricks and D. F. Hornig (to be published). [e] Obtained by combined use of infrared and molecular dipole moments.

TABLE IV

VALUES OF μ AND $\partial\mu/\partial r$ IN SOME MULTIPLE BONDS

Molecule	Bond	μ in D	$\partial\mu/\partial r$ in D/Å.
NO[a]	NO	0.1	1.7
N_2O[b]	NO	+0.7[k,l]	6.5
	NN	+0.5[k,l]	3.3
CO[c]	CO	0.1	3.1
CO_2[d]	CO	1.1	5.4
C_3O_2[e]	CO	?	8.8
	CC	?	5.6
COS[b]	CO	?	8.5
	CS	?	5.9
CS_2[f]	CS	?	5.9
$(CN)_2$[g]	CN	?	0.7
HCN[h]	CN	+1.9[l]	0.6
CH_3CN[i]	CN	+1.8 or +1.3[l]	0.8
	C–C	*ca.* +2.0[l]	0.5
ClCN[j]	CN	+1.4	0.3–0.7
BrCN[j]	CN	+1.3	0.5–0.8

[a] S. S. Penner and D. Weber, *J. Chem. Phys.*, 21, 649 (1953). [b] H. J. Callomon, D. C. McKean and H. W. Thompson, *Proc. Roy. Soc.* (*London*), A208, 332, 341 (1951). [c] S. S. Penner and D. Weber, *J. Chem. Phys.*, 19, 807, 817, 974 (1951). [d] See D. F. Eggers, and B. L. Crawford, *ibid.*, 19, 1554 (1951). [e] R. L. Williams, *ibid.*, 22, 345 (1954). [f] D. C. McKean, H. J. Callomon and H. W. Thompson, *ibid.*, 20, 520 (1952). [g] E. R. Nixon and P. C. Cross, *ibid.*, 18, 1316 (1950). [h] See ref. 10. [i] A. V. Golton, Dissertation, Oxford, 1953. [j] See Table III, ref. *d*. [k] A. M. Thorndike, A. J. Wells and E. B. Wilson, *J. Chem. Phys.*, 15, 157 (1947). [l] Combined use of infrared and molecular dipole moment data.

The values of the bond moment derivatives, $\partial\mu/\partial r$, for both C–F and C–Cl bonds are consistently remarkably big. The values of the moments themselves are reasonable although the trend in the C–Cl moment in passing from CH_3Cl to $C_2H_2Cl_2$ is interesting. It should be noted that most of them have been calculated by combining infrared data with dipole moments, and in many cases the original work has been recalculated. This is a proper procedure because if the second assumption is valid the static moment is the μ_0 associated with the zero frequency motion, pure rotation. Any other procedure is usually inaccurate because in compounds like CH_3Cl and CH_3F the displacements of the halogen atoms are so small that the C–X moments have practically no effect on infra-

red intensities.[6] Attempts to use such devices as isotopic substitution, particularly of hydrogen by deuterium, to replace the static dipole moments are therefore likely to lead to fallacious results because of other effects such as anharmonicity of the potential function. In other molecules, such as $CHCl_3$ or CHF_3, the C–X moment could be determined from infrared intensities alone but the potential function was not sufficiently accurate.[7] However, the values derived purely from intensities in CF_4, SiF_4 and SF_6 are in reasonable agreement with the others.[8]

The most remarkable conclusion which emerges from Table III is that Cl and Br are at the positive poles of large C–X dipoles in Cl–CN and Br–CN. The trend in passing from these compounds to CH_3Cl comes largely from the variation in the staticdipole moment. There are certainly very real variations in the character of these C–X bonds, of which some other evidence is given in Tables V and VI. This suggests that in CH_3Cl the Cl is indeed negative. This is, of course, the "common sense" conclusion in the first place but it should be cautioned that Smyth[9] has already pointed out that in polyatomic molecules there is practically no correlation between electronegativity differences and bond moments. At least one of the factors which affect the polarity of bonds, the relative *size* of the two atoms, tends always to make Cl positive in a C–Cl bond.

TABLE V

INTERATOMIC DISTANCES AND FORCE CONSTANTS

Bond	Molecule	r in Å.	k in m. dynes/Å.
CH	CH_4	1.094[a] (r_0)	5.39[b] (har)[n]
	C_2H_6[b]	1.102 (r_0)	5.35 (har)[n]
	C_2H_4	1.071[a] (r_0)	6.13[c] (har)[n]
	C_2H_2	1.064[d] (r_e)	6.37[e] (har)[n]
	HCN[f]	1.066 (r_e)	6.29 (har)[n]
CCl	CH_3Cl	1.781[g] (r_0)	3.4[h]
	CH_2Cl_2	1.772[g]	3.4[h]
	$CHCl_3$	1.767[g] (r_0)	3.4[h]
	C_2Cl_4	1.72[i] (r_0)	?
	ClCN	1.629[g] (r_0)	4.9–5.2[j]
	ClC_2H	1.632[g] (r_0)	5.51[k]
CN	$(CN)_2$		17.5[a]
	HCN[f]	1.153 (r_e)	18.6 (har)
	CH_3CN	1.158[g] (r_0)	18.4[l]
	BrCN	1.159[g] (r_0)	17.0–18.2[m]
	ClCN	1.163[g] (r_0)	16.9–18.2[j]

[a] See ref. 1. [b] G. E. Handson and D. M. Dennison, *J. Chem. Phys.*, **20**, 313 (1952). [c] B. L. Crawford, J. E. Lancaster and R. G. Inskeep, *ibid.*, **21**, 678 (1953). [d] B. D. Saksena, *ibid.*, **20**, 95 (1952). [e] D. F. Eggers, ref. 5. [f] A. E. Douglas and D. Sharma, *J. Chem. Phys.*, **21**, 448 (1953). [g] W. Gordy, W. V. Smith and R. F. Trambarulo, "Microwave Spectroscopy," John Wiley and Sons, New York, N. Y., 1953. [h] J. C. Decius, *J. Chem. Phys.*, **16**, 214 (1948). [i] I. L. Karle and J. Karle, *ibid.*, **20**, 63 (1952). [j] W. S. Richardson and E. B. Wilson, *ibid.*, **18**, 155 (1950). [k] W. S. Richardson and J. H. Goldstein, *ibid.*, **18**, 1314 (1950). [l] See Table IV, ref. *i*. [m] See Table III, ref. *d*. [n] Force constants denoted (har) were obtained from harmonic frequencies.

(6) G. M. Barrow and D. C. McKean, *Proc. Roy. Soc.* (*London*), **A213**, 27 (1952).

(7) D. C. McKean and H. W. Thompson (to be published).

(8) P. N. Schatz and D. F. Hornig, *J. Chem. Phys.*, **21**, 1516 (1953).

(9) C. P. Smyth, THIS JOURNAL, **59**, 1121 (1955).

TABLE VI

QUADRUPOLE COUPLING CONSTANTS

		eqQ (mc.)
N^{14}	NH_3	− 4.10
	HCN	− 4.58
	CH_3CN	− 4.35
	ClCN	− 3.63
	BrCN	− 3.83
	NO	− 1.7
Cl^{35}	ClCN	− 83.2
	ClC_2H	− 79.7
	CH_3Cl	− 75.3
Br^{79}	BrCN	+686.1
	CH_3Br	+577.3
D^2	HD[a]	−114 ± 1 (kc.)
	DCN[a]	±145 ± 60 (kc.)
	DC_2Cl[a]	+175 ± 20 (kc.)

[a] R. L. White, *Phys. Rev.*, 94, 789 (1954). Other values are taken from ref. *g*., Table V.

Table IV is chiefly of interest in that it shows that in resonating systems the values of $\partial\mu/\partial r$ become very large. On the other hand, both μ_0 and $\partial\mu/\partial r$ appear to be reasonably consistent.

With regard to our first question, then, we are now in a position to say that using the assumptions originally outlined, the moments and derivatives obtained are consistent as far as order of magnitude is concerned. However, the variations obtained are so large that either these properties of a bond are very sensitive to small changes in the environment or the factors which were neglected make contributions which cannot be neglected in the long run.

The second question, whether "effective bond moments" from the infrared are equal to static bond moments, is hard to answer with assurance but it seems certain that in some cases, such as the C–N bond, there are real differences. One line of approach which has been attempted is to obtain purely infrared values of all of the moments so that the total moment of the molecule thus predicted can be compared with that observed experimentally. The difficulties of this approach are shown by the following example. By measuring the infrared intensities of the bending modes in HCN and DCN, $d\mu/d\theta$ was measured, where θ is the angle of bend. Since

$$\frac{d\mu}{d\theta} = \mu_{CH} \times \frac{\partial\alpha}{\partial\theta} + \mu_{CN} \times \frac{\partial\beta}{\partial\theta}$$

if α and β are the angles the two bonds make to the original axis of the molecule, one thus obtains[10]

$$0.667 = 0.848\mu_{CH} + 0.152\mu_{CN}\ (HCN)$$
$$0.456 = 0.761\mu_{CH} + 0.239\mu_{CN}\ (DCN)$$

These yield $\mu_{CH} = -1.03\ D$ and $\mu_{CN} = 1.35\ D$ so that the predicted dipole moment is only 2.38 D, compared with 2.96 D observed. The disagreement is only apparent however. The average of the values obtained from each of these equations plus the dipole moment are $\mu_{CH} = -1.18\ D$ and $\mu_{CN} = 1.78\ D$. If these are inserted into the previous equations, $(d\mu/d\theta)_{HCN} = 0.698$ and $(\alpha\mu/\alpha\theta)_{DCN} = 0.432$, so that the predicted intensities are 9% high for HCN and 13% low for DCN, neither of them outside the possible experimental error. Hence no

(10) G. E. Hyde and D. F. Hornig, *J. Chem. Phys.*, **20**, 647 (1952).

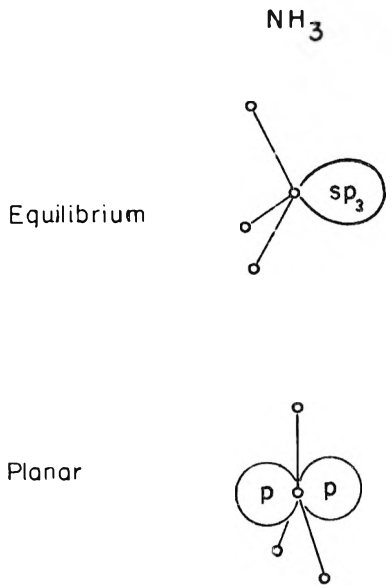

Fig. 2.—Orbitals for unshared pair electrons in NH_3.

decision is possible although disagreement is suggested. The point involved here is that the C–N bond moves so little that the infrared intensity is quite insensitive to its moment. A similar situation arises in many other molecules.

Most of the values of μ_0 in the tables were derived with the use of the dipole moment so they are necessarily in agreement. Either value for μ_0 in CF_4 is reasonably close to those of CH_3F, CH_2F_2 and CHF_3 but not coincident. However, the infrared value of μ_0 in CO_2, 1.1 *D*, is much smaller than the usual bond moment of CO in ketones, 2.3 *D*.[9] Similarly, the infrared value of 1.5–1.8 *D* for C–N is well out of line with the value 3.5 *D*[9] which is usually considered the bond moment. The infrared value is quite difficult to reconcile with a dipole moment of 3.96 *D* in CH_3CN, 3.6 *D* in cyanoacetylene or 3.9 *D* in vinyl cyanide, particularly since in the last case it has been shown that the molecular moment is parallel to the C–N axis, ruling out any substantial induced moment in the C=C linkage.[11]

It appears probable then that the "effective bond moments" obtained with the assumption of independent bond dipoles are not the same physical quantities as the static bond dipole moments.

The over-all situation is therefore inconclusive. The tables are fairly consistent; however, some of this consistency is certainly obtained because when multiple solutions are available, consistency with other molecules is used as a basis for selection. Furthermore, there are internal inconsistencies within molecules. Finally, there is inconsistency with dipole moment evidence. On balance, it seems, then, that not only the accuracy but the meaningfulness of the numbers derived with the usual assumptions is open to serious question.

The Question of Unshared Pairs

It is quite generally realized that one of the hazards in the usual assumptions is that when a given bond is distorted electrons may be redistributed in other parts of the molecule. This question becomes most serious when unshared pairs are involved.

They are included with the bond moments in static measurements. If the assumptions of the previous section are correct they are also included with the bond moments in the infrared measurements, with the additional assumption that the direction and magnitude of their moment does not change relative to that of the bond when it is distorted. If a typical case, NH_3, is considered, it seems most unlikely that this is even approximately correct. This can be seen from Fig. 2. In the equilibrium configuration the unshared pair contributes a substantial part of the total dipole moment of NH_3, 1.47 *D*. Absolute calculations have not been made but in H_2O Pople[12] has calculated a moment of 1.67 *D* for the oxygen pairs. If the NH_3 is deformed into the symmetrical planar configuration, this moment vanishes. It may therefore be expected to make a substantial contribution to the change of moment in the symmetrical bending vibration On the other hand, symmetry considerations require that there be no change in the unshared pair moment during the perpendicular bending vibration. Consequently, if the unshared pair contribution is important the apparent bond moment should differ in the two vibrations which are illustrated in Fig. 3.

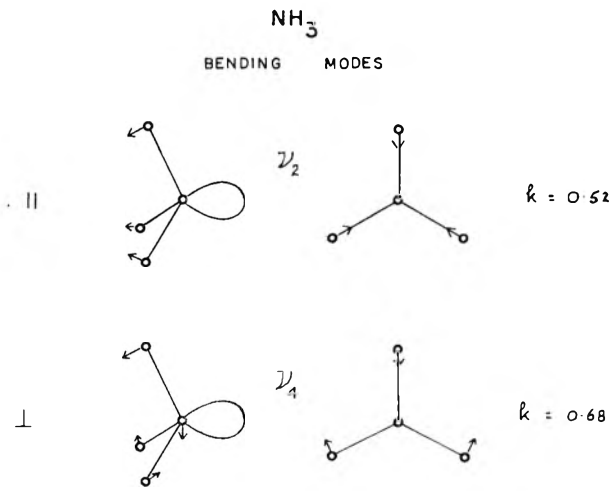

Fig. 3.—Bending vibrations and force constants in NH_3 (k in units 10^{11} ergs/radian^2).

With this in mind, one of us (D.C.M.) has measured the infrared intensities of the bending modes in NH_3. The results obtained for the apparent moments is that in the parallel bending vibration $\mu_{NH} = 0.92$ *D* while in the perpendicular vibration $\mu_{NH} = 0.68$ *D* (H^+) or 0.13 *D*(H^-). The two choices in the perpendicular case depend on whether the *z* component of the N–H bond moment is parallel or opposed to the molecular moment. The value 0.68 *D* (H^+) corresponds to an unshared pair moment of 0.70 *D* while the second corresponds to 1.62 *D*. A clear-cut decision is not possible but in the light of Pople's calculation the second (H^-) seems preferable, although shocking. In either case, there is a clear difference between the values ob-

(11) W. S. Wilcox, J. H. Goldstein and J. W. Simmons, *J. Chem. Phys.*, **22**, 516 (1954).

(12) J. A. Pople, *ibid.*, **21**, 2234 (1953).

tained from the two modes and in addition the value obtained from the parallel vibration is in definite conflict with the dipole moment of the molecule.

It is possible to understand this situation, however. Schatz[13] has derived an expression for the contribution of the unshared pair, utilizing the orbital following concept which has previously been applied to molecular force fields.[14] Assuming that the N orbitals are directed toward the hydrogen atoms throughout the vibration but that μ_{NH} is substantially constant (that is, that the effect of the change in hybridization appears only in the variation of the unshared pair moment) he obtained

$$\frac{\partial \mu_z}{\partial S_2} = \frac{1}{\sqrt{3}}(2.55\mu_{NH} - 12.18M_{sp}) =$$

$$\pm 1.36 \text{ (from infrared intensity)}$$

where $S_2 = 1/\sqrt{3}(\Delta\alpha_1 + \Delta\alpha_2 + \Delta\alpha_3)$ is the symmetry coördinate, α being the H–N–H angle, and

$$M_{sp} = e \int \psi_s z \psi_{p_z} \, d\upsilon$$

In this same notation the unshared pair moment is

$$\mu_{up} = 9.017M_{sp}$$

and the molecular moment.

$$\mu_{NH_3} = (9.017M_{sp} - 1.125\mu_{NH}) = \pm 1.47 \; D$$

These equations lead to the result $\mu_{NH} = 0.36$ D (H^+) and $\mu_{up} = 1.06$ D. The value for the unshared pair moment is quite reasonable. The value of μ_{NH} is decidedly lower than that obtained from the perpendicular mode and there are several possible explanations. For one thing, orbital following is not possible in the perpendicular mode so the effective moment may really be different. On the other hand, following is probably incomplete in the parallel mode. If the degree of following is 75%, $\mu_{up} = 0.70$ D and $\mu_{NH} = 0.68$ D is obtained, in exact agreement with the values from the perpendicular vibration. The other possibility ($\mu_{NH} = 0.13$ D, H^-) is inconsistent with any degree of following. At this stage it can only be said that by separating the effect of the unshared pair the inconsistencies in the various measurements can be eliminated and a reasonable moment for the unshared pair obtained.

The X–CN molecules are another class in which the explicit introduction of the unshared pair drastically alters the interpretation. If the bending motion of HCN, for example, is considered, two extremes of what may happen are easily visualized. The positions of the orbitals in each are illustrated in Fig. 4. Here the σ-orbitals are omitted from the triple bond for clarity. In the first case, the proton and its electron are displaced but the lone pair retains its equilibrium relation to the C–N group. This corresponds roughly to the model implied by the usual bond moment interpretation. However, in this model the overlap in the C–H bond is reduced and repulsive overlap between the hydrogen and π-orbitals is introduced. The resulting strain can be relieved very simply by a p_x, p_z rehybridization which is actually a simple rotation of the orbitals about the C and N atoms. The extreme case of this type of following is also shown in Fig. 4. The truth is certainly between these extremes since when the orbitals rotate, the overlap in the σ-bond is reduced. In the extreme of complete following it is interesting to observe that the unshared pair moment would appear, not as a part of the C–N moment as in the static case, but as a part of the C–H moment. We suggest that this is the origin of the previously mentioned discrepancy in the C–N moment. If the unshared pair moment in HCN is the same as in NH_3 (1.1 D) (the similarity in the quadrupole coupling constant shows that the electron distribution about the nitrogen is not much different), and the orbital following were complete in the sense of Fig. 4, the moments in HCN would be

$$\mu_{CH} = 0.08 \; D \; (H^+)$$
$$\mu_{CN} = 1.78 \; D$$
$$\mu_{up} = 1.1 \; D$$

Since the degree of following and the unshared pair moment are not known, these figures are speculative but it seems certain that the common assumption that an acetylenic C–H bond has a moment of about 1.0 D is completely unfounded.

These notions can be tested on acetylene. Acetylene has the two bending modes shown schematically in Fig. 5. The dotted lines represent the π-orbitals. In the infrared inactive mode the orbitals behave as in the HCN bending modes; in the active mode the π-orbitals are pushed together, in the inactive they remain parallel. If the previous arguments are qualitatively correct the energy required for the distortion in the active mode should be much greater than for the other; in fact, it is about twice as great as shown by the symmetry force constants for the two modes.[15] Hence it appears that the force constant is determined to a considerable extent by the degree to which the π-electron system can follow the rotation of the end atom.

The interesting and important question which now arises is this: if a considerable part of the apparent C–H moment in HCN is really the moment of the unshared pair, why is the apparent C≡H moment in HC≡CH so nearly the same when it has no unshared pair. One answer may be that according to the model just explored (Fig. 4), if the orbitals follow the hydrogen atoms, the σ-orbital in the triple bond is bent and the σ-orbital from each carbon atom plays the same role as the unshared pair in HCN, contributing a moment perpendicular to the C≡C axis when the hydrogens are displaced.[16]

An extension of this argument to the cases of ethylene and ethane would predict that the effective CH moments obtained in the boat type skeletal bending modes for these molecules would be

(13) P. N. Schatz, private communication.

(14) J. W. Linnett and D. F. Heath, *Trans. Faraday Soc.*, **44**, 561, 878, 884 (1948).

(15) Proton–proton repulsion can give rise to maximum force constants of 0.07 and 0.19 m. dynes/Å. in the g and μ modes, respectively. The experimental values are 0.15 and 0.33 m dynes/Å.

(16) Since the charge distribution in a bonded orbital differs very little from that of a non-bonded orbital, the moment of the σ-orbital from each carbon should be somewhat greater than one half that of the unshared pair in HCN, there being but one electron per C–H in the bonding orbital, but two in the unshared pair; the effective nuclear charge is probably greater for the pair, reducing its relative moment somewhat.

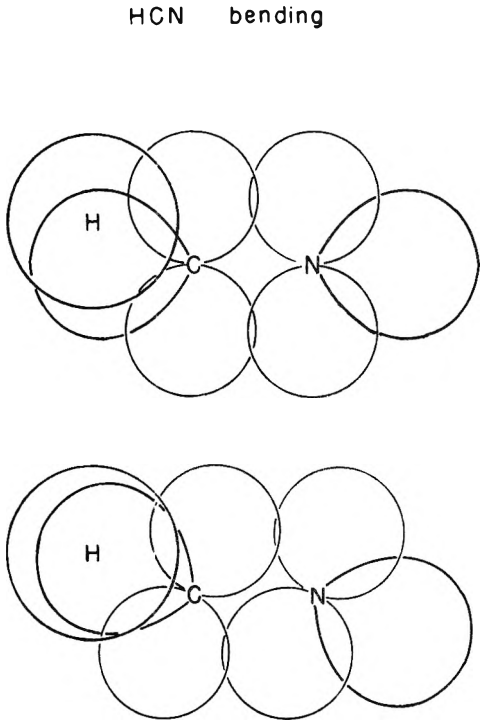

Fig. 4.—Possible orbital movements during the bending vibration of HCN.

rather different from those measured in the CH_2 or CH_3 deformation vibrations, which are symmetrical with respect to the carbon-carbon axes. The rotating σ-orbitals here would be of the sp_2 or sp_3 type. This effect, however, apparently does not exist. Only one value of μ_{CH} is found which differs greatly from about 0.3 D in C_2H_6 or C_2H_4 and this is derived from the out-of-plane bending vibration of C_2H_4, where it is 0.7 D. This vibration is one in which the hydrogen atoms move in the plane of the electrons in the double bond and is the one most nearly comparable with the acetylene bending motion. While it seems likely, therefore, that the high values of μ_{CH} in acetylene and ethylene arise at least partly from a displacement of charge in the triple or double bond, whether this is to be described by an orbital-rotation model or by some other possibility, such as a rehybridization of the carbon σ orbitals is not yet clear. We may conclude in any case that there is as yet no solid evidence for a systematic variation in the "free" CH moment along the series

$$\equiv C-H \qquad \begin{matrix} \diagdown \\ =C-H \\ \diagup \end{matrix} \text{ and } \qquad \begin{matrix} \diagdown \\ -C-H \\ \diagup \end{matrix}$$

This line of reasoning can be extended to many other substances but until quantitative quantum mechanical calculations have been made it is premature to do so.

Conclusions

In the light of these considerations a series of conclusions emerges.

1. In reducing infrared intensity measurements to molecular parameters the sensitivity of the result to uncertainties in the potential function must be explored if the reliability of the resulting moments and derivatives is to be known.

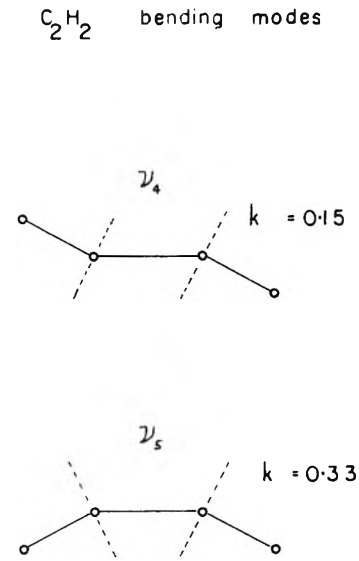

Fig. 5.—Orbital movements and force constants in bending vibrations of C_2H_2 (k in units 10^{11} ergs/radian^2).

2. At the present time the consistencies in the reported moments are so tenuous that choices among alternative solutions should not be made on consistency grounds unless really unreasonable alternatives are involved.

3. It appears that the independent, rigid-bond

TABLE VII

DIPOLE MOMENTS (IN D)

HCN[a]	3.00	HC_2H	0	NH_3[a]	1.47
ClCN[a]	2.80	ClC_2H[a]	0.44	PH_3[a]	0.55
BrCN[c]	2.93	BrC_2H[b]	0.0		
CH_3CN[a]	3.95	CH_3C_2H[a]	0.75	N_2O[a]	0.166
HC_2CN[a]	3.60				
$H_2C{:}CHCN$[d]	3.83				
CH_3Cl[a]	1.87	CH_3F[a]	1.79	CH_3Br[a]	1.80
CH_2Cl_2[a]	1.62	CH_2F_2[a]	1.93	CH_2Br_2[b]	1.43
$CHCl_3$[b]	1.01	CHF_3[a]	1.645		
cis-$C_2H_2Cl_2$[b]	1.90				

[a] See ref. *g* Table V. [b] A. A. Maryott and F. Buckley, U. S. National Bureau of Standards Circular 537, U. S. Government Printing Office, Washington, D. C., 1953. [c] L. G. Wesson "Tables of Electric Dipole Moments," Laboratory of Insulation Research, Massachusetts Institute of Technology, 1947. [d] See ref. 11.

TABLE VIII

SYMMETRY FORCE CONSTANTS FOR SKELETAL BENDING VIBRATIONS ANALOGOUS TO THOSE FOR ACETYLENE

Units: 10^{11} ergs/radian^2

Molecule	Chair-like mode	Boat-like mode
C_2H_2[a]	0.15 π_g	0.33 π_u
C_2N_2[a]	.33 π_g	.26 π_u
C_2H_4[f] (in plane)[b]	.65 B_{1g}	.80 B_{2u}
(out of plane)[c]	.20 B_{2g}	.26 B_{1u}
C_2F_4[d,f] (out of plane)[e]	.20 B_{2g}	.45 B_{1u}
C_2Cl_2[e,f] (out of plane)[c]	.27 B_{2g}	.45 B_{1u}

[a] See ref. 1. [b] See ref. *c*, Table V. [c] R. L. Arnett and B. L. Crawford, *J. Chem. Phys.*, **18**, 118 (1950). [d] Calculated from data of J. R. Nielson, H. H. Claassen and D. C. Smith, *ibid.*, **18**, 812 (1950). [e] Calculated from data of H. J. Bernstein, *ibid.*, **18**, 478 (1950). [f] Symmetry coordinates are those of J. E. Kilpatrick and K. S. Pitzer, *J. Research Natl. Bur. Standards*, **38**, 191 (1947).

model of the molecule is on such insecure ground that results reported in terms of $\partial\mu/\partial r$ and μ_0 may not only be in error but in some cases may be quite meaningless.

4. Therefore, the most important form in which to report conclusions is the rate of change of dipole moment with distortions of given symmetry, *i.e.*, $\partial\mu/\partial S$.

5. In molecules containing unshared electron pairs, their contribution may be so great that their effect must be taken into account explicitly.

6. Since unshared pairs affect infrared intensities and equilibrium dipole moments differently, they must be considered when making a comparison.

7. Bond moments obtained from some motions, such as rocking motions, may reflect a considerable effect of electronic displacement. Other motions, such as the perpendicular distortion of a methyl group, may yield reasonably reliable bond moments.

8. Because of the sensitivity to electron structure, the measurement of infrared intensities should be a powerful tool in understanding the electronic structure of molecules and the effect of deformation on that structure.

STUDIES ON THE CRYSTAL GROWTH OF SOLUBLE METAL SALTS: PART I. THE EFFECT OF "PROTECTING AGENTS" ON THE INTERFACE REACTION

BY A. PACKTER*

F. W. Berk & Co., London Colney, Herts, England

Received January 19, 1955

The effects of chelating organic acids, polyelectrolytes and long-chain surface active agents have been studied on the crystal growth of crystals of typical soluble, silver, copper, lead and aluminum salts. The final crystal weight increases exponentially with the concentration of protecting agent, according to the relation obtained in a previous work for systems of insoluble metal salts. The experimental results demonstrate that the rate of formation of nuclei by aggregation and their growth to form crystals may be markedly reduced by adsorption of single molecules of the "protecting agent."

Introduction

Traces of impurities may cause marked modifications in the growth and habit of both insoluble and soluble metal salts. Early investigators of this phenomenon studied the effect of dyes and metal chlorides on the growth habits of the silver halides,[1] ammonium chloride[2] and alum[3]; while more recently, Bunn[4] has examined the adsorption of dyestuffs on lead nitrate. Strong adsorption occurs on certain crystal faces only, and their rate of growth is markedly reduced. The growth of sodium chloride crystals, also, is modified by small additions of polyvalent metal ions; and similar effects have been observed with other strongly ionized salts, that may form complexes with the additive.[5]

Neuhaus[6] systematically investigated the oriented overgrowth of a large variety of organic "guest" substances on such inorganic "host" crystals as the alkali halides, calcium fluoride and zinc sulfide, and demonstrated that an oriented association of the two lattices occurred, caused by polar forces. The nuclei of the guest crystal must possess at least one plane with similar parameters to those of the host. Generally, modifications in crystal habit have been studied in detail, but few quantitative data have been presented for the changes in the rate of crystal growth brought about by the additive.

The author[7,8] recently has investigated the effects of chelating organic acids, polyelectrolytes, etc., on the rate of growth of insoluble metal salts from their peptized sols, and has shown that, as previously demonstrated by v. Weimarn,[9] there is no change in the mechanism of crystal growth, as the solubility product approaches that of the "soluble" salts. Crystal growth in such systems follows an oriented aggregation of coagulated micelles; the final crystal size depends on the rate of coagulation, which in turn is determined by the adsorption of the peptizing agent onto the surface of the sol micelle.

The present work extends the above studies to soluble metal salts; the effects of chelating organic acids, polyelectrolytes, and long-chain surface active agents have been studied on the growth of crystals of typical silver, copper, lead and aluminum salts. (Such "protecting agents" may withdraw the metal cation from solution, and increase the degree of "supersaturation,"[10-12] and it is to be expected that their addition to solutions containing such ions would cause a reduction in the rate of crystal growth (*cf.* 13).

Determination of growth rates at the crystal face is a most complicated problem but by introducing several simplifying assumptions, these rates may be approximately estimated from the reciprocal of the final average crystal weight. This latter in-

* Glaxo Laboratories, Ltd., Greenford, Middlesex, England.

(1) W. Reinders, *Z. physik. Chem.*, **77**, 677 (1911).
(2) J. Gaubert, *Chem. Revs.*, **157**, 1537 (1913).
(3) W. Keen and R. R. France, *J. Amer. Ceram. Soc.*, **10**, 821 (1927).
(4) C. W. Bunn, *Proc. Roy. Soc. (London)*, **A141**, 567 (1930).
(5) C. W. Bunn and R. Emmett, *Disc. Faraday Soc.*, **5**, 119 (1949).
(6) K. Neuhaus, *Z. physik. Chem.*, **A191**, 359 (1943); **A192**, 309 (1943).
(7) A. Packter and R. Matalon, *Disc. Faraday Soc.*, in press.
(8) A. Packter, 1955, unpublished.
(9) P. P. v. Weimarn, *Chem. Revs.*, 2, 1 (1926).
(10) C. B. Monk, *Trans. Faraday Soc.*, **47**, 285 (1951).
(11) A. Van Hook, THIS JOURNAL, **45**, 422 (1941).
(12) R. C. Warner and I. Weber, *J. Am. Chem. Soc.*, **75**, 5086 (1953).

creases exponentially with concentration of protecting agent; but at high concentrations the rate of growth is so retarded that the crystal size (even after 100 hours of growth) again decreases. Certain reagents may also completely inhibit the growth of a particular face, and modify the crystal habit. The experimental results demonstrate that the rate of formation of nuclei and their growth to form crystals may be markedly reduced by adsorption of single molecules of the protecting agent, which modify the whole process of aggregation and deposition involved in crystal growth.

Experimental

The rate of crystal growth from supersaturated solution depends on two main factors, the rate of transfer of solute from the bulk of the system to the environment of the growing nucleus or crystal, and the rate of deposition of material from this region onto the faces of the growing crystal. In the first part of this work, we have kept the viscosity of the systems under examination constant at 1.00–1.05 centipoise; and under these conditions, the rate of crystal growth is mainly determined by the second interface reaction.

The effects of additives on this reaction have been studied.

Materials.—Metal salts, organic acids and salts were Analar reagents. Gelatine, agar and surface active reagents were commercial products of at least 90% purity.

Technique.—Five ml. of the solution of protecting agent is added to 20 ml. of the saturated metal salt solution contained in a covered Petri dish; both solutions have been filtered free of dust particles through Whatman's Number 4 filter paper, and their temperature raised to 95°. The dish is immersed in a water-bath held at 20.0°. The solution cools from 95 to 20° in ten minutes, and is kept at this temperature for 100 hours without stirring.

The crop of crystals is washed free of mother liquor with cold distilled water, dried in warm air at 40°, and examined for weight and size. In those cases where a large number of small crystals have grown, a random batch of fifty is taken for study.

Crystal dimensions have been measured at low magnification with a Zeiss microscope against an internal graticule; and the diameter (d) determined as that of the sphere of volume equivalent to that of the crystal under examination.

The Number of Crystals.—The number of crystals in each crop is observed; and for each concentration (C_p) of protecting agent is expressed as N_c, the number grown per liter of initially supersaturated solution.

The Final Average Crystal Weight. (1) The Arithmetical Mean Weight.—The arithmetical mean weight (m_c) in g. for any C_p value is determined as

$$m_c = M_c/N_c$$

where M_c is the total weight of crystals grown from one liter of solution.

For low values of $C_p = 0 - C_p'$, $M_c = (M_i - M_{sp})$, where M_i is the initial weight of solute and M_{sp} is the saturation solubility in distilled water at 20.0° (all M values expressed in g. per l.).

Beyond $C_p = C_p'$, the rate of growth is so slow that the mother liquor is still supersaturated after 100 hours growth; *i.e.*, $M_i - M_c > M_{sp}$. However, since growth will finally cease for all C_p values, when $M_c = M_{sp}$, m_c may be corrected for incompleteness of growth, and generally

$$(m_c)\text{cor.} = (M_i - M_{sp})/N_c$$

The arithmetical mean diameter (d_c) is also determined at each C_p value.

(2) The Mode Weight.—The mode weight (m_c) represents the weight of the type of crystal formed from those nuclei on which most growth has occurred; and corresponds to the mode on the graph of weight fraction against diameter. $\bar{m}_c$ is determined as follows: the crop is subdivided into ten groups of diameter 0–0.1, 0.1–0.2 . . . 0.9–1.0 d_m, where d_m is the diameter of the largest crystal in the crop. The weight fraction (f_n) for each group is determined as

$$f_n = m_n / \sum_{n=0}^{n=10} m_n$$

where m_n is the total weight of the nth group.

m_c is taken as the mean weight of that group for which f_n is the maximum.

The mode diameter ($\bar{d}_c$) corresponding to maximum f_n is also observed.

"Orderliness" of Growth.—The assymmetry or "skewness" of crystal weight distribution will be represented for any system by the factor

$$\Delta m = (\bar{m}_c - m_c)/m_c$$

The maximum f_n value (for subdivision into ten groups) is a measure of the "orderliness" of the crystal growth. (Very rapid growth leads to a distribution of all sizes and weights, and $f_n \rightarrow 0.10$; while very slow growth leads to formation of a few crystals of very similar size and weight, for which collection, $f_n \rightarrow 0.90$.) The "orderliness" has been further measured in terms of the standard deviation (σ_m) for the m_n values by the usual statistical methods.

Results

The effects of a series of simple organic acids, polyelectrolytes and long-chain surface active agents on the rate of crystal growth of typical soluble metal salts have been studied by following the change in final average crystal size and weight.

Generally, low concentrations of these "protecting agents" markedly reduce the rate of crystal growth, except when the metal salt cation forms an insoluble precipitate with the anion of the additive. (This leads to formation of a large number of nuclei on which rapid growth of the soluble salt occurs, and the effects of such protecting agents as the hydroxyorganic acids cannot be investigated.)

The Effect of Protecting Agents on Final Average Crystal Weight.—With increasing C_p/C_s—the protecting agent–solute concentration ratio—the average crystal weight (m_c) after 100 hours crystal growth, rises to an optimum at $C_p = C_p'$, and then falls in value as $C_p > C_p'$. The values of $(m_c)_{cor}$ however, increase continuously with C_p/C_s over the range investigated (0 to 0.3). N_c/N_0, m_c/m_0 vary with C_p/C_s according to the relation

$$-\log_{10} N_c/N_0 = \log_{10} (m_c)_{cor}/m_0 = F(C_p/C_s) \quad (1)$$

where m_c, N_c are the values of m, N at concentration C_p of protecting agent; m_0, N_0 at $C_p = 0$ (refer to Figs. 1, 2).

F is a constant for a particular metal salt, protecting agent system, and varies with the structure of the latter, and is the reciprocal of the C_p/C_s value at which $m_c/m_0 = 10$; $N_c/N_0 = 0.1$.

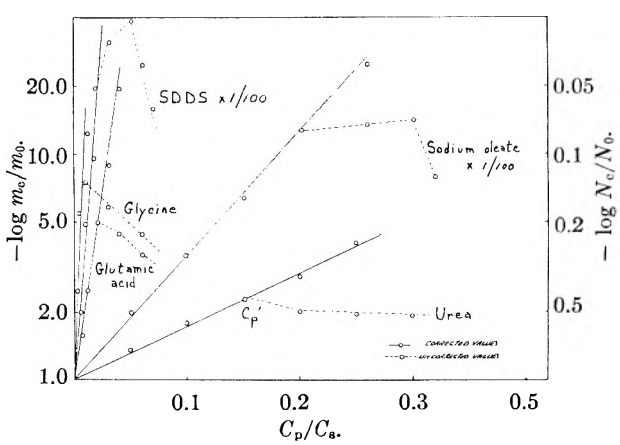

Fig. 1.—Crystal growth of copper sulfate at 20.0° (S = 2.9). Variation of average crystal weight with protecting agent–copper sulfate concentration ratio.

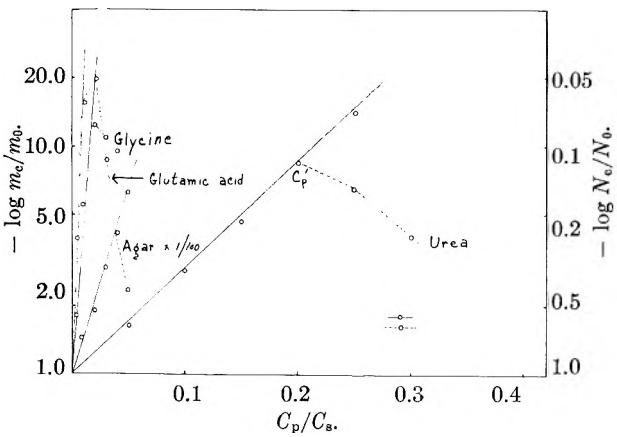

Fig. 2.—Crystal growth of lead nitrate at 20.0° (S = 1.4). Variation of average crystal weight with protecting agent–lead nitrate concentration ratio.

A similar relation has been observed between the final average weight of the crystals of insoluble metal salts, and the protecting agent–solute concentration ratio.[8]

Values of F, for the systems examined, are compared with the results for typical insoluble metal salt systems (with the same cation), at corresponding supersaturations (s), in Table I.

For a particular metal cation, the F value at corresponding supersaturation is appreciably higher for the more soluble salts.

The effects of long-chain surface active agents that may complex with the metal cation is especially marked.

"Orderliness of Growth."—In all the systems examined, the orderliness of growth increases continuously with addition of protecting agent. Values of f_n and σ_m for typical systems are presented in Table II.

TABLE I

CRYSTAL GROWTH IN THE PRESENCE OF PROTECTING AGENTS

	Values of F	
(A) Copper salts (s = 2.9)	Copper sulfate	Copper chromate
Glycine	45	12
Glutamic acid	35	10
Urea	3	< 1
Gelatine	2000[a]	15
Gluconic acid	Pptn.	20
Agar	Pptn.	3
Sodium dodecyl sulfate	3000	...
Sodium oleate	3700	...
"Cetab"	2500	...
(B) Lead salts (s = 1.4)	Lead nitrate	Lead iodide
Glycine	35	1.0
Glutamic acid	52	3.0
Urea	4	0.1
Gelatine	1200	1.0
Gluconic acid	Pptn.	3.0
Agar	2250[b]	1.0
(C) Aluminum salts (s = 8.3)	Potassium aluminum sulfate	
Sodium dodecyl sulfate	9600	
Sodium oleate	8000	
"Cetab"	6000	
(D) Silver salts (s = 1.2)	Silver nitrate	Silver oxalate
Glycine	Pptn.	< 0.1
Glutamic acid	Pptn.	2.0
Urea	10	0.1
Gelatine	1600	0.5
Gluconic acid	Pptn.	0.6
Agar	Pptn.	< 0.1
Sodium dodecyl sulfate	2400	...
Sodium oleate	2000	...
"Cetab"	Pptn.	Pptn.

[a] Calculated on the basis of an equivalent weight of 800; *i.e.*, one free glutamic acid residue per eight amino acid groups. [b] Calculated on the basis of an equivalent weight of 2000; *i.e.*, one free sulfonic acid residue per ten galactose units.

TABLE II

"ORDERLINESS OF CRYSTAL GROWTH," f_n AND σ_m VALUES (FOR SUBDIVISION INTO TEN GROUPS)

	C_p/C_s	f_n	σ_m
A. Copper Sulfate Soln.			
Glutamic acid	0	0.18	0.65
	.004	.24	.48
	.010	.31	.40
	.020	.35	.35
Sodium dodecyl sulfate	0	0.18	0.65
	.0004	.35	.49
	.0006	.61	.30
	.0008	> .90	< .10
B. Lead nitrate soln.			
Glutamic acid	0	0.13	
	.004	.25	0.62
	.010	.33	.50
	.020	.38	.47
"Agar"	0	0.13	0.62
	.002	.36	.47
	.004	.51	.36
C. Potassium aluminum sulfate soln.			
Sodium dodecyl sulfate	0	0.24	0.58
	0.00015	.35	.52
	.00031	.51	.45
	.00047	.65	.39
	.00063	.76	.32

With copper sulfate and potash alum solution sodium dodecyl sulfate may reduce the growth of all but a few nuclei to negligible proportions.

Generally, the skewness of distribution also increases with increasing C_p/C_s; $\bar{d}_c$ increases from 0.52 to 0.60 $\bar{d}_c$; while $\bar{m}_c$ increases from 1.1–1.6m_c; *i.e.*, the main growth occurs on the largest of the initially formed nuclei.

Modifications in Crystal Habit

Addition of protecting agent may not only reduce the over-all rate of growth, but may also preferentially inhibit the rate of growth of certain crystal faces, with appreciable variation in crystal habit.

Traces of long-chain anion inhibit the growth of the 100 faces of copper sulfate crystals, while low power microscopic examination indicates a step-like growth on the 111 face. A similar step-like growth is induced by such reagents on the 110 and 010 faces of alum crystals: while traces of agar

TABLE III

MODIFICATIONS IN CRYSTAL HABIT

	Copper sulfate Face			Lead nitrate Face			Potassium aluminum sulfate Face			Silver nitrate Face		
	100	110	111	001	010	110	001	010	110	001	010	110
Sod. dodecyl sulfate	0.2	4.2	4.0[a]	0.1	6.0[b]	5.0[b]	8.5	8.5[a]	8.5	0.3	1.0	2.0[b]
Sod. oleate	0.3	3.5	3.1[a]		Pptn.		7.0	7.0[a]	7.5		Pptn.	
Cetab	0.8	2.0[b]	1.0		Pptn.		3.0	3.0	3.0		Pptn.	
Gelatine		...		0.5	5.0	3.0		...		0.1	0.5	11.5[b]
Agar		Pptn.		0.4	3.5[a]	3.1[a]						

[a] Step-like growth on this face. [b] Dendritic growth in direction perpendicular to this face.

cause such effects on the 110 faces of lead nitrate crystals.

Traces of gelatine similarly reduce the growth of the 001 faces of silver nitrate crystals; while concentrations >0.001 N induce formation of thin dendritic aggregations along the axis perpendicular to the 110 face.

These modifications in crystal habit are summarized in Table III and are expressed in terms of the ratio of the crystal dimension in presence of optimum concentration (C_p') of the protecting agent for 100 hours growth to that observed in the absence of additive. (For outline of crystallography nomenclature refer to 13.)

Discussion

Two main processes determine the rate of growth of nuclei and crystals from a solution, the transfer of material from the bulk of the solution to the region of the growing nucleus (or crystal), and the deposition of solute ions onto a growing face from material in its close vicinity. In this work, the rate (k_D) of diffusion has been kept practically constant, and far higher than the rate (k_F) of deposition, and under these conditions this latter determines the reaction rate of the whole process.

We may apply a similar mathematical treatment to the systems studied, to that of van Hook,[14] who extended the Volmer theory for condensed systems to supersaturated aqueous solutions.

The number (δN) of nuclei formed in the first small time interval (δt) of cooling is expressed in the relation

$$\delta N/\delta t = \exp\left[-(\Delta A_0 + \Delta A_{visc})/kT\right] \qquad (2)$$

where $(\Delta A)_0$ is the free energy of activation involved in forming a nucleus, in the absence of protecting agent; and ΔA_{visc} is the free energy of activation of viscosity, that remains constant.

If we further assume that $(\Delta A)_c$ varies linearly with (C_p/C_s) according to a simple relation

$$(\Delta A)_c = (\Delta A)_0 + \alpha(C_p/C_s) \qquad (3)$$

then for constant δt

$$\delta N_c/\delta N_0 = \exp\left[-(\alpha/kT \times C_p/C_s)\right] \qquad (4)$$

i.e.

$$\log_{10} \delta N_c/\delta N_0 = -2.303\ \alpha/kT \times C_p/C_s = -F(C_p/C_s) \qquad (5)$$

where F varies directly with α.

According to the Berthoud–Valeton theory,[15,16] the rate of crystal growth (dc/dt) onto nuclei is given by the equation

$$k_x = dc/dt = k_F A s \qquad (6)$$

where A is the surface area and s is the supersaturation.

Crystal growth is thus a very complex process since both the surface area and the supersaturation may vary continuously throughout the whole period of growth.[17] However, the main growth may well occur on those "nuclei" of sufficiently large initial surface area that are formed during the first short period of cooling. In such systems the final average crystal weight m_c will be inversely proportional to δN_c, *i.e.*

$$-\log_{10}(\delta N_c/\delta N_0) = \log_{10} m_c/m_0 = F(C_p/C_s) \qquad (7)$$

Such a relation has indeed been verified experimentally; and the values of F, determined from the data for m_c, represents the effect of a particular protecting agent on the over-all rate of crystal growth. For it follows from equation 6 that

$$\log_{10}(k_x)c/(k_x)_0 = \log_{10}(k_F)_c/(k_F)_0 \qquad (8)$$

and if we assume that $\delta N/\delta t$ is directly related to k_F then

$$\log_{10}(k_F)_c/(k_F)_0 = -\log_{10}(\delta N_c/\delta t)/(\delta N_c/\delta t) = F(C_p/C_s) \qquad (9)$$

The experimental results thus demonstrate that very low concentrations of protecting agent (corresponding to C_p/C_s <0.05) may reduce the rate of the interface reaction, and thence that of nucleus formation (and crystal growth) to less than one-twentieth of the rate in distilled water. Two main hypotheses have been put forward to explain such latter phenomena. Christiansen[18] and Duke and Brown[19] consider that the nucleus for crystal growth is the "embryo" that consists of a small number of atoms, and that its rate of formation varies with the supersaturation according to mass-action laws; while Traube[20] and Balarev[21] have earlier demonstrated that crystal growth may well occur by aggregation of stable groups or "submicrons" formed from a large number of ions and similar to the "micelle" of an insoluble metal salt. The effects of protecting agents cannot be directly explained by application of mass-action law, since the decrease in supersaturation that results from withdrawal of such small proportions cation (by forma-

(13) C. W. Bunn, "Chemical Crystallography," Clarendon Press, London, 1945, Ch. 2.

(14) A. v. Hook and J. Bruno, *Disc. Faraday Soc.*, **5**, 112 (1949).

(15) A. Berthoud, *J. chim. phys.*, **10**, 625 (1912).

(16) R. Valeton, *Z. Kryst.*, **59**, 335 (1923).

(17) S. H. Branson, W. J. Dunning and B. Millard, *Disc. Faraday Soc.*, **5**, 83 (1949).

(18) J. A. Christiansen, *Acta Chem. Scand.*, **5**, 673 (1951).

(19) F. R. Duke and L. M. Brown, *J. Am. Chem. Soc.*, **76**, 1443 (1954).

(20) J. Traube, *Z. physik. Chem.*, **A146**, 1 (1929).

(21) D. Balarev, *Kolloid Beihefte*, **50**, 1 (1939).

tion of chelation complexes[11,12]) would only account for a fraction of the observed effects: but the results do, however, confirm the concepts of Juliard[22] that a single molecule of amino acid or hydroxy acid when complexed with a cation from such an "embryo" may completely distort and hence reduce any further growth. Alternatively, such protecting agents, when adsorbed onto the surface of a larger "micelle," reduce the process of aggregation to form crystals.[8]

Long-chain polypeptides, polysaccharides and colloidal electrolytes adsorbed or complexed through similar polar groups are especially effective; and the high F values (in Table I) demonstrate that such adsorption is very much more active in solutions of the highly soluble metal salts than on the sols of the less soluble metal salts of corresponding cation.

During the early stages of growth, the above additives may completely inhibit the formation of "embryo" or "micelle": while at a later stage they may preferentially reduce the growth of some specific crystal face. Furthermore, as might be expected from statistical considerations,[23] rapid rate of growth onto a large number of nuclei will lead to a wide distribution of crystal sizes, while addition of protecting agents which retard the rate of growth favors the "ordered" formation of a small number of larger well-formed crystals with a narrow size distribution.

Acknowledgments.—This work was carried out during a period of post-graduate research at Kings College, University of London (England). I wish to thank Prof. Sir E. K. Rideal for his helpful interest and encouragement, and my colleagues for valuable discussion.

(22) A. Juliard, *Disc. Faraday Soc.*, **5**, 191 (1949).

(23) W. H. Carothers, *Trans. Faraday Soc.*, **32**, 39 (1936).

THE MELTING POINT OF GERMANIUM AS A FUNCTION OF PRESSURE TO 180,000 ATMOSPHERES

H. TRACY HALL*

Research Laboratory, General Electric Co., Schenectady, N. Y.

Received April 28, 1955

The melting point of germanium has been found to decrease linearly with increasing pressure from 936° at one atmosphere to 347 ± 18° at 180,000 atmospheres. The linear dependence indicates that there are no new solid phases formed in the region investigated. Resistance measurements indicate that the solid remains a semi-conductor while the liquid displays metallic conduction over the entire pressure range.

Experimental Procedure

The "belt" ultra-high pressure, high temperature apparatus[1] was used to measure the melting point of germanium as a function of pressure. A graphite cylinder 0.150 inch o.d., 0.090 inch i.d. and 0.450 inch long served as container and as electrical resistance element for heating the germanium. The germanium (high purity, single crystal used in semi-conductor work) was a cylinder 0.090 inch diameter and 0.300 inch long. Graphite plugs 0.090 inch in diameter and 0.075 inch long were placed in the ends of the tube. A thermocouple (Pt–Pt 10% Rh, wire diameter 0.010 inch) imbedded in the graphite cylinder measured the temperature.

After the high pressure assembly was in place, the press load was increased to the desired pressure. The pressure calibration was made by observing transitions in bismuth, thallium, cesium and barium[2] (see Fig. 1). Then the voltage across the heating tube was raised until the germanium melted. The e.m.f. of the thermocouple (with 0° reference junction) was recorded automatically. The voltage across the heating tube and the current through it were also recorded. Each of the recorders detected the melting point of the germanium as shown in Fig. 2. When germanium melts, its electrical conductivity increases by a factor of about ten. This was ascertained from the voltage and current measurements before and after melting, the geometry of the system, and the known conductances of solid germanium and graphite near the germanium melting point. On melting, then, the electrical resistance of the germanium–graphite assembly decreases appreciably. This causes a large increase in the current through the assembly and a corresponding drop in the voltage across the sample. The final balance of current and voltage is determined by the internal impedance of the power supply. When the germanium melts, its thermal conductivity also increases considerably. This causes a larger flow of heat to pass out through the ends of the sample and supercools the molten germanium. This and possibly latent heat effects cause a sharp dip to occur in the e.m.f. curve. More power is required to raise the temperature of the assembly a given amount after the germanium has melted than when it is solid. This is again due to the greater heat loss out the ends when the germanium is molten.

On lowering the power input to the sample, the germanium would eventually freeze. The freezing point could not be detected nearly as well as the melting point. The germanium usually supercooled in a non-reproducible manner. There seemed to be no relationship between the amount of supercooling and the pressure.

Experimental Results

Six runs were made. Five of them covered the range from 1 to 100,000 atmospheres. They all showed a linear decrease in melting point with increasing pressure. The slopes obtained were -3.20, -3.18, -3.36, -3.32 and -3.33×10^{-3}°/atm. The sixth run covered the range from 1 to 180,000 atmospheres, showing also a linear decrease in melting point with a slope of -3.21×10^{-3}°/atm. Considering all slopes, the average and the standard deviation from the mean were $-(3.27 \pm 0.07) \times 10^{-3}$°/atm. Data from one of the runs are displayed in Fig. 3. The lower line is drawn through the points as they were measured. Note that the line intersects the melting point axis at 895°. This is 28° below the one atmosphere melting point of 936°.[3] The thermocouple, because of its location, was probably conducting away enough

* Brigham Young University, Provo, Utah.

(1) H. T. Hall, to be published.

(2) P. W. Bridgman, *Proc. Am. Acad. Arts & Sci.*, **81**, [4] 165 (1952).

(3) Esther Conwell, U.R.E., 1336, November, 1952.

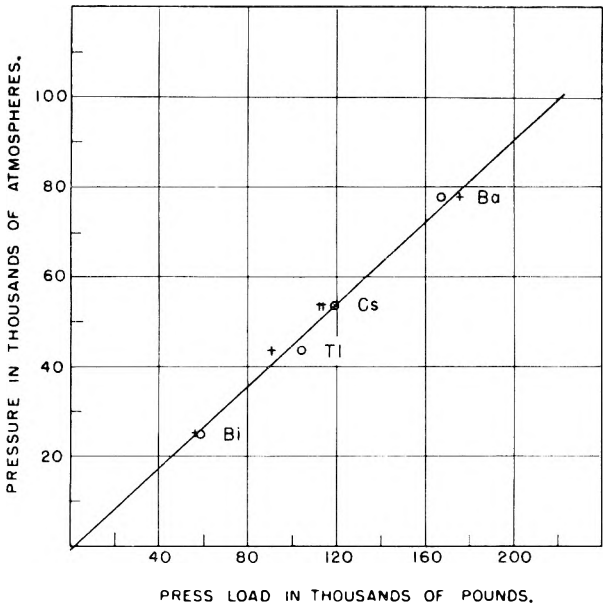

Fig. 1.—Pressure calibration of "belt" apparatus.

heat to lower the junction temperature this amount. Consequently, a corrected line (the upper line) was drawn. Its upper end was located at 936°. The position of its lower end at 180,000 atmospheres was determined by assuming the relationship

$$\frac{936 - 895°}{936 - 40°} = \frac{y}{345° + (x - 40°)}$$

where 40° was the average temperature of the sink to which heat was flowing, 345° is the lower line melting point at 180,000 atmospheres, and x is the correction to be added to this value. The other runs were corrected in like manner.

Effect of Pressure on Thermocouple E.M.F.—This is a peculiarly difficult problem and will be discussed in detail in a future paper. For the present, let it be known that the temperatures (from standard, one atmosphere e.m.f. *vs.* temperature charts) recorded by the couples, platinum–platinum 10% rhodium and chromel–alumel, have been compared at pressures to 100,000 atmospheres and simultaneous temperatures to 900°. Both couples give the same temperature within the limits of experimental reproducibility of the measurements. This reproducibility has an average deviation from the mean temperature of ±3° at 900° (the deviation is smaller at lower temperatures). This means that the effect of pressure on the e.m.f. of these couples is negligible within the limits of the experimental error or that the pressure affects both couples in an identical manner. The latter seems improbable; so the assumption has been made that the e.m.f.'s of these couples are not affected by more than the equivalent of 3° by the pressures and temperatures used in the germanium melting point experiments.

Discussion

Sulman and VanWinkle[4] by application of the Clapeyron–Clausius equation have calculated $dT/dp = -2.4 \times 10^{-3}$ degree/kg./cm.^{2} for the melting

(4) R. G. Sulman and D. M. VanWinkle, *J. Appl. Phys.*, **24**, 224 (1953).

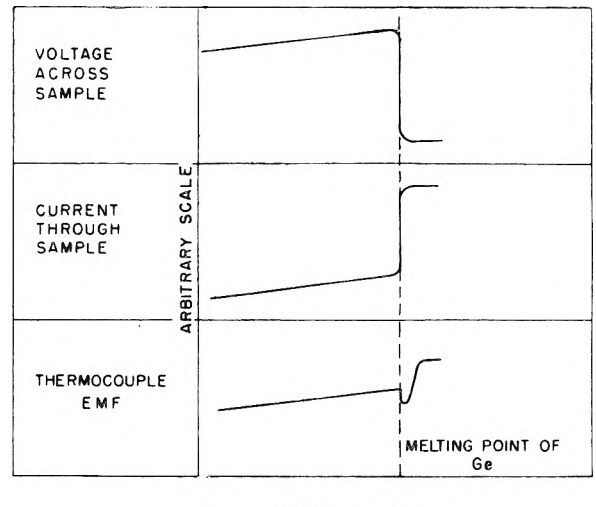

Fig. 2.

point of germanium. They used 935° as the melting point, 5% for the volume change on melting, and 110 cal./g. as the latent heat of fusion. The source of their data is not given. The 5% volume change is probably an estimate and if changed to 6.7% would bring their calculation into line with the results of this work.

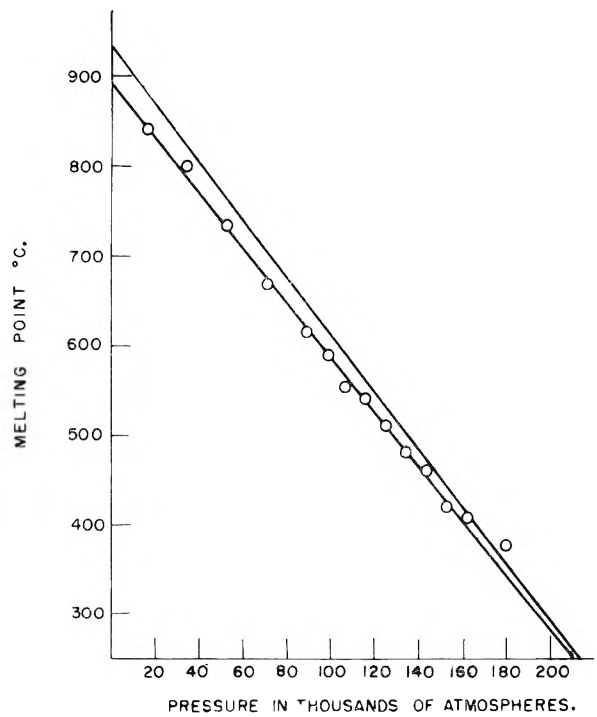

Fig. 3.—Sample of melting point data lower line, as obtained upper line, corrected.

The linear dependence of melting point on pressure up to 180,000 atmospheres indicates that no new solid phases are formed, and that the liquid remains the denser phase at this extreme pressure. The electrical resistance (from the current and voltage measurements on the sample) indicated that over the entire pressure range the conductance of the molten germanium is greater than that of the solid germanium. This means that the solid re-

mains a semi-conductor while the liquid displays metallic conduction even at these extreme pressures.

The germanium melting curve does not give the usual "concave downward" curvature found by Bridgman for many substances.[5]

The determination of the melting point of germanium in a high pressure, high temperature apparatus can be used as a secondary pressure standard. In designing new equipment, the problem of determining its ultimate capabilities is always encountered. The measurement of the germanium melting point as a function of applied load will give this information. When the pressure limit of an experimental design is approached, the melting point will cease to fall with increasing press load. At lower pressures, the change in electrical resistance of a manganin wire has been used for this purpose.[6] However, mechanical deformation of the wire in the necessarily solid pressure transmitting media at the very high pressures used here causes the gage to give uncertain results. The germanium melting point, being a discontinuous phenomenon, is independent of change in shape brought about by application of pressure.

(5) P. W. Bridgman, "The Physics of High Pressure," G. Bell and Sons, London 1949, see Chapter VII.

(6) See reference 4, Chapter III.

Conclusion

The melting point of germanium has been measured as a function of pressure up to 180,000 atmospheres. The melting point decreases linearly from 936° at one atmosphere with a slope of $-(3.27 \pm 0.07) \times 10^{-3}$°/atm. As far as is known, this represents the most extreme condition of simultaneous high pressure, high temperature under which a measurement of this nature has been made. An extension of the techniques employed here to measure the melting points of other materials should eventually shed light on the old question as to the eventual character of the melting curve as pressure is indefinitely increased. Does it end in a critical point, rise to a maximum, or behave otherwise?

KINETICS OF THE OXIDATION OF PYROLYTIC CARBON[1]

By Mei Chio Chen, Carl J. Christensen and Henry Eyring

Department of Chemistry, University of Utah, Salt Lake City, Utah

Received May 2, 1955

A method for determining the kinetics of carbon oxidation by measuring the rate of decrease in the electrical conductivity of the carbon in film form is elucidated. This method is applied to films of pure pyrolytic carbon and a rate equation is determined. An activation energy of 21 kcal. and an activation entropy of −28 e.u. are found to apply to the oxidation of this particular carbon when oxidized at temperatures up to 550°. The oxidation rate is found to be first order with respect to oxygen pressure.

Introduction

A pure pyrolytic carbon film[2] can be uniformly deposited on a ceramic base[3] to give an electrical resistor,[4] the conductance values of which can readily be measured.

Carbon produced in this manner is pure with the exception of a fraction of a per cent. of hydrogen.[5] The structure of such films has been examined[6] and found to consist of "pseudo-crystals, each made up of 3 or 4 parallel and uniformly spaced, but otherwise randomly disposed, atomic planes in each of which the carbon atoms are hexagonally arranged as in graphite." The crystals are small, 10 to 50 ångströms in each dimension, and tend to be oriented with their planes parallel to the supporting surface.

The conductivity of a carbon film decreases with oxidation of the film. It is the purpose of this study to show that this phenomenon can be used to determine the kinetics of carbon oxidation at low temperatures, and by this method to determine the kinetics of oxidation of pure pyrolytic carbon at temperatures up to 550°.

(1) This study was supported by the U. S. Air Force through the Office of Scientific Research of Air Research and Development Command.

(2) K. A. Hofmann and C. Rochling, *Ber.*, **66**, 2071 (1923).

(3) M. D. Rigternik, *Ceramic Age*, **63**, 10 (1954).

(4) C. J. Christensen, U. S. Patent No. 2,161,950 (June 13, 1939); U. S. Patent No. 2,285,017 (June 2, 1942); U. S. Patent No. 2,328,422 (Aug. 31, 1943); R. O. Grisdale, A. C. Pfister and W. Van Roosbroeck, *Bell System Tech. J.*, **30**, 271 (1951).

(5) R. Iley and H. L. Riley, *J. Chem. Soc.*, 1362 (1948).

(6) A. H. White and L. Germer, *J. Chem. Phys.*, **9**, 492 (1941).

Experimental Method

The carbon films used in this study were of the order of 2×10^{-4} cm. thick[4] and were deposited on a solid ceramic cylinder[3] 2 inches long by $^{7}/_{32}$ inches in diameter and had an approximate initial resistance of 10 ohms end to end of the cylinder. Electrode terminations were applied over about $^{1}/_{4}$ inch of each end of the cylinder so that the carbon tube contributing to the resistance was approximately 1.5 inches long. The terminations were applied in three ways: (1) a heavy graphite layer was produced by painting an aquadag paste followed by heating in a reducing atmosphere to volatilize the liquids from the paste and compact the graphite flakes; (2) a layer of gold was produced from "liquid bright gold" (Hanovia, Grade N) by firing in a neutral nitrogen atmosphere; (3) a silver paste layer was produced from du Pont Silver Paste No. 4545 and firing in a neutral atmosphere at 600°. In each case care was taken to properly mature the electrode by heating so that it was adherent and clean and the carbon layer was undamaged.

Oxidation studies on samples with these three terminations showed no differences. Since one termination was substantially pure graphite, which would not be expected to affect the oxidation reaction, it was concluded that each of these terminations is without effect. Since the silver paste termination is the easiest to apply, and in other ways is superior, it was used as the standard termination for specimens in this study.

The surface of a deposited carbon film is roughened by a given burning condition until a steady state roughness is reached. Beyond this the thickness of the film decreases at a uniform rate which is characteristic of the condition under which the burning takes place.

The electrical conductance (C) of such a film can be considered to be made up of two parts: the conductance of the rough surface layer (C_s), and the conductance of the film inside this roughened surface layer (C_f). Accordingly

$$C = C_s + C_f \quad (1)$$

After the steady-state roughness is reached C_s is constant. For a given burning condition the decrease in carbon film conductance, C, is linear with time, t. Accordingly

$$C = C_0 + mt \quad (2)$$

where C_0 is the conductance value at the beginning of a run where the steady-state roughness of the film has been established. The value of m for each experimental condition is obtained from the plot of C *vs.* t.

The conductance of the film was measured by the potentiometer method with current through the resistor being held at such low values as to avoid heating the carbon film due to the passage of current. An unsteady ammeter was evidence of poor contacts between the carbon film and the electrodes at the ends of the film. When such a condition developed the data were not used in our considerations.

The oxidation took place in a cylindrical tube furnace controlled to ±1°. The carbon film resistor was positioned along the axis of the furnace. The furnace was so constructed as to give a zone of substantially uniform heat for a length of 8 inches.

The oxidizing gas was oxygen with nitrogen diluent, dried over magnesium perchlorate and passed through "ascarite" to remove carbon dioxide. These gases were mixed in the ratios desired and fed to the furnace at the desired velocity by means of small sensitive flowmeters.

Experimental Procedure.—The carbon resistors were carefully cleaned with distilled water, absolute alcohol and carbon tetrachloride, in that order. They were then placed in position at the center of the furnace and the furnace protected from oxidation by a flow of oxygen-free nitrogen. After the furnace had reached the desired temperature and a steady state had been achieved the oxidizing gas was turned on and the conductance followed over a period of 10 to 20 minutes. In no case was a substantial portion of the carbon film burned away. Accordingly, equations 1 and 2 would apply.

Theoretical Considerations

The electrical conductance of the carbon film is given by equation 1. The value of C_f can be written as

$$C_f = \frac{\pi D\tau}{\rho L} \quad (3)$$

where D is the diameter of the film tube, τ is the film thickness, L is the length of the film tube and ρ is the specific electrical resistivity of the carbon making up the film.

From equations 1 and 3

$$\frac{dc}{dt} = \frac{\pi D}{\rho L}\frac{d\tau}{dt} \quad (4)$$

where $-d\tau/dt$ is the rate of thinning of the carbon tube due to oxidation. This can also be written

$$-\frac{d\tau}{dt} = \delta k' p \quad (5)$$

where δ is the thickness of an atomic layer of carbon, k' is the rate of removal by oxidation of an atomic layer, and p is the oxygen pressure in the ambient gaseous atmosphere. This expresses the assumption that the reaction is first order with respect to oxygen pressure.

Substituting the usual expression[7] for k' in equation 5 we obtain

$$-\frac{d\tau}{dt} = \delta p\kappa \frac{kT}{h}\exp\left(\frac{\Delta S^{\pm}}{R}\right)\exp\left(-\frac{\Delta H^{\pm}}{RT}\right) \quad (6)$$

(7) S. Glasstone, K. Laidler and H. Eyring, "The Theory of Rate Processes," McGraw-Hill Book Co., New York, N. Y., 1941, p. 14.

From equations 4 and 6

$$-\frac{dc}{dt} = \frac{\pi D}{\rho L} \times \delta p\kappa \frac{kT}{h}\exp\left(\frac{\Delta S^{\pm}}{R}\right)\exp\left(-\frac{\Delta H^{\pm}}{RT}\right) \quad (7)$$

To make equation 7 dimensionally correct p must be a dimensionless number. Accordingly, p is a ratio of the oxygen pressure used to that at an arbitrarily chosen standard state, which standard state we take to be 1 atmosphere (760 mm. pressure). If some other standard state is chosen the value of $\Delta S^{\pm}$ will be altered to conform.

From equation 2

$$\frac{dc}{dt} = -m$$

With equation 7 this becomes

$$m = \frac{\pi D}{\rho L} \times \delta p\kappa \frac{kT}{h}\exp\left(\frac{\Delta S^{\pm}}{R}\right)\exp\left(-\frac{\Delta H^{\pm}}{RT}\right) \quad (8)$$

This becomes

$$\frac{m}{pT} = \frac{\pi D}{\rho L}\delta\kappa\frac{k}{h}\exp\left(\frac{\Delta S^{\pm}}{R}\right)\exp\left(-\frac{\Delta H^{\pm}}{RT}\right) \quad (9)$$

In logarithmic form

$$\log\left(\frac{m}{pT}\right) = \log\left[\frac{\pi D}{\rho L}\delta\kappa\frac{k}{h}\left(\exp\frac{\Delta S^{\pm}}{R}\right)\right] - 0.4343\left(\frac{\Delta H^{\pm}}{RT}\right) \quad (10)$$

For experimental analysis equation 10 can be written

$$\log A = -B\left(\frac{1}{T}\right) + \log Q \quad (11)$$

where

$$A = \left(\frac{m}{pT}\right), \quad B = \left(\frac{0.4343\Delta H^{\pm}}{R}\right)$$

and

$$Q = \frac{\pi D}{\rho L}\delta\kappa\frac{k}{h}\exp\left(\frac{\Delta S^{\pm}}{R}\right)$$

Since all quantities in Q are known with reasonable accuracy we can measure $\Delta S^{\pm}$ for the burning process as well as $\Delta H^{\pm}$.

Experimental Results

According to equation 8 the burning rate is linearly proportional to the oxygen pressure. This relationship is confirmed over a 4 to 1 range in oxygen pressure. In this series of runs the oxygen was diluted with nitrogen so that the total pressure was atmospheric (635 mm. at the laboratory). The temperature was held constant at 450°.

The values of the parameters which enter into Q of equation 11 are

D = 7/32 inches = 0.555 cm.
L = 1 1/2 inches = 3.81 cm.
ρ = 1.5×10^{-3} ohm/cm.[4,8]
δ = 3.6×10^{-8} cm.[6]
κ = 1 (assumed)
k and h have their usual values.

The value of Q is then

$$Q = 2.30 \times 10^5 \exp\left(\frac{\Delta S^{\pm}}{R}\right) \quad (12)$$

The results of our measurements are summarized in Table I.

(8) This value has a temperature coefficient of -1.8×10^{-4} ohms per deg. centigrade. Thus at 500° the resistance would decrease by 8.5%. Our measurements are not sufficiently accurate to warrant this refinement in our calculations.

Table I

Gas flow (cc./min.)	p (atm.)	T, °K.	$m \times 10^6$	log (A)	$B \times 10^{-4}$	$\Delta H^{\pm}$, kcal.	Q	$\Delta S^{\pm}$, e.u.
352	0.836	623	2.60	−8.301				
		673	9.00	−7.796				
		723	29.3	−7.314	4.62	21.2	0.123	−28.7
		773	88.4	−6.863				
352	.418	623	1.0	−8.416				
		673	4.2	−7.824				
		723	12.2	−7.395	4.62	21.2	.093	−29.3
		773	30.7	−7.022				
239	.836	623	4.60	−8.054				
		623	4.00	−8.115				
		673	15.6	−7.558				
		723	55.6	−7.036	4.62	21.2	.204	−28.0
		773	159.0	−6.609				
		823	305.0	−6.354				
458	.836	623	1.60	−8.513				
		623	1.88	−8.444				
		673	7.00	−7.903	4.62	21.2	.092	−29.4
		723	23.4	−7.412				
		773	62.8	−7.013				

Discussion of Results

For ideal conditions and according to the theory outlined, all values of $\Delta S^{\pm}$ and $\Delta H^{\pm}$ should be identical. Values of $\Delta H^{\pm}$ are identical. The values of $\Delta S^{\pm}$ are found to spread by 1.4 entropy units in the extreme. This discrepancy we attribute to the condition that temperature equilibrium between the reacting gas and the furnace is not attained under our experimental conditions, and that the departure from equilibrium is increased as the rate of gas flow is increased. This condition comes about because the gas flow is not turbulent, and the gas flowing along the axis of the tube must reach temperature equilibrium through diffusion, a slow process. Future work will take account of this condition and devices to insure temperature equilibrium between the reacting gas and the furnace will be employed. The true value of the activation entropy is proposed as -28 ± 1 e.u.

Such an activation entropy value is consistent with expectations. Oxygen has an entropy change of about −20 e.u. in going from gas to liquid, according to Trouton's rule. It is likely that the adsorbed form of oxygen, to form the activated complex on the carbon surface, will have more restricted degrees of freedom than oxygen in the liquid form, accounting for still further loss of entropy which could be expected to be 3 or 4 entropy units. It is not likely that each carbon site is a candidate for forming the activated complex characteristic of the reaction studied, and further entropy decrease would be accounted for by the probability of a particular carbon being a candidate to form the activated complex. For example, suppose that only edge atoms of a graphite sheet are capable of undergoing the reaction studied and that the sheet is about 20 Å. per dimension.[6] The probability of an atom being an edge or corner atom is then about $^1/_4$. Because of the manner in which the crystals are packed together to form the carbon films only a fraction of the edge atoms of carbon will be available to complex with oxygen. It is thus reasonable to assume that not more than $^1/_{10}$ of the carbon atoms are in a favorable situation to react. This gives an additional entropy of −4.6 entropy units. Thus the −28 e.u. as the value of $\Delta S^{\pm}$ might have been anticipated considering our choice of the standard state.

The fact that the reaction is first order with respect to oxygen pressure p signifies that only a few of the carbon sites which are candidates for reaction are complexed with oxygen at any instant. This in turn signifies that there is a reversible reaction between the carbon–oxygen complex and the carbon site and oxygen gas, or that once the activated complex is formed it reacts very quickly to give carbon monoxide or carbon dioxide gas, thus preparing new carbon sites which are candidates for reaction.

Some observers have shown that carbon with adsorbed oxygen cannot be outgassed except by removal of the oxygen as carbon monoxide. This observation and our findings seem to demand that carbon adsorbs oxygen in two ways and that only one of these gives an activated complex leading to rapid removal of carbon in the burning process, at least at the low temperatures studied.

This work is being continued, extending it to catalyzed reactions.

THE DYNAMICS OF THE DIFFUSION OF FLUIDS IN RELATION TO THE CHOICE OF COMPONENTS

BY OLE LAMM

Division of Physical Chemistry, The Royal Institute of Technology, Stockholm, Sweden

Received May 13, 1955

The present paper is a continuation of earlier ones about the "dynamical theory" of diffusion. The term "dynamical theory" is used to describe the theory in which diffusion is considered to be a motion of molecules caused by a driving force and approved by frictional forces between the diffusing molecules. Such theory aims to be of general application to all systems and is to be distinguished from physical theories invoking precise physical mechanisms appropriate to particular systems. By way of the dynamical theory an attempt is made to provide a background against which practical diffusion problems can be examined, partly in order to distinguish which factors are general to all diffusion processes and which are special to a particular system.

In connection with the fundamentals of the diffusion theory,[1] it is of importance to realize that no special knowledge of the system is necessary for its applicability. In this article we will investigate the conditions for the diffusion formulas in question to be invariant with the choice of components, in the same sense as in thermodynamics, where only the number, and not the special choice of components is essential. An often used example is aqueous sulfuric acid with the components alternatively H_2SO_4, H_2O or SO_3, H_2O or SO_3, H_2SO_4, etc., *regardless of the real molecular constitution* and the composition of the mixture.

In other connections[3,4] we have discussed the adaptability of the theory in other respect, without pretensions concerning originality, *e.g.*, different assumptions regarding the molecular weights of the components. This was necessary in connection with the use of molar quantities of concentration, chemical potential and friction. The chemical potential gradients, which regulate the diffusion forces, are characterized by a considerable flexibility of application. This is a matter of classical physical chemistry, which is made use of in the diffusion theory.

In attempts to prove the generality and adaptability of the equations, obviously the question of the unambiguity and magnitude of the molar frictions in the case of associated components and chemical equilibria between the components is of interest. An essential point is that it is possible to ascribe frictional coefficients not only to the separate molecular species contained in the mixture, but also to each component in the thermodynamic sense of the word.

Similarly, it is justified to calculate with the velocity of the component as a whole, in spite of the fact that different molecular species within this have different mobilities and even may form molecules with matter belonging to other components of the mixture. It is, of course, necessary that the adjustment of the inner equilibrium shall be rapid in comparison with the disturbance of that which is caused by the diffusion.

In order to fix the ideas it may be added that while the physical theories of diffusion use the simplest possible, appropriate assumptions regarding the displacement of atoms or molecules, *the dynamic theory makes a point of being independent of special assumptions* concerning the structure and the mode of transfer of matter. In this way a greater generality and exactness is attained although, of course, within a narrower compass.

We will limit our further discussion to the equation[3]

$$D_{12} = \frac{RTB_{12}}{\Phi_{12}} \qquad (1)$$

valid for a case of two components, where $B_{12} = \partial \ln a_1/\partial \ln x_1 \equiv \partial \ln a_2/\partial \ln x_2$. x is mole fraction, a activity, and Φ_{12} is the friction between the components in the volume $1/c_1 + 1/c_2$ cu. cm.; the sum of the inverse concentrations in moles/cu. cm. This equation may alternatively be written

$$D_{12} = \frac{c_1c_2^2\bar{v}_1}{\varphi_{12}}\frac{\partial\mu^2}{\partial c_2} \equiv \frac{c_1^2c_2\bar{v}_2}{\varphi_{12}}\frac{\partial\mu_1}{\partial c_1} \qquad (2)$$

where φ_{12} is the mutual friction between the accepted components in a volume of 1 cu. cm., $\bar{v}_1$ and $\bar{v}_2$ the partial molar volumes, and μ_1 and μ_2 the chemical potentials.

The differential diffusion coefficient D_{12} is a direct property of the mixture and is accordingly independent of the way in which the components of a given mixture are chosen. It shall therefore be *invariant with the special choice* made in each case. The components being A_1 and A_2 in one case, we will investigate the condition for invariance during a change to the components A_1 and A_1A_2.

We will assume that the magnitudes μ, c, $\bar{v}$ and φ defined above, and used in the equations 2 relate to A_1 and A_2 as components, and will use the same symbols with the addition of an asterisk* for the case A_1 and A_1A_2. We obtain

$$\bar{v}_1^* = \bar{v}_1 \qquad c_1^* = c_1 - c_2$$
$$\bar{v}_2^* = \bar{v}_2 + \bar{v}_1[5] \qquad c_2^* = c_2 \qquad (3)$$

and

$$c_1\,d\mu_1 + c_2\,d\mu_2 = 0 \qquad \bar{v}_1\,dc_1 + \bar{v}_2\,dc_2 = 0$$
$$c_1^*\,d\mu_1^* + c_2^*\,d\mu_2^* = 0 \qquad \bar{v}_1^*\,dc_1^* + \bar{v}_2^*\,dc_2^* = 0 \qquad (4)$$

That the identity expressed in equation 2 is maintained, is easily shown. The invariance of D_{12}, however, imposes a condition upon the frictions φ_{12}

(1) The kind of theory referred to here has alternatively been called "hydrodynamic," "formal" or "phenomenological." The idea conveyed by the term "dynamical theory of diffusion" is also partly conveyed by Guggenheim's[2] use of the term "kinematic" diffusion coefficient in a special sense.

(2) E. A. Guggenheim, *Trans. Faraday Soc.*, **50**, 1048 (1954).

(3) O. Lamm, THIS JOURNAL, **51**, 1063 (1947).

(4) O. Lamm, *Acta Chem. Scand.*, **6**, 1331 (1952).

(5) This is immediately seen, considering that the partial molar volume is the volume change obtained by adding one mole of the component to a very large amount of the mixture. A_1A_2 is one mole A_1 and one mole A_2, as we do not in a general sense refer components to special kinds of molecules.

and φ^*_{12}, which we are going to deduce. For this purpose, we observe the additional relation

$$\mu_1 = \mu_1^* \tag{5}$$

The *concentration* of the first component has, however, changed. In order to elucidate equation 5 we may connect the activity a_1, defined by $\mu_1 = \mu^\circ_1 + RT \ln a_1$, with the partial vapor pressure of the special *molecules* A_1.[6] Neither this pressure nor its deviation from the ideal laws is changed by choosing A_1A_2 as the second component instead of A_2. Thus $a_1 = a_1^*$ and equation 5 is obtained provided that the standard state μ°_1 is maintained. A suitable standard state is the pure component.

From equations 3, 4 and 5 we obtain

$$\frac{\partial \mu_2}{\partial \mu_2^*} = \frac{c_1}{c_1 - c_2} \tag{6}$$

Applying equation 2 to the new choice of components gives at once

$$D_{12} = \frac{c_1^* c_2^{*2} \bar{v}_1^*}{\varphi^*_{12}} \frac{\partial \mu_2^*}{\partial c_2^*} \tag{7}$$

Exchange of variables transforms this to

$$D_{12} = \frac{(c_1 - c_2)^2 c_2^2 \bar{v}_1}{\varphi^*_{12} c_1} \frac{\partial \mu_2}{\partial c_2} \tag{8}$$

The identity with equation 2 requires

$$\frac{\varphi^*_{12}}{\varphi_{12}} = \left(\frac{c_1 - c_2}{c_1}\right)^2 \tag{9}$$

The form of this equation seems intelligible. In order to fix the ideas, let the point of departure be sulfuric acid with the components H_2O of concentration c_1, and SO_3 of concentration c_2, and let the case denoted by an asterisk be H_2O and H_2SO_4. If $c_1 = c_2$, equation 9 gives $\varphi^*_{12}/\varphi_{12} = 0$. This is correct, observing that φ_{12} is the friction/cu. cm. between H_2SO_4 and a zero quantity of water. Thus $\varphi^*_{12} \to 0$ as usual in a dilute solution, whereas φ_{12} is a quantity of a normal order of magnitude. We also observe that $\varphi^*_{12} \to \varphi_{12}$ if $c_2 \to 0$.

In connection with problems of solvation[3,7,8] the more general transformation from A_1 and A_2 to A_1 and $A_2(A_1)_\gamma$ is of interest. The only modification needed is that $c_2\gamma$ enters equation 9 instead of c_2

$$\frac{\varphi^*_{12}}{\varphi_{12}} = \left(\frac{c_1 - c_2\gamma}{c_1}\right)^2 \tag{10}$$

as is seen by direct computation or by calculating a series of successive steps from the case treated above.

We finally write the formula for a transformation from the friction φ_{12} of the components A_1 of c_1, mole/cm.^{3} and A_2 of c_2, mole/cu. cm. to the friction φ^*_{12} of the components $(A_1)_{p_1}(A_2)_{q_1}$ and $(A_1)_{p_2}(A_2)_{q_2}$

$$\frac{\varphi^*_{12}}{\varphi_{12}} = \left[\frac{(c_1q_1 - c_2p_1)(c_1q_2 - c_2p_2)}{c_1c_2(p_1q_2 - q_1p_2)}\right]^2 \tag{11}$$

It is easily shown that a transformation, which only affects the molecular weights, say to $(A_1)_{\gamma_1}$ and $(A_2)_{\gamma_2}$, does not at all change φ_{12}. (Naturally, the molecular weights, which are expressed by this component choice, have to be used in the calculation of the molar quantities contained in the diffusion equations 1 or 2. Consequently, the *molar* frictions depend upon γ_1 and γ_2, respectively). Equation 11 is most simply deduced from this point of departure, and by applying two successive steps analogous to equation 10 upon this choice of components.

The quadratic form of the equations 9, 10 and 11 shows that the friction/cu. cm. cannot become negative by a special choice of components. This is, however, not always true of the molar frictions (*e.g.*, $\Phi_{1(2)} = \varphi_{12}/c_1$, etc.), which may become negative in connection with negative concentrations. Previously, writing on self-diffusion,[9] it was taken for granted that the frictions are positive quantities. This is evidently not a formal necessity, but the special cases considered above, where negative molar frictions occur, cannot be seen to have any real bearing on the previously treated self-diffusion problem. The statements made regarding inequality relations[9] are, however, mathematically correct only if the components are so chosen that the frictions are positive. An eventual existence of negative component contributions to the total molar friction even in a normal, *physical* sense (in several component systems), cannot be excluded from merely dynamic reasonings.

We will with a few remarks return to our general problem: in order to make a suitable choice of components one has simply to consider *which friction one likes to determine* by the diffusion measurement. Equations like 1 or 2 are directly applicable, provided the molar quantities are calculated according to the molecular composition, expressed by the choice of components, *e.g.*, $(A_1)_{\gamma_1}$ or A_1A_2, etc. But it will often be more expedient to stick to the simplest molecular weights A_1 and A_2 and to use the equations 9, 10 or 11 to calculate the frictional coefficient, which corresponds to another choice.

The simultaneous diffusion of *three* components[3,10] is already much more complicated.[11] We will not treat the corresponding invariance problem in this article. As shortly indicated in an earlier work the choice of the components is of very great interest also in connection with the ultracentrifugal sedimentation of solvated substances. In this theory, as in the case of pure diffusion, the question of the frame of reference for the magnitudes involved has been a main point to examine. Thus "the question of to which frame of reference the driving force is acting relative to" (Baldwin and Ogston[12]) and related questions seem to have become clearly settled, compare also[13] and the verification by aid of the thermodynamics of irreversible processes by Hooyman, Holtan, Mazur and de Groot.[14]

(6) This procedure is quite general in all cases of thermodynamic equilibrium.

(7) Ping-Tao Cheng, *J. Chem. Phys.*, **23**, 191 (1955).

(8) O. Lamm, *Acta Chem. Scand.*, **7**, 173 (1953).

(9) O. Lamm, *ibid.*, **8**, 1120 (1954).

(10) O. Lamm, *Arkiv Kemi. Mineral. Geol.*, **18A**, No. 2 (1944).

(11) It may be noted here that the differential equations for the three-component diffusion, although complicated, were given an even oversimplified appearance. The diffusion force naturally in this case depends on *two* concentration gradients. This was, however, unfortunately obscured by the special choice of thermodynamic factors.

(12) R. L. Baldwin and A. G. Ogston, *Trans. Faraday Soc.*, **50**, 749 (1954).

(13) O. Lamm, *Arkiv Kemi Mineral. Geol.*, **17A**, No. 9 (1943).

(14) G. J. Hooyman, H. Holtan, Jr., P. Mazur and S. R. de Groot, *Physica*, **19**, 1095 (1953).

LITHIUM ABSORPTION BY KAOLIN MINERALS

By R. Greene-Kelly

Contribution from Rothamsted Experimental Station, Harpenden, Herts, England

Received May 16, 1955

Lithium ions introduced into the cation exchange positions on kaolin minerals are found to be non-exchangeable after the minerals are dried by heating to 200°.

Introduction

Recent investigations[1,2] on the effect of drying of montmorillonite minerals as a prelude to adsorption studies have shown that under certain conditions interlamellar sorption is inhibited at room temperature. Minerals that are dioctahedral, possess a large proportion of the silicate sheet charge due to octahedral substitution, and are saturated with cations of small size (*e.g.*, Li^+) are particularly susceptible to irreversible changes during drying. The inhibition of interlamellar sorption is always accompanied by a decrease in the cation-exchange capacity due to the fixation of the interlamellar cations.

It was naturally of interest to see whether other clay minerals showed the effect of ion fixation on drying and if so how far this affected their adsorption of water. Preliminary unpublished work on illites indicated that these minerals did not fix lithium ions. The kaolin group of minerals were found, however, to show lithium fixation and this result appeared of particular interest in view of the work of Keenan, Mooney and Wood[3] who found that lithium kaolinite (Peerless No. 2) showed the lowest water adsorption at any relative vapor pressure of water compared with kaolinites saturated with ions of hydrogen, sodium, potassium, rubidium, cesium, calcium, strontium and barium. This paper presents the results of ion-exchange work on three kaolinites and a halloysite and discusses the fixation effects in relation to the adsorption of water.

Table I

Mineral	Origin	Impurities	Ammonia retention, meq./100 g.	Surface area, sq. m./g.
Kaolinite	Merck Colloidal Kaolin	None	1.9	10
Kaolinite	English Clays RLO/314 Cornwall	Trace mica	1.6	...
Kaolinite	Peerless No. 2 (Vanderbilt Co.)	Trace mica	3.5	17
Halloysite	Eureka, Utah	Trace gibbsite	10	...

Experimental Methods

The selected minerals were examined by X-ray diffraction for impurities and their "exchange capacities" and surface areas determined by ammonia retention and carbon dioxide adsorption at its sublimation point, respectively. The latter values were obtained by use of the B.E.T. equation and proved to be in excellent agreement with those determined by other authors using nitrogen on kaolinites of the same origin.[3,4] These preliminary results are given in Table I.

The minerals were washed four times with normal solutions of the chlorides of the cations to be introduced and then washed free of chloride ions with alcohol or water. The samples were then dried at various temperatures and when this was completed the cations introduced were washed off with normal ammonium acetate (*p*H 7) over a period of several days. The resultant solutions were analyzed by the Lundegärdh flame spectrographic method. By this procedure it was found possible to introduce the desired cation into a proportion of the cation-exchange positions. If the washing of the excess chloride was carried out with water substantially lower amounts were introduced owing apparently to hydrolysis of the "clay-salt." For example Merck kaolinite was found to bind 0.3 meq./100 g. of lithium when the mineral was washed with water, whilst with alcohol washing, 1.6 meq./100 g. of lithium was introduced. This difficulty of preparing homogeneously saturated kaolinites has been a major factor in the development of special methods of determining the net change of kaolinite where the excess salt is not removed by washing with water or alcohol but is displaced by another electrolyte.[5] Clearly such methods could not be used in this work. Keenan, *et al.*,[3] prepared their samples by electrodialysis followed by titration with the appropriate hydroxide to neutrality. This procedure has been criticised on the grounds that the resultant titration curve represents at least in part the precipitation of aluminum oxides released during electrodialysis.[6]

Finally the ammonium acetate treated kaolin minerals were washed free of excess ammonium ions with alcohol and the minerals analyzed for retained ammonia by steam distillation of samples with sodium hydroxide, the evolved ammonia being collected in boric acid.

Results

Tables II and III summarize the experimental results for different cations and different minerals. It will be noticed that the excess salt was removed by washing with water in the first series and by al-

Table II

Merck Kaolinite

Cation introduced[a]	Drying temp., °C.	Cations recovered, meq./100 g.	NH_4^+ retained, meq./100 g.
Li^+	Unheated	0.3	1.8
	300	.02	1.5
Na^+	Unheated	.6	1.8
	100	.7	...
	200	.8	...
	300	.6	1.4
Mg^{2+}	Unheated	1.8	2.1
	100	1.6	...
	200	1.4	...
	300	0.9	1.1
Ca^{2+}	Unheated	1.1	2.3
	100	1.0	...
	200	1.0	...
	300	0.5	1.8

[a] Excess salt washed off with water.

(1) U. Hofmann and R. Klemenc, *Zeit. anorg. Chem.*, **262**, 95 (1950).

(2) R. Greene-Kelly, *Clay Min. Bulletin*, **2**, 52 (1953).

(3) A. G. Keenan, R. W. Mooney and L. A. Wood, This Journal, **55**, 1462 (1951).

(4) H. R. Samson, Ph.D. Thesis, London, p. 115, 1953.

(5) R. K. Schofield, *J. Soil Science*, **1**, 1 (1949).

(6) R. K. Schofield and H. R. Samson, *Clay Min., Bulletin*, **2**, 45 (1953).

cohol in the second series. The ammonia retention determinations refer to the ammonium ions retained by the clay mineral after alcohol washing.

TABLE III

LITHIUM EXCHANGED CLAY MINERALS[a]

Mineral source	Drying temp., °C.	Lithium recovered, meq./100 g.	NH_4^+ retained, meq./100 g.
Merck	Unheated	1.6	2.0
	100	0.8	1.6
	200	<0.1	1.4
	300	<0.1	1.3
E.C.	Unheated	1.1	1.5
	100	0.4	1.1
	200	0.1	0.8
	300	0.1	0.9
Peerless	Unheated	2.0	3.5
	100	1.0	2.9
	200	0.2	2.0
	300	0.1	1.9
Eureka	Unheated	6.0	10
	100	3.0	7
	200	2.7	9
	300	1.7	10

[a] Excess salt washed off with alcohol.

The results show that kaolin minerals fix exchangeable cations during drying, but that the fixation is most marked when lithium ions are introduced. The fixation of lithium ions is not generally accompanied by the full expected decrease in the ammonia retention value and this suggests that some other ion is also taking part in the exchange process. An attempt was therefore made to repeat the introduction of lithium on the same sample to see whether an indefinite amount could be introduced, the samples being analyzed for total lithium at various stages. The Merck and Peerless kaolinites were thus found to fix 11 and 13 meq. Li^+/100 g., respectively, after nine treatments after which the lithium introduced at each treatment diminished. The Peerless kaolinite could however still retain 1.4 and the Merck 1.1 meq./100 g. of ammonia. These samples deflocculated readily with alkali and showed no difference in their X-ray diffraction diagrams or electron micrographs. Similar results were obtained with Eureka halloysite although a drop in the ammonia retention figure was not observed. Incidentally the maintenance of the ammonia retention value after being heated to 200° is an indication that the exchangeable cations are concentrated on the external surface since the internal surface is no longer available to water molecules after severe drying.

An attempt was made to find the ions from the heated mineral which were being exchanged against ammonium ions. There was some evidence that slightly larger amounts of sodium ions were removed from the Merck kaolinite after heating but this did not amount to more than one fifth of the amount of fixed ions. Of potassium, magnesium and calcium the amount was unchanged on heating. To determine whether aluminum was released during the fixation process the solution obtained after washing the kaolinite with 0.001 *N* HCl and *N* NH_4Cl was analyzed for aluminum. Both before and after heating the amounts were both small and the same.

Discussion

The conclusion of Keenan, *et al.*,[3] that lithium ions are absent from adsorbed water films on kaolinite is supported by the observed fixation of lithium ions during drying. It is noteworthy however that drying appears to be necessary for fixation which suggests that lithium ions are present in the adsorbed water film during the first desorption and consequently there should be hysteresis between it and subsequent adsorption–desorption cycles. Keenan, *et al.*, attributed the peculiarities of lithium kaolinite to the fact that the size of the lithium ion is just such as to cause it to fit into a position in the surface of the kaolinite crystal where its hydration is prevented by steric factors. The strong fixation of lithium ions suggests that the ions are not located in the surface layer of atoms of the crystal but buried in the crystal, possibly in the vacant octahedrally coördinated sites as has also been suggested to explain a similar phenomenon with montmorillonite.

The repeated introduction of lithium ions by the fixation process is thought to be evidence that structural exchange is also occurring. The absence of metallic ions makes it necessary to postulate a process by which hydrogen ions are ejected during fixation of lithium and these are then re-exchanged during the succeeding treatment. If it is assumed that half the surface of kaolinite consists of close packed hydroxyl groups of area 6 Å.^{2} then the area per fixed lithium ion after nine treatments is 7 Å.^{2} for Merck kaolinite and 11 Å.^{2} for Peerless kaolinite, and hence it seems that the surface may become sparse of easily available hydrogen ions as the lithium fixation becomes more difficult. It is interesting to note that the oxides of aluminum and ferric ion appear to show related phenomena with regard to the similar roles played by lithium and hydrogen ions. The compounds $LiAl_5O_8$ and $LiFe_5O_8$ have shown to have the same superstructure as certain samples of γ-ferric oxide known to contain traces of water molecules and with a probable limiting composition of HFe_5O_8. The compound HAl_5O_8 is also known. Clearly the hydrogen ions are not present merely as adsorbed water but are incorporated in the lattice in the same way as lithium ions.[7,8]

Acknowledgments.—The author thanks Mr. H. H. Le Riche for carrying out spectrographic analyses and Mr. H. Nixon for taking electron micrographs. Acknowledgment is also made to the late Dr. H. Samson and the Vanderbilt Export Corporation, New York, for gifts of minerals.

(7) P. B. Braun, *Nature*, **170**, 1123 (1952).

(8) I am indebted to Mr. H. P. Rooksby for bringing this paper to my notice.

STRUCTURE OF THE CARBON DEPOSITED FROM CARBON MONOXIDE ON IRON, COBALT AND NICKEL

BY L. J. E. HOFER,[1a] E. STERLING[1b] AND J. T. MCCARTNEY[1c]

Contribution of Division of Solid Fuels Technology, Bureau of Mines, Region V, Pittsburgh, Pa., and Coal Research Laboratories, Department of Chemistry, Carnegie Institute of Technology, Pittsburgh, Pa.

Received May 17, 1955

The carbon deposits formed by the action of carbon monoxide at 390° on iron, cobalt and nickel have been studied by electron microscopy. These deposits are in the form of filaments from 0.01 to 0.2 μ in diameter. These filaments of the deposits on iron are single solid strands. The carbon deposits on nickel seemed to consist almost entirely of either tubules or, less likely, of untwisted bifilaments. The deposits on cobalt exhibit both the form of solid filaments and of tubules or bifilaments. Most of these filaments contain dense nuclei of about the same diameter as the diameter of the filaments in which they lie. The nuclei are about midway from the ends of the corresponding filaments. The nuclei in the deposits formed on iron have the form of discs, the short axis of which parallels the fiber axis of the carbon deposit. The nuclei in the cobalt deposits are well-formed octahedra in which one of the [001] axes parallels the fiber axis. The nuclei in the nickel deposits seem to have crystalline faces but these cannot be positively identified. Powder diffraction analysis suggests that these nuclei contain face-centered cubic nickel metal and/or the hexagonal close-packed nickel carbide.

Introduction

The catalytic deposition of carbon from carbon monoxide by the reaction $2CO \rightarrow C + CO_2$ is highly deleterious in several industrial processes. At atmospheric pressure the reaction takes place between 300 and 800°. The Fischer–Tropsch process used for the synthesis of hydrocarbons is subject to this carbon deposition, which may lead to blockage of the reaction vessel and to deactivation and disintegration of the catalyst.[2] Ceramic brick linings containing iron undergo physical disintegration whenever exposed to carbon monoxide under suitable conditions of diffusion and temperature.[3] The reaction is involved in blast furnace operation.[4]

The structure of carbon formed by decomposition of carbon monoxide on an iron catalyst was described by Radushkevich and Luk'yanovich in 1952.[5] They reported that the carbon particles formed at a temperature of 600° had elongated thread-like shapes. They postulated that thread-like nuclei, apparently consisting of iron carbides, were formed first and that these grew transversely by deposition of carbon. They also noted the presence of twisted multiple threads. Tesner and Echeistova[6] reported the growth of similar threads on lampblack particles exposed to CH_4, C_6H_6 or cyclohexane atmospheres at temperatures above 977°.

Davis, Slawson and Rigby[7] have published electron micrographs of filamentary carbon growths formed by the interaction of carbon monoxide and iron oxide in blast furnace brickwork. They observed that these structures were formed at temperatures of 450° on different forms of iron oxide. X-Ray examination showed the presence of "amorphous carbon, cementite (Fe_3C), and an iron percarbide ($Fe_{20}C_9$)." (The present authors believe the term iron percarbide as used by Davis, *et al.*, is identical to the Hägg iron carbide.) They postulated that the catalyst for the reaction, either iron or iron carbide, formed on the surface of the oxide as a speck which in turn gave rise to a thread of carbon. Threads from a collection of specks became twisted together and probably coalesced to form the characteristic filament. They suggested that after deposition began the catalyst particles were located on the growing ends of the threads.

Although growth of carbon deposits on iron has been investigated, similar observations on cobalt and nickel have been lacking. The aim of the present paper has been, therefore, to study the morphology of the carbon deposits on cobalt and nickel.

Experimental Procedure

The nickel catalyst specimen was precipitated $Ni(OH)_2$ prepared by the method described elsewhere.[8] The cobalt catalyst was in the form of Co_3O_4 spinel prepared according to the method described elsewhere.[9] The iron catalyst was P-1028 of the Bureau of Mines, which was prepared by pre-neutralizing reagent grade $Fe(NO_3)_3$ solution with ammonia at room temperature and then heating rapidly to 70° and precipitating with ammonia at that temperature. The precipitate was then filtered and dried.

The apparatus used to obtain carbon deposits on catalysts is simple. A sample of approximately 1 g. of fine-crushed catalyst was placed in the porcelain combustion boat and this in turn was pushed into a (1.5 cm. i.d.) Vycor combustion tube heated by an electric furnace. Temperatures were measured with a thermocouple and potentiometer. Since samples were not in a reduced state, a stream of hydrogen was passed over the sample at a rate of 25 cm.^{3}/min. The reduction was carried out at 390° for the nickel and iron specimens and 350° for the cobalt specimens. The reduction periods varied from 8 to 24 hours.

Commercial carbon monoxide was used for the carbon deposition. The gas was purified by passing through a hot porcelain tube at 350–400° in order to decompose the iron carbonyl usually found in carbon monoxide stored under pressure in steel tanks. It was then passed through (8–20 mesh) Caroxite, a CO_2 indicating absorbent manufactured by the Fisher Scientific Co. The gas was then dried in a

(1) (a) Physical Chemist, Branch of Coal-to-Oil Research, Bureau of Mines, Bruceton, Pa. (b) Member of staff, Coal Research Laboratory, Dept. of Chemistry, Carnegie Institute of Technology, Pittsburgh; now with Explosives Department, Eastern Laboratories, E. I. du Pont de Nemours & Co., Gibbstown, N. J. (c) Physicist, Coal Constitution and Miscellaneous Analysis Section, Bureau of Mines, Pittsburgh, Pa.

(2) H. Pichler and H. Merkel, U. S. Bureau of Mines, Tech. Paper, 718 (1949).

(3) R. F. Potnik and R. B. Sosman, *J. Am. Ceramic Soc.*, **32**, 133 (1949).

(4) S. Klementaski, *J. Iron & Steel Inst., London*, **171**, 176 (1952).

(5) L. V. Radushkevich and V. M. Luk'yanovich, *Zhur. Fiz. Khim.*, **26**, 88 (1952); *C. A.*, **47**, 6210 (1953).

(6) P. A. Tesner and A. I. Echeistova, *Doklady Akad. Nauk. U.S.S.R.*, **87**, 1029 (1952); *C. A.*, **47**, 6210 (1953).

(7) W. R. Davis, R. J. Slawson and G. R. Rigby, *Nature*, **171**, 756 (1953).

(8) L. J. E. Hofer, E. M. Cohn and W. C. Peebles, THIS JOURNAL, **54**, 1161 (1950).

(9) L. J. E. Hofer and W. C. Peebles, *J. Am. Chem. Soc.*, **69**, 893 (1947).

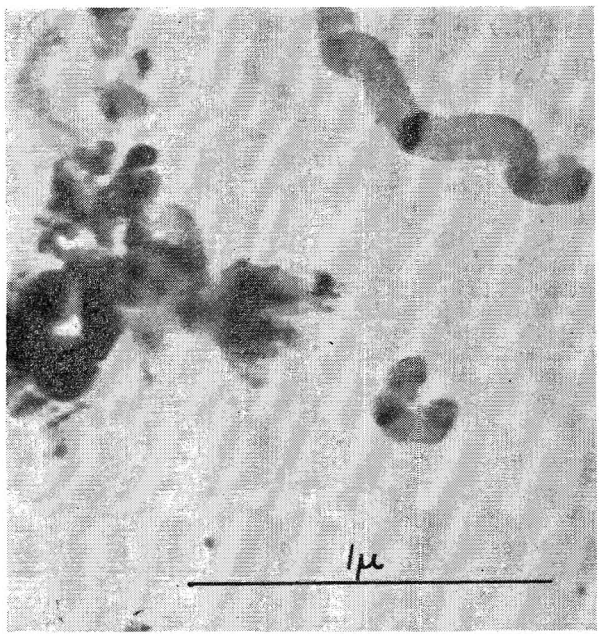

Fig. 1.—Carbon deposited on iron; sample 212. Note extension of filaments in two directions from central nucleus.

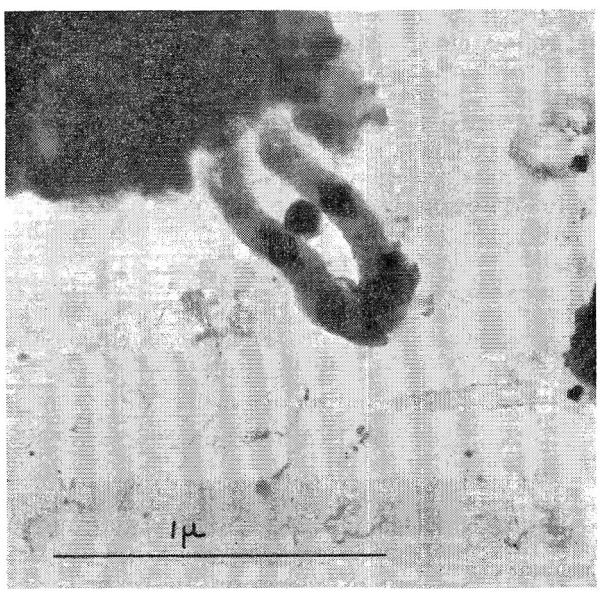

Fig. 2.—Carbon deposited on cobalt; sample 216. Note octahedral nuclei within large filaments. The ends of these filaments are obliterated; note also fine filaments.

drying tube containing granulated anhydrous magnesium perchlorate. A second Caroxite absorbent was placed on the downstream side of the reaction tube. This tube allowed visual qualitative observation of the rate of carbon dioxide production resulting from the decomposition of carbon monoxide. Carburization was carried out at 390°.

When the carbonaceous deposit was built up to 20 to 30 times the volume of the original catalyst, its top layer was removed. This fraction was pyrophoric and was stored under nitrogen in a sealed bottle.

Specimens of the carbon deposits were prepared for electron microscopy by adding to a few milligrams of the deposit 3 or 4 drops of a 2% solution of collodion in amyl acetate plus 7 or 8 drops of amyl acetate and mulling with a glass rod until a good dispersion was obtained. A little of the suspension adhering to the rod was then rapidly drawn over a clean microscope slide. This operation yielded a thin collodion film containing the dispersed particles. After the film was scored in 1/4-inch squares, it was floated off on a water surface. Two superimposed 200-mesh specimen

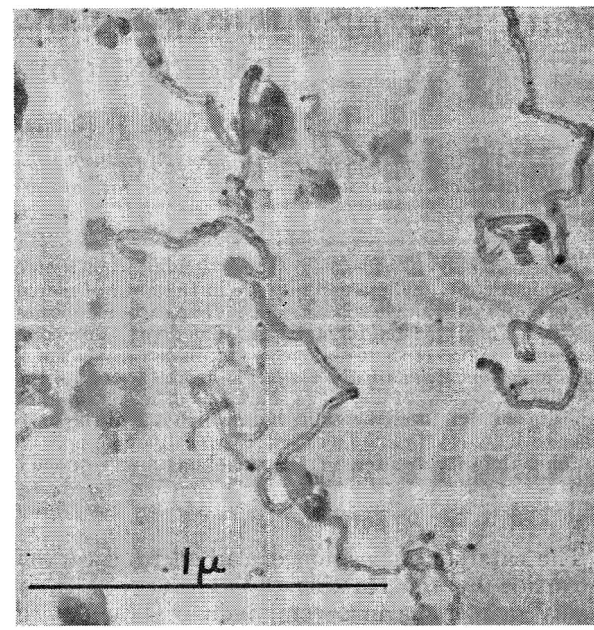

Fig. 3.—Carbon deposited on nickel [from $Ni(OH)_2$]; sample 215. Note well developed bifilamentary or tubular structure.

screens were brought up under a square of film of proper particle dispersions. The mount was then allowed to dry. The top screen containing the film was then removed and examined by electron microscope.

The X-ray diffraction patterns were made with a simple Debye–Scherrer powder camera of 71.62 mm. inside diameter. Radiation was obtained from a sealed-off iron target tube equipped with beryllium windows and manganese dioxide filters and operated at 40-peak kilovolts and 7.0 milliamperes. The samples were ground to a fine paste with collodion cement (Duco) and extruded from a short section of 19 gage 0.7 mm. i.d. stainless steel tubing. The results are shown in Table I.

TABLE I

X-RAY DIFFRACTION DATA ON CARBURIZATION PRODUCTS

Sample	Analysis[a]
212	C,[b] Fe_3O_4,[c] Fe_2C[d]
215	C,[b] Ni[e]
216	C,[b] $\beta Co'$, αCo^{g}

[a] The phases are listed in the order of decreasing intensity of the diffraction patterns. [b] Turbostratic carbon showing chiefly the 002 band of graphite and some evidence of 100 and 110 bands. [c] Magnetite. [d] Hägg iron carbide, *Z. Krist.*, 89, 92 (1934). [e] Face-centered cubic nickel. [f] Face-centered cubic cobalt. [g] Hexagonal close-packed cobalt.

Results and Discussion

In general, when carbon monoxide reacts with iron or cobalt at temperatures below 225° and with nickel below 270°,[10,11] carbides of these metals are formed almost exclusively. Above these temperatures free carbon deposition occurs. At various higher temperatures these carbides undergo reactions, transitions and/or decompositions.[12,13] Therefore, when carbon monoxide reacts with the

(10) (a) H. A. Bahr and V. Jessen, *Ber.*, **66**, 1238 (1933); (b) *ibid.* **63**, 2226 (1930).

(11) H. A. Bahr and Th. Bahr, *ibid.*, **61**, 1277 (1929).

(12) L. J. E. Hofer, E. M. Cohn and W. C. Peebles, THIS JOURNAL, **53**, 661 (1949); **54**, 1161 (1950).

(13) L. J. E. Hofer, E. M. Cohn and W. C. Peebles, *J. Am. Chem. Soc.*, **71**, 189 (1949).

above metals at a high temperature—for example, 390°—free carbon as well as various forms of carbides and the original metals may be present. Their relative amounts will depend upon the experimental conditions, *i.e.*, time, temperature, composition of gas, flow rates, etc.

Figures 1 to 3 show electron micrographs of various carbonaceous deposits obtained in this study. The filamentary particles of carbon deposited on iron reported by previous investigators were also observed here on cobalt and nickel in addition to iron. The filaments deposited on iron are characteristically about 0.1 μ in diameter and usually contain an elliptical dark spot near the center (Fig. 1). Powder-diffraction analysis of the whole carbon deposit suggests these nuclei to be Hägg carbide and/or α-iron from which the growth of the fiber occurs. The magnetite reported in Table I may have been present originally or formed from the reaction with carbon dioxide. As has been previously mentioned, Davis, Slawson and Rigby found such spots only at the ends of filaments; thus their filaments seem to have grown exclusively in one direction, whereas in most cases the growth of the fibers here observed proceeded in two opposite directions from the same center.

The deposits on cobalt appear to contain fibers of two size ranges. The larger fibers average 0.1 μ in diameter and up to 2 μ in length while smaller fibers are about 0.01 μ in diameter and up to 2 μ in length. The larger fibers, as in the case of iron, have a dense nucleus near the center. Such a nucleus appears on the electron micrograph as a tiny, diamond-shaped area, which may be interpreted as the projection of an octahedron, one of whose [001] axes coincides with the axis of the fiber.

One can conceive that, if the two other axes of the octahedra are at 45° with the line of sight, the diamond-shaped area will appear elongated in the direction of the fiber axis. The long axis of the diamond would in this instance be longer than the transverse axis by a factor of $\sqrt{2}$. If, on the other hand, one of the two axes of the octahedron transverse to the fiber axis coincides with the line of sight, the diamond-shaped area will be square. All the diamond-shaped nuclei observed here vary between the two extremes described above. This means that under the microscope the two octahedral axes other than the one lined up with the fiber axis are randomly oriented in space. Since carburization is carried out in the temperature range where cobalt has cubic symmetry, the octahedron is a very probable crystal habit which arises when the crystal is bounded by 111 planes.

Leidheiser and Gwathmey[14] found that single crystals of nickel machined into spheres deposited carbon from carbon monoxide preferentially on the 111 planes. Kehrer and Leidheiser[15] found that this also occurs on single crystal cobalt spheres. Removal of nickel or cobalt atoms from the surface may accompany this carbon deposition. Such a process removing nickel or cobalt preferentially from the 111 planes will eventually convert a single crystal into an octahedron whatever the initial shape is.

It should also be noted that the particles of cobalt which are not included in carbonaceous filaments present irregular contours (Fig. 2). This fact suggests that the growth of the carbonaceous filament is causally related to the evolution of 111 planes.

The above-described threads grown on cobalt are relatively large in diameter and homogeneous in their cross-sectional density. Some very fine (10 mμ) threads also were found, and close examination reveals that some of these appear as two fine parallel lines suggesting either double threads or tiny tubules (*cf.*, deposition on nickel, immediately following).

The carbon formed on nickel contained both coarse and fine threads (Fig. 3). Many of the threads appeared to be double or were tubules. The lines were remarkably parallel and never seemed to be twisted as one would expect them to be if they were double threads; it seems most likely that they are tubules. It is conceivable that these tubules may not actually be hollow but only contain material less dense than the outside walls. Nuclei appeared almost invariably at the ends of the threads if they appeared at all. The dark nuclei of the larger threads have angular edges suggesting a crystalline form but the exact crystal habit is not determinable. It is possible that the carbon-deposition process has not gone far enough to reduce the nuclei to a recognizable crystalline form. From the reasoning employed to explain the results found with cobalt, one would expect an octahedral crystal habit in nickel.

Acknowledgment.—The authors wish to thank Mrs. W. C. Peebles for the X-ray diffraction analyses presented here.

(14) H. Leidheiser, Jr., and A. T. Gwathmey, *J. Am. Ch m. Soc.*, **70**, 1206 (1948).

(15) V. J. Kehrer and H. Leidheiser, Jr., THIS JOURNAL, **58**, 550 (1954).

THE EFFECT OF USING THE PRESSED SALT TECHNIQUE TO OBTAIN THE SPECTRUM OF CHEMISORBED AMMONIA

BY W. A. PLISKIN AND R. P. EISCHENS

Beacon Laboratories, The Texas Company, Beacon, New York

Received May 19, 1955

Recently French, *et al.*, have published pressed disk spectra from which they attribute a band at 7.2 μ to ammonia chemisorbed on cracking catalysts.[1] This does not agree with the results of Mapes and Eischens,[2] who, in an investigation of ammonia chemisorbed on cracking catalysts, obtained a band at 6.9 μ which they attribute to chemisorbed NH_4^+. The latter investigators examined the catalysts directly, overcoming scattering by using very small particle size catalysts. Investigation of a cracking catalyst and γ-alumina by both techniques has established that the discrepancy is due to the difference in the technique used to obtain the spectra. In fact the exact band position depends on the alkali halide used as the disk material. The shift in band positions can be explained by assuming that ion exchange between the alkali ion and NH_4^+ takes place and that in the pressed disk technique one actually obtains the spectrum of the ammonium halide and not NH_4^+ adsorbed on cracking catalysts. Verification of the existence of the ammonium halide was obtained by examining the exchange between the ammonium group and the alkali ion for various ammonium halides in alkali halide disks. It has also been found that in some cases the ammonium ions exist in the form of a solid solution with the alkali halides.

I. Introduction

Recently French, *et al.*, have published spectra from which they attribute a band at 7.2 μ to ammonia chemisorbed as NH_4^+ on silica gel, on Filtrol Catalyst Grade 58 and on Houdry Catalyst S-45.[1] This result is not in agreement with that reported by Mapes and Eischens, who, in an investigation of ammonia chemisorbed on a fresh American Cyanamid MS-B silica–alumina cracking catalyst, obtained a band at 6.9 μ[2] due to the non-symmetrical N–H bending vibration of the chemisorbed ammonium ion NH_4^+. The present work shows that the difference is due to the fact that French, *et al.*, used the pressed disk technique[3-5] to obtain the spectra, whereas Mapes and Eischens examined the catalysts directly, overcoming scattering by using very small particle size catalysts.

The work reported here was undertaken because it seemed unreasonable to assume that this discrepancy in the bending vibration band position was due to a difference in the nature of the catalysts. The NH_4^+ ion was visualized as being held to the surface by electrostatic forces and there is no reason to expect a difference between the band position on the American Cyanmid MS-B and the Houdry S-45 catalysts, which are both synthetic silica–alumina cracking catalysts. This is supported by the fact that with the silica gel, Filtrol grade 58 and Houdry S-45 catalysts, French, *et al.*, obtained the same band positions although these materials differ in structure and chemical composition.

The experimental work was designed to test the hypothesis that ion exchange occurs during use of the pressed salt technique so that the NH_4^+ in the catalyst is replaced by the alkali ion of the salt. If this occurred the spectrum would be that of the ammonium halide corresponding to the salt used, rather than the spectrum of adsorbed NH_4^+.

The infrared spectra of ammonia chemisorbed on the American Cyanamid cracking catalyst and on Alon C[6] were obtained both directly and by use of the pressed disk technique. To verify the exchange phenomenon and to help interpret the infrared spectra of adsorbed NH_4^+, various alkali halide salts were used as disk materials and the spectra of a variety of ammonium halides pressed in alkali halide disks were obtained.

II. Experimental Procedure

The spectra were obtained with a Perkin–Elmer Model 12B which was modified to be equivalent to a Model 12C. A CaF_2 prism was used as the dispersing element. The spectral region fron 2.6 to 8.3 μ was investigated.

Since it was possible to use very small particle sizes of Alon C or cracking catalyst,[7] spectra of thin films of these substances could be obtained directly. Spectra of NH_4^+ adsorbed on either of these materials could be obtained by merely exposing the films to a stream of ammonia at room temperature.

The alkali halide salts and most of the mixtures were ground in a mechanical mortar and pestle which was enclosed in a dry box. In some cases the catalyst was heated from one to three hours at 500° before grinding and at about 200° after grinding. In other cases a fine powder of the cracking catalyst and the ground alkali halide were mixed only with a spatula. The mixtures were then exposed for about 10 to 15 minutes to ammonia at room temperature after which they were pressed into disks.

Two simple dies were constructed for making the pressed disks. One die makes 13 mm. pellets and the other 22 mm. pellets. Most of the former weighed 0.20 g. and the latter weighed about 0.6 to 0.8 g. depending on the alkali halide being used.

The chemicals used were reagent grade. The weight ratio of alkali halide to catalyst varied from about 30:1 to 70:1, whereas the weight ratio of alkali halide to ammonium halide varied from about 250:1 to 3000:1, depending on the combination of ammonium halide and alkali halide. Most of the molar ratios of alkali to ammonium halide were about 250:1 to 500:1.

The slit widths which were used depended on the sample under investigation. For most of the samples the resolution was about 10 $cm.^{-1}$ in the 3 μ region and 2 to 3 $cm.^{-1}$ in the 7 μ region. Representative details on the resolution are tabulated below.

	3 μ	7 μ
Pressed disks:		
Ammonium halides in NaCl, NaBr, KCl, KBr, KI, CsCl	9–10 $cm.^{-1}$	2–3 $cm.^{-1}$
Ammonium halides in NaI	20–40 $cm.^{-1}$	7–10 $cm.^{-1}$

(1) R. O. French, M. E. Wadsworth, M. A. Cook and J. B. Cutler, THIS JOURNAL, **58**, 805 (1954).

(2) J. E. Mapes and R. P. Eischens, Reprints of General Papers of the Division of Petroleum Chemistry, Chicago Meeting, A.C.S., Sept. 1953, pp. 23–28, and THIS JOURNAL, **58**, 1059 (1954).

(3) E. S. Cook, C. W. Kreke, E. B. Barnes and W. Motzel, *Nature*, **174**, 1144 (1954).

(4) M. M. Stimson, Abstracts of Symposium on Molecular Structure and Spectroscopy, Ohio State University, 1951, p. 59, and M. M. Stimson and M. V. O'Donnell, *J. Am. Chem. Soc.*, **74**, 1805 (1952).

(5) U. Scheidt and H. Reinwein, *Z. Naturforsch.*, **7b**, 270 (1952).

(6) A commercial product of small particle size (50–200 Å.) γ-alumina available from Godfrey L. Cabot, Boston, Massachusetts.

(7) See reference 2 for details on the preparation of small particle catalysts.

Catalyst in NaCl, NaBr, KCl, KBr, KI, CsCl	10–16 cm.$^{-1}$	3–4	cm.$^{-1}$
Catalyst in NaBr (one sample having a larger relative amount of catalyst than normal)	33	cm.$^{-1}$	8	cm.$^{-1}$
Alon C direct	25	cm.$^{-1}$	4	cm.$^{-1}$

III. Results and Discussion

A. Exchange of Adsorbed Ammonia to Form Ammonium Halides.—Reinvestigation of ammonia chemisorbed on an incompletely dried cracking catalyst verified the previous work of Mapes and Eischens in that the non-symmetric N–H bending vibration of the chemisorbed ammonium ion NH_4^+ produces a band at 6.9 μ. Furthermore ammonia was chemisorbed on incompletely dried γ-alumina (Alon C) and from direct examination by infrared the band was found to be at 6.84 μ as shown in Fig. 1.[8] On the other hand, Fig. 1 also shows the spectrum of a sample of Alon C which had been subjected to NH_3 and thence pressed with ground KBr into a disk. The pelleting shifted the band to 7.14 μ. Similar results were also found in the investigation of American Cyanamid MS-B silica–alumina cracking catalyst. In addition it was found that in the pressed disk technique this band position depends on which particular potassium halide was used. Use of KBr disks, as shown in Fig. 1, resulted in a band at 7.14 μ; whereas, pressing in KI disks resulted in a band at 7.17 μ.

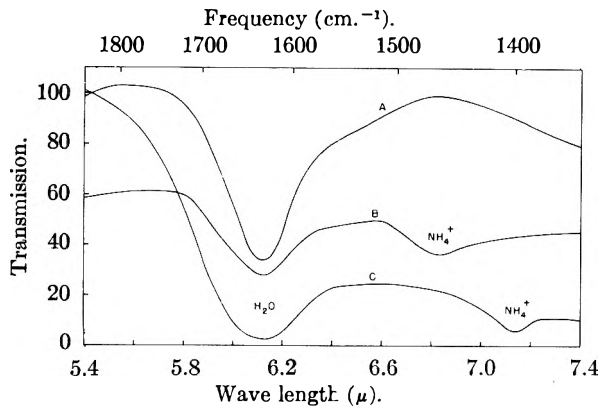

Fig. 1.—Effect of pelleting technique on the infrared spectra of Alon C exposed to ammonia: A, Alon C; B, Alon C after ammonia exposure; C, ammonia exposed Alon C in a KBr disk.

The shift from 6.9 μ to the 7.2 μ region can be explained by assuming that ion exchange between the K^+ and NH_4^+ takes place and that in the pressed disk technique one actually obtains the spectrum of NH_4I or NH_4Br and not NH_4^+ adsorbed on the cracking catalyst. This is substantiated by an examination of the spectrum of either NH_4Br in KBr or NH_4I in KI. Figure 2 compares the essential portions of the infrared spectrum of ammonia-exposed silica–alumina cracking catalyst pressed into a KI disk with the spectrum of NH_4I pressed into a KI disk. Spectrum A is for the silica–alumina cracking catalyst and spectrum B is for the NH_4I. Outside of the 2.9 μ band due to water adsorbed on the cracking catalyst, the positions of the strongest bands coincide exactly, with maxima at 3.17 and 7.17 μ. The absorptivity is such as to indicate that the catalyst had adsorbed 2.2×10^{-3} meq. of ammonia per gram of catalyst.[9] When the cracking catalyst with adsorbed ammonia was pressed into a KBr disk, the two strongest ammonium bands were at 3.20 and 7.14 μ, which coincides with the band positions in the spectrum of NH_4Br pressed into a KBr disk.

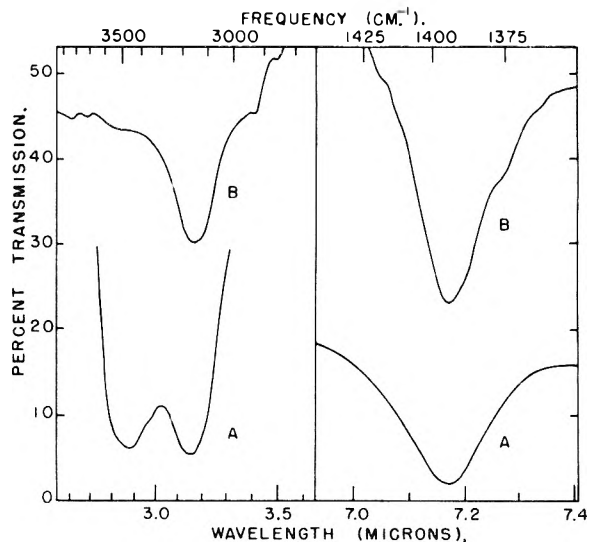

Fig. 2.—Comparison of pressed disk spectra of NH_4^+: A, ammonia exposed cracking catalyst in KI disk; and B, NH_4I in KI disk.

B. Comparison of Spectra of Ammonium Halides in Pressed Disks.—Although the aforementioned spectra in KBr are the same, they do not agree with the spectra of thin films of NH_4Br at room temperature,[10,11] and therefore the NH_4Br obtained by pelleting ammonia-exposed cracking catalyst in KBr is not ordinary NH_4Br. It seemed as if an explanation might be obtained by investigating the spectra of various ammonium halides pressed into alkali halide disks.

The exchange between adsorbed ammonium ions and the alkali halide disks suggested that exchange between ammonium halides and alkali halides would occur in using this technique. This was found to be the case for all combinations of ammonium and alkali halides that were tried. Table I shows the positions of the major ammonium bands which were obtained by pressing various ammonium halides in alkali halide disks. Table II shows the combinations of ammonium halides and alkali halides that were tried. Due to exchange

(8) Investigation of ammonia (NH_3) chemisorbed on dried Alon C revealed absorption bands at 2.96, 3.06 and 6.1 μ due to the two N–H stretching vibrations and the non-symmetric bending vibration.

(9) The maximum absorptivity of the 7.17 μ band as calculated from the spectrum of NH_4I in KI was found to be 82×10^{-20} cm.^{2} per NH_4^+ ion. With a 13 mm. diameter disk having a KI–catalyst ratio of 70 and weighing 0.203 g., the absorbance of the 7.17 μ band was 1.00. Therefore on the assumption that the NH_4^+ absorptivities are the same we have for the amount of NH_4^+ adsorbed

$$\left(\frac{(1.00)(2.303)}{82 \times 10^{-20}}\right)\left(\frac{(70)(0.65)^2\pi}{0.203}\right)\left(\frac{1}{6.02 \times 10^{20}}\right) =$$

2.2 meq. of ammonia/g. catalyst

(10) E. L. Wagner and D. F. Hornig, *J. Chem. Phys.*, **18**, 305 (1950).

(11) L. F. H. Bovey, *J. Opt. Soc. Am.*, **41**, 836 (1951).

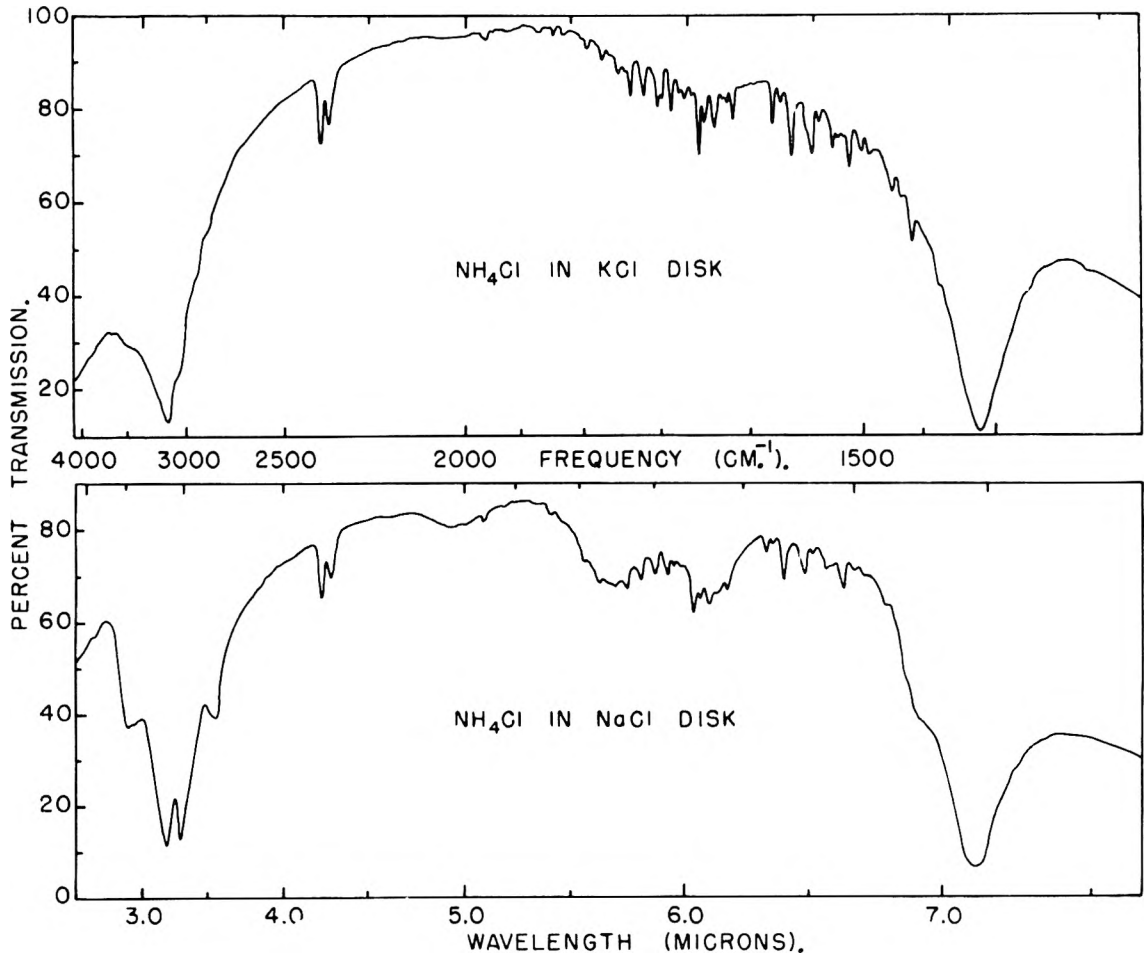

Fig. 3.—Comparison of spectrum of NH_4Cl in KCl disk with spectrum of NH_4Cl in NaCl disk.

the results were independent of the ammonium halide used and are therefore presented in Table I according to the alkali halide used. As an example the spectra of ammonium halides pressed in sodium chloride disks were essentially the same, having three strong bands at 3.19, 3.29 and 7.11 μ. On the other hand when the ammonium halides were pressed into potassium chloride disks, there were only two strong bands at 3.22 and 7.10 μ.

TABLE I

WAVE LENGTH POSITIONS IN μ OF THE MAJOR AMMONIUM BANDS IN VARIOUS ALKALI HALIDE DISKS

NaCl	KCl	CsCl	NaBr	KBr	NaI	KI
3.19	3.22	3.19	3.20	3.20	3.12	3.17
3.29		3.29	3.30			
7.11	7.10	6.99	7.13	7.14	7.18	7.17

TABLE II

COMBINATIONS OF AMMONIUM HALIDES AND ALKALI HALIDES WHICH WERE INVESTIGATED

In NaCl	In KCl	In CsCl	In NaBr	In KBr	In NaI	In KI
NH_4F	NH_4F	NH_4Cl	NH_4F	NH_4F	NH_4F	NH_4F
NH_4Cl	NH_4Cl	NH_4I	NH_4Br	NH_4Cl	NH_4Br	NH_4Br
	NH_4Br			NH_4Br		NH_4I
				NH_4I		

A study of Table I shows that there are two general types of spectra. A comparison between the two different types of spectra is shown in Fig. 3. The spectra of the ammonium halides pressed into NaCl disks are essentially the same as the spectra of thin films of ammonium chloride at room temperature,[10,12] having three strong bands as shown. But the spectra of the ammonium halides pressed into KCl disks resemble (except for exact band positions) the spectra of thin films of ammonium iodide at room temperature.[11] In the latter type there are only two strong bands: one in the 3 μ region and one in the 7 μ region.

The results for the ammonium bromides were the same as for the chlorides. For ammonium halides pressed into NaBr disks the spectra were essentially the same as the spectra of thin films of ammonium bromide at room temperature,[10,11] whereas in KBr disks the spectra resembled the spectra of thin films of ammonium iodide at room temperature. The spectrum of ammonium iodide pressed into either a NaI disk or a KI disk was similar to the spectrum of thin films of ammonium iodide at room temperature, and thus in this case all three spectra are of the same type.

C. Crystal Structure and Ammonium Halides in Solid Solution.—The essential difference between the spectra of thin films of ammonium iodide at room temperature and thin films of either ammonium chloride or bromide at room temperature is attributed to the difference in their crystal

(12) E. L. Wagner and D. F. Hornig, *J. Chem. Phys.*, **18**, 296 (1950).

structure.[11] At room temperature both ammonium chloride and bromide crystallize in the simple cubic (s.c.) CsCl type structure, whereas ammonium iodide crystallizes in the NaCl face centered cubic (f.c.c.) type structure. Thus by comparing the spectra it appears as if the NH_4^+ ions of the ammonium halides pressed into potassium halide disks are in f.c.c. type structures. This can be explained on the assumption that the ammonium exists in a solid solution in the potassium halide. In effect the NH_4^+ ions replace some of the K^+ ions in the potassium halide lattice so that the spectrum of the ammonium halide will indicate an f.c.c. structure, corresponding to the f.c.c. structure of the potassium halide. Similarly on pressing a catalyst with adsorbed NH_4^+, the K^+ and NH_4^+ can exchange and since the NH_4^+ is not too large to go into solid solution with the f.c.c. potassium halide, the observed spectrum is that of ammonium halide in an f.c.c. structure.

To further check the hypothesis that the NH_4^+ ions can exist in a solid solution with the alkali halide whenever the alkali ion is large enough to be replaced by the NH_4^+ ion, the spectra of NH_4Cl and of ammonia-exposed cracking catalyst pressed in CsCl disks were obtained. CsCl like NH_4Cl crystallizes in a simple cubic lattice. As expected the spectra of the ammonium halides and ammonia-exposed cracking catalyst pressed in the CsCl disks were the same. The spectra were similar to that obtained for thin films of NH_4Cl in that two of the strong bands were at 3.19 and 3.29 μ, thus indicating that the NH_4^+ ion is in a simple cubic type structure. It is concluded that the observed spectrum of NH_4Cl is that of NH_4^+ ions dissolved in the simple cubic CsCl lattice and not that of ordinary simple cubic NH_4Cl. The latter conclusion is based on the fact that the spectra are considerably different from that of ordinary NH_4Cl in that the 7.11 μ band is displaced to 6.99 μ and its overtone is displaced from 3.56 to 3.52 μ in addition to both these bands being sharper[13] and the overtone being much stronger than in the spectrum of s.c. NH_4Cl at room temperature as obtained from thin films.[11,12]

D. Use of Sodium Halide Disks.—In the case of pressed sodium halide disks even when exchange is possible, one would not expect the NH_4^+ ion to replace the Na^+ ion in the sodium halide crystal lattice due to the small relative size of the Na^+ ion. Thus, although exchange between the ammonium halides and sodium halides occurs, the spectra of the resulting ammonium halides are the same as the spectra of thin films of the corresponding ammonium halides at room temperature. Similarly in the case of NH_4^+ adsorbed on cracking catalysts and pressed into sodium halide disks, any adsorbed NH_4^+ ions which exchange with Na^+ ions would be too large to form a solid solution in the alkali halide lattice. But unlike pressing a mixture of particles of ammonium halide and sodium halide, the adsorbed NH_4^+ ions are scattered on the catalyst surface. Thus the ammonium halide molecules formed by the exchange would also be scattered and without a suitable medium for migration may be incapable of assembling in large enough quantities to form ammonium halide crystals. The observed spectra would then be those for ammonium ions in uncrystallized small groups of ammonium halide molecules. Therefore the resulting spectra should not be expected to correspond to either type of ammonium halide spectra previously discussed.

Not surprisingly the spectra obtained by the pressed disk technique of an ammonia-exposed mixture of silica–alumina cracking catalyst (or Alon C) and NaCl (or NaBr) are different from the other pressed disk spectra. The spectra show a broad band, presumably due to uncrystallized NH_4Cl (or NH_4Br), at about 6.8 μ, and bands at 3.11 and 3.29 μ. The latter two appear only as shoulders on the strong 2.9 μ band of water adsorbed on the cracking catalyst. Whether the 6.8 μ band is due to ammonium chloride (or bromide) formed by exchange or whether it is NH_4^+ chemisorbed on the cracking catalyst (or Alon C) cannot be definitely determined at this time. But since it was found that exchange occurs with the ammonium halide–alkali halide mixtures and since exchange occurred with all catalyst–potassium halide (and cesium chloride) mixtures, it is believed that the observed band at 6.8 μ in the pressed disks is mainly ammonium chloride (or bromide) in an uncrystallized form. Exchange between the adsorbed NH_4^+ and Na^+ ions is not unreasonable in view of the high concentration of alkali halide compared to adsorbed NH_4^+ ions and in view of the known base exchange properties of cracking catalysts.[14]

Whether moisture is absolutely necessary or how much moisture is necessary to get exchange has not been established. The only precaution taken to exclude water was to grind the materials in a dry box. Exchange is strongly favored by the fact that very low ammonium halide concentrations are required in order to obtain good spectra, and therefore if moisture is necessary for exchange, minute quantities would probably be sufficient to effect a significant amount of exchange during the pressing of the disk. It is believed that with the materials investigated such minute quantities of moisture could be easily picked up by momentary exposure to the atmosphere.

Acknowledgment.—The authors are grateful to Dr. L. C. Roess and Dr. S. A. Francis for the interest they have shown in this work, and to E. J. Bane, D. H. McKinney and J. E. Scardefield for their help with the experimental work.

(13) The half widths are 12 cm.$^{-1}$ for the 6.99 μ band and 25 cm.$^{-1}$ for the 3.52 μ band.

(14) A. G. Oblad, T. H. Milliken, Jr., and G. A. Mills, "Advances in Catalysis," Vol. III, Academic Press, Inc., New York, N. Y., 1951, p. 202.

THE EXPLOSIVE REACTION OF CARBON MONOXIDE AND OXYGEN AT THE SECOND EXPLOSION LIMIT IN QUARTZ VESSELS

BY ALVIN S. GORDON AND R. H. KNIPE

Chemistry Division, U. S. Naval Ordnance Test Station, China Lake, California

Received May 24, 1955

The second explosion limits of pure dry CO–O_2 mixtures have been studied over a range of pressures, temperatures and composition, including the effect of water vapor. On the basis of these studies and previous work on the explosion limits, a mechanism is proposed and discussed.

Introduction

Only a few studies of the explosive reaction between CO and O_2 have been reported. Hadman, Thompson and Hinshelwood (HTH),[1] Gordon,[2] and Hoare and Walsh[3] worked with dry mixtures in a static system. Kopp, Kowalsky, Sagulin and N. Semenoff (KKSS)[4] worked with wet mixtures of CO and O_2 in a flow system. In this present investigation, the technique of HTH[1] has been used.

In chain-branched explosions, the mapping of the second explosion limit is most instructive in ascertaining the mechanism of the reaction; therefore, most studies concentrate on this region.

There are two general methods of obtaining the second explosion limit. In method I, the explosive gases are made up at a high pressure, well above the second explosion limit; the pressure is then reduced until the limit is crossed and the mixture explodes.

In method II, the explosive mixture is made up at low temperatures and the furnace is heated until the mixture explodes when the second explosion limit is crossed.

HTH[1] noted that method I failed for CO–O_2 mixtures and so used method II, as have other workers.[3] Gordon[2] used a furnace on a track so that the mixture could be admitted at low temperature and the hot furnace raised around the reaction vessel; the vessel could be brought to explosion temperature in a minute to a minute and a half. He has reported considerably higher values for the explosion temperature of pure, dry mixtures than those reported by other investigators.[1,3]

In the present investigation the pure, dry mixture has been reinvestigated, using method II with a rate of heating approximately the same as that used by HTH.[1] Also, the effect of very small percentages of water vapor on the second explosive limit was investigated.

Apparatus, Materials and Procedure

A 7″ i.d. vertical cylindrical furnace was employed. A fan in the bottom of the furnace reduced the thermal gradient to less than 15° from the bottom to the top of a 4″ quartz sphere; over most of the vessel the gradient was less than 10°. Explosion temperatures recorded in this work were for the hottest region of the reaction vessel. The gases were admitted to the vessel at low temperatures and heated at 10–15°/min. until explosion occurred. This procedure approximates that employed by HTH.[1]

In some of the experiments gases were admitted to the reaction vessel one at a time at high enough pressures so that the mixture did not explode; the mixture was evacuated until it crossed the limit and exploded.

A Wallace and Tiernan pressure gage was employed in conjunction with the reaction vessel. The diffusion of mercury vapor from the Hg diffusion pump to the reaction vessel was prevented by a Dry Ice trap and by two gold-leaf traps.

CO was generated by phosphoric acid dehydration of formic acid. The gas was passed through a KOH trap and through a coil held at −150° before it was condensed in a liquid N_2 trap. About one third of the liquid CO was evaporated to rid the material of a trace of H_2. CO gas was was distilled to storage directly from the remaining liquid. A glass-wool trap just above the liquid prevented mechanical entrainment of ice particles which might be present in the liquid.

Tank O_2 was condensed in a liquid air trap. About one third of the liquid was evaporated to eliminate most of the N_2 impurity. The gas was distilled to storage from the liquid. A glass-wool trap was employed as above.

Results

From the data plotted in Fig. 1, the following general observations may be made on the $1CO:2O_2$ mixture:

(1) The pure, dry mixture explodes at higher temperatures than those reported by HTH[1] or by Walsh and Hoare,[3] who used a rapid-heating method.

(2) The presence of very small amounts of water vapor has a large effect on the explosion, raising the limit very markedly. Further addition of water vapor raises the limit, but the effect is not nearly as striking as for the first extremely small addition. The effect of water vapor on the second explosion limit was first reported by Gordon,[2] and confirmed by Hoare and Walsh.[5]

(3) If water vapor is present in an explosion, there is a "memory" effect, and the succeeding one or two explosions with the dry mixture have a higher explosion limit than that corresponding to the normal mixture. This effect is not due to absorbed water. Treatment of the surface at low or high temperatures with water vapor prior to the explosion, followed by flushing with a dry gas, does not have any appreciable effect on the succeeding explosion limits of the dry mixture.

(4) The presence of mercury vapor, generated by placing a drop of liquid mercury in the cool vessel, raises the limit. The effect is not as severe or as reproducible as the effect of water vapor.

The work of Gordon[2] has been criticized by Hoare and Walsh[3] on the basis that the fast heating prior to explosion and fast cooling of the quartz surface subsequent to explosion left a film of ab-

(1) G. Hadman, H. W. Thompson and C. N. Hinshelwood, *Proc. Roy. Soc.* (*London*), **A137**, 87 (1932).

(2) A. S. Gordon, *J. Chem. Phys.*, **20**, 340 (1952).

(3) D. E. Hoare and A. D. Walsh, *Trans. Faraday Soc.*, **50**, 37 (1954).

(4) D. Kopp, A. Kowalsky, A. Sagulin and N. Semenoff, *Z. physik. Chem.*, **B6**, 307 (1930).

(5) D. E. Hoare and A. D. Walsh, *Nature*, **170**, 838 (1952).

sorbed gas which accounted for his low explosion limits compared to other investigators. To check this point, the reaction vessel was heated to temperatures of *ca.* 900° for about one hour while it was evacuated with a mercury diffusion pump. Then dry O_2 was admitted to the vessel. The O_2 was pumped out and the vessel heated for about four hours while it was pumped on by the diffusion pump. Finally, the furnace was allowed to cool with the diffusion pump in operation. This type of pre-treatment had no effect on the explosion limit of the dry mixture, within experimental error. The above pre-treatment was employed a number of times during the course of this work, and in no case did it show any effect on the explosion limit. Since these results all gave explosion limits in reasonable agreement with those of Gordon,[2] the explanation advanced by Hoare and Walsh[3] is not tenable.

In the present work we have noted that the addition of a few hundredths of 1% of water vapor to the explosive mixtures increase the explosion limits so that they are in fair agreement with the results of Hoare and Walsh[3] and of HTH.[1] Since H_2 would undoubtedly oxidize to water at a lower temperature than the temperature of the CO–O_2 explosions, our observations offer a possible explanation of the differences in explosion limits.

When the explosive mixture was made up at high temperature and at a pressure above the second explosion limit it could usually be exploded on evacuation. In general, the limits obtained in this manner were erratic and lower than the limits obtained by heating the mixture from low temperature. The treatment of the surface was important in this type of experiment. The mixture was found to be more explosive if a pressure of O_2 was kept in the reaction vessel overnight. Otherwise, the limits got lower with time and eventually no limit could be obtained by the evacuation technique. HTH[1] previously reported on inability to obtain explosions by the evacuation technique.

It is of interest to know the effect of CO_2, the product of the reaction, on the explosion limits. Gordon[2] has shown that the addition of up to 10% of CO_2 lowered the total pressure of the limit. Heating the mixture of CO and O_2 to about 700° from room temperature at about 10°/min. and holding it at 700° for five minutes generates about 3 to 4% CO_2. At higher temperatures more CO_2 is generated before explosion, but for most of our results, the CO_2 present at explosion has no effect on our qualitative conclusions.

When we employed a 4-in. diameter spherical quartz reaction vessel, no light was ever observed prior to explosion of the pure and dry mixture. With traces of water vapor, light was observed prior to explosion.

HTH[1] reported light prior to explosion when they used a cylindrical reaction vessel and dry gases. When we used a cylindrical quartz reaction vessel about 2.5 in. diameter and 6 in. long, a faint glow, rapidly growing in intensity just prior to the explosion, was observed from a temperature starting 50° prior to explosion. HTH[1] used a $1CO:2O_2$ mixture and reported that the manometer fell with increasing temperature when the mixture was heated in the temperature range close to the explosion. We observed this phenomenon only when water vapor was present.

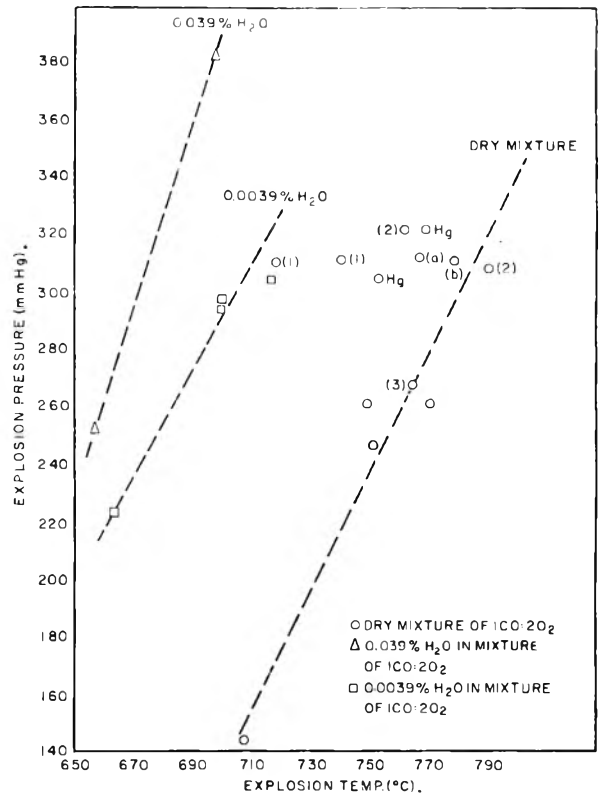

Fig. 1.—Explosion pressure *vs.* explosion temperature for $1CO:2O_2$ showing effect of H_2O vapor and of Hg vapor: (1) first explosion using dry mixture after explosion with H_2O vapor present; (2) second explosion using dry mixture after explosion with H_2O vapor present; (3) third explosion using dry mixture after explosion with H_2O vapor present; (a) surface treated with 0.0058% H_2O in O_2 at 800°, then the reaction vessel is evacuated while it is cooled to about 350° prior to the experiment with a dry mixture of $1CO:2O_2$; (b) second explosion limit experiment after (a) treatment.

Discussion

All the investigators agree that at the second limit the explosion temperature increases with increased explosion pressure and that the pressure limit decreases with increasing CO/O_2. Gordon[2] reported that the limit of both the wet and the dry mixtures decreased with increasing surface/volume of the quartz reaction vessel. Kopp, Kowalsky and Semenoff[4] reported no effect of surface/volume on the second explosion limit of wet mixtures of CO and O_2 in a flow system.

In the present work it was noted that the withdrawal method gave erratic results in mapping the second explosion limit. These results emphasize the important role played by the surface in the CO/O_2 explosion. Since a limit could be obtained by this withdrawal method, the explosion is probably chain-branched. The chain-branched character is also shown because the "slow" reaction is extremely slow, a few millimeters above the limit.

Contrary to the results of KKSS,[4] who used wet mixtures and a flow system, Gordon reported that up to 17% N_2 and up to 10% CO_2 could replace the corresponding percentage of the explosive mixture and raise the total limit pressure (the mixture with

the inerts is more explosive than the inert-free mixture).

Finally, the strong effect of water vapor in raising the second explosion limit of CO/O_2 mixtures seems to be well established.

From the foregoing qualitative findings, the mechanism of the explosion must have a chain branching step of lower order than the chain quenching step, since increasing pressure quenches the explosion. Also, the energy of activation of the chain-branching reaction must be higher than the chain quenching reaction, since the quench of the explosion by the increase in pressure is overcome by increasing the temperature. Finally, the effect of composition and inerts must be taken into account.

The chain branched character must involve O atoms since the >200 kcal. bond of the CO molecule is not likely to be broken as part of the explosion mechanism. O atoms may form O_3, O_2*, O_2, CO_2*, CO_2 molecules. Experiments with O atoms in the presence of CO and O_2 at temperatures up to 100° show the formation of O_3 to be about 100 times as fast as the total formation of CO_2.[6] However, O_3 is not a likely chain carrier because: (1) the equilibrium constant relating its concentration to that of O and O_2 is most unfavorable as the temperature is increased.

(2) Garvin[7] has reported that O_3 and CO do not react appreciably at about 200°, and that CO is oxidized by O atoms.

(3) Both CO and O_3 have singlet ground states and we have been unable to find any clear-cut cases where two singlet molecules react directly. This is no doubt analogous to the failure of atoms with singlet ground states to react readily with one another.[7a]

From energy considerations the elimination of O_3 leaves only O_2*, O_2, CO_2* and CO_2 as molecules which can be important in the explosion. O_2* probably cannot be formed from two O atoms in a bimolecular collision.

Although an O_2 molecule could be formed from two oxygen atoms in a termolecular collision, this process would be chain quenching and would be second order with respect to oxygen atoms. Unless the chain-branch process were also at least second order with respect to O atoms, an explosion would not be possible since the quenching process would be more efficient than the branch as the oxygen atom concentration built up. Under these conditions the branching reaction would be minimal third order. Thus, the breaking process would have to be minimal fourth order, which is quite impossible in the pressure range we explored.

Only CO_2 and CO_2* remain as products of O atom reaction. For the chain branching reactions, CO_2* could transfer its energy to O_2 forming O_2*, but this is unlikely because the Schuman-Runge O_2 bands, which are present in the CO–O_2 explosion, have been shown to be probably thermal by Wolfhard and Parker.[8]

From all the foregoing, we believe the CO–O_2 explosion mechanism to be

$$CO + O \longrightarrow CO_2^* \quad (1)$$

$$CO_2^* + O_2 \longrightarrow CO_2 + 2O \quad (2)$$

$$CO_2^* + M \longrightarrow CO_2 + M \quad (3)$$

$$CO + O + M \longrightarrow CO_2 + M \quad (4)$$

$$\left.\begin{matrix} O \\ CO_2^* \end{matrix}\right\} \text{diffusion to the wall with subsequent quench} \quad (5)$$

For a chain branched explosion at the second explosion limit, the rate of chain-branch reaction equals the rate of chain-break reactions. This may be stated for the above mechanism as

for CO_2*

$$k_1[CO][O] = k_2[CO_2^*][O_2] + k_3[CO_2^*][M] + Q_1[CO_2^*]$$

for O

$$2k_2[CO_2^*][O_2] = k_1[CO][O] + k_4[CO][O][M] + Q_2[O]$$

Eliminating $[CO_2^*]$ and $[O]$ in the above, the pressure is given by

$$P = \frac{k_2 - k_3\frac{[M]}{[O_2]} - \frac{Q_1}{[O_2]} - \frac{Q_2}{k_1[CO]}\left(k_2 + k_3\frac{[M]}{[O_2]} + \frac{Q_1}{[O_2]}\right)}{\frac{k_4[M]}{k_1P}\left(k_2 + k_3\frac{[M]}{[O_2]} + \frac{Q_1}{[O_2]}\right)} \quad (6)$$

In the above expression $[CO]/[O_2]$ is one of the terms in $[M]/[O_2]$. k_1 and k_2 are the pressure and composition independent rate constants of reactions (1) and (2). k_1 is tacitly assumed to have an energy of activation. We think this is more likely than that k_2 has an energy of activation, because at low temperatures oxygen atoms form O_3 in preference to CO_2 in a mixture of CO and O_2.[6] $k_3[M]/[O_2]$ and $k_4[M]/P$ are composition dependent, pressure independent rate constants for reactions (3) and (4); $Q_1/[O_2]$ and $Q_2/[CO]$ represent the effect of quenching the CO_2* and O at the wall. According to Kassel and Storch,[9] these latter quantities should vary from zero with no heterogeneous quenching to $\gamma/r_0^2P^2$ in the case of complete quenching where γ is dependent on the composition and temperature, and r_0 is the radius of the vessel.

Equation 6 qualitatively satisfies all the experimental observations, including the effects of temperature, CO/O_2 ratio, inerts and surface on the pressure limit of explosion. An attempt to obtain quantitatively the large observed effect of surface has failed even though a wide range of reasonable values of the rate constants has been considered. This quantitative failure appears to be characteristic of any mechanism where the second limit is due to the competition of a bimolecular branch and a termolecular quench reaction. The observed pressures make it unreasonable to expect the higher order quench reaction necessary to get predicted effects of the same magnitude as those observed. For this reason, we believe the quantitative failure to be due primarily to shortcomings in the theory of the heterogeneous quenching terms Q_1 and Q_2, rather than to shortcomings in the postulated mechanism.

The mechanism which is presented here is essentially that which was suggested by Semenoff[10] as

(6) W. B. Jackson, *J. Am. Chem. Soc.*, **56**, 2631 (1934).

(7) D. Garvin, *ibid.*, **76**, 1523 (1954).

(7a) NOTE ADDED IN PROOF:—A discussion of the high activation energy requirements for the reaction of two singlet molecules has recently been given by V. Griffing, *J. Chem. Phys.*, **23** 1015 (1955).

(8) H. G. Wolfhard and W. G. Parker, *Proc. Phys. Soc., London*, **A65**, 2 (1952).

(9) L. S. Kassel and H. H. Storch, *J. Am. Chem. Soc.*, **57**, 672 (1935).

(10) N. Semenoff, *Chem. Revs.*, **6**, 347 (129).

one possibility which could qualitatively fit the observations. No attempt was made to justify the elementary steps. Reaction (1) is especially difficult to justify, and it has been criticized by Lewis and von Elbe[11] because the CO_2^* resulting from a bimolecular collision would be expected to have too short a half-life to be effective as a chain carrier. If the lifetime of the CO_2^* molecule is calculated on the basis of the probability that the binding energy accumulates in the correct bond, a lifetime of about 10^{-11} sec. results, while the time between collisions is $\sim 10^{-10}$ sec.

To explore other possibilities for bimolecular formation of stable CO_2^*, qualitative potential energy surfaces were constructed on the basis of the correlation diagram of Walsh[12] (see Appendix). The symmetry properties of the collision complex allow for crossings of the surfaces of the type discussed by Teller.[13] These crossings can lead to the binding of an excited CO_2 for a time considerably in excess of that to be expected from bimolecular collision without the crossings. Thus, it is expected that the CO_2^* formed in reaction (1) will be sufficiently long lived to take part in the reactions (2) and (3). As a result, the effective concentration of the CO_2^* will probably be quite low, consistent with all the experimental observations.

Hoare and Walsh[3] have discussed the CO–O_2 mechanism of Laidler and Lewis and von Elbe

$$O + O_2 + M = O_3 + M \quad (7)$$

$$O_3 + CO = CO_2 + 2O \quad (8)$$

$$O_3 + CO + M = CO_2 + O_2 + M \quad (9)$$

They point out that there is no *a priori* reason to expect (9) to be termolecular. In the bimolecular reaction of CO and O_3 to give CO_2 and O_2, the CO_2 must be in a low lying triplet state to satisfy the multiplicity requirements. If M is exclusively O_2 in reaction (9), then the CO_2 may be singlet. However, the experimental observations are now in conflict with the prediction from the mechanism. The existence of a low lying triplet state of CO_2 has been postulated by Walsh.[12] We have also assumed this species in reactions (3) and (4).

Hoare and Walsh[3] state that the chain-branch reaction may be as in reaction (2) and they assume the chain-break reaction to be

$$CO_2^* + O_2 + M \longrightarrow \text{inert products} \quad (10)$$

We believe that their criticism of reaction (9) applies equally to reaction (10).

Appendix

The Bimolecular Reaction of Carbon Monoxide and an Oxygen Atom.—To investigate the possibility of the bimolecular reaction of CO and O, qualitative potential energy surfaces for the CO–O collision have been constructed and studied. Since spectroscopic information for these states is meager, the surfaces have been based on the correlation diagram of Walsh[12] which is consistent with what is known about CO_2 and a number of related molecules. Potential surfaces for a linear O–C–O approach, which we shall refer to as a 180° approach have been considered by Goodeve[14] and Weeks.[15] These considerations were based on a correlation diagram of Mulliken,[16] and offer no evidence that the 180° collision will result in a bound CO_2 molecule with a sufficiently high probability to be of kinetic significance. This situation is more favorable in the case of Walsh's correlation diagram as we shall illustrate.

The collision of CO and O involves three atoms, hence may be considered to take place in a plane. The only symmetry element for the collision is the reflection across this plane. For a description of the internal motion in this plane, we choose the distance r between the center of mass of the CO and the colliding oxygen atom, and the angle (θ) between the CO bond and the line along which r is measured. The internal motion of the CO is neglected, so that the collision is considered as the interaction of two bodies, the interaction being dependent on r and a coördinate u proportional to θ. We justify neglecting the effect of the internal motion of the CO on the basis that if the collision is to be effective in forming a bound CO_2, the change in CO distance in the CO molecule is small compared to the change in r.

Since we wish to consider the collision of CO and O in their ground states, we consider only the triplet surfaces. According to the correlation diagram of Walsh,[12] the lowest configurations for the linear molecule, in order of increasing energy, are

electronic configuration		molecular terms
$(\pi_g)^3(\bar{\pi}_u)$	⟶	$^3\Delta_u$, $^3\Sigma_u^-$, $^3\Sigma_u^+$
$(\pi_g)^3(\bar{\sigma}_g)$	⟶	$^3\Pi_g$

The colliding reactants present the following low-lying configurations, again in order of increasing energy

CO	O		molecular terms[17]
($^1\Sigma^+$)	(^{3}P)	⟶	$^3\Pi$, $^3\Sigma^-$
($^3\Pi_r$)	(^{3}P)	⟶	$^3\Delta$, $^3\Pi$, $^3\Sigma^-$, $^3\Sigma^+$

The correlation of the reactants with the linear O–C–O is then

CO	O		molecular term		electronic configuration
($^3\Pi_r$)	(^{3}P)	⟶	$^3\Delta$	⟵	$(\pi_g)^3(\bar{\pi}_u)$
($^1\Sigma^+$)	(^{3}P)	⟶	$^3\Sigma^-$	⟵	$(\pi_g)^3(\bar{\pi}_u)$
($^3\Pi_r$)	(^{3}P)	⟶	$^3\Sigma^+$	⟵	$(\pi_g)^3(\pi_u)$
($^1\Sigma^+$)	(^{3}P)	⟶	$^3\Pi$	⟵	$(\pi_g)^3(\bar{\sigma}_g)$

It is significant that it is necessary to bring in the excited CO($^3\Pi_r$) in order to obtain a correlation with the $^3\Delta$ and $^3\Sigma^+$ belonging to the lowest O–C–O configuration. Further, if the formation of the O–C–O in the $^3\Pi$ state may be considered as an attack of the lone pσ electron of the colliding oxygen on the lone pair of electrons on the carbon of CO, no activation energy is expected. In an association to form the O–C–O($^3\Sigma^-$) from the ground state of the reactants, some activation energy is expected to be required in order to localize a lone p_{xy} electron as a pσ so that it may effectively attack the lone pair on the carbon. Therefore, we expect the $^3\Sigma^-$ to have initially a repulsive profile for a 180° approach.

(11) B. Lewis and G. von Elbe, "Combustion, Flames and Explosions of Gases," Academic Press, Inc., New York, N. Y., 1951, p. 78.

(12) A. D. Walsh, *J. Chem. Soc.*, 2266 (1953).

(13) E. Teller, THIS JOURNAL, **41**, 109 (1937).

(14) C. F. Goodeve, *Trans. Faraday Soc.*, **30**, 60 (1934).

(15) I. F. Weeks, "3rd Symposium on Combustion," The Williams and Wilkins Co., Baltimore, Md., 1949, p. 552.

(16) R. S. Mulliken, *Rev. Mod. Phys.*, **14**, 204 (1942).

(17) The correlations between the reactant terms and molecular terms are given by K. E. Shuler, *J. Chem. Phys.*, **21**, 624 (1953).

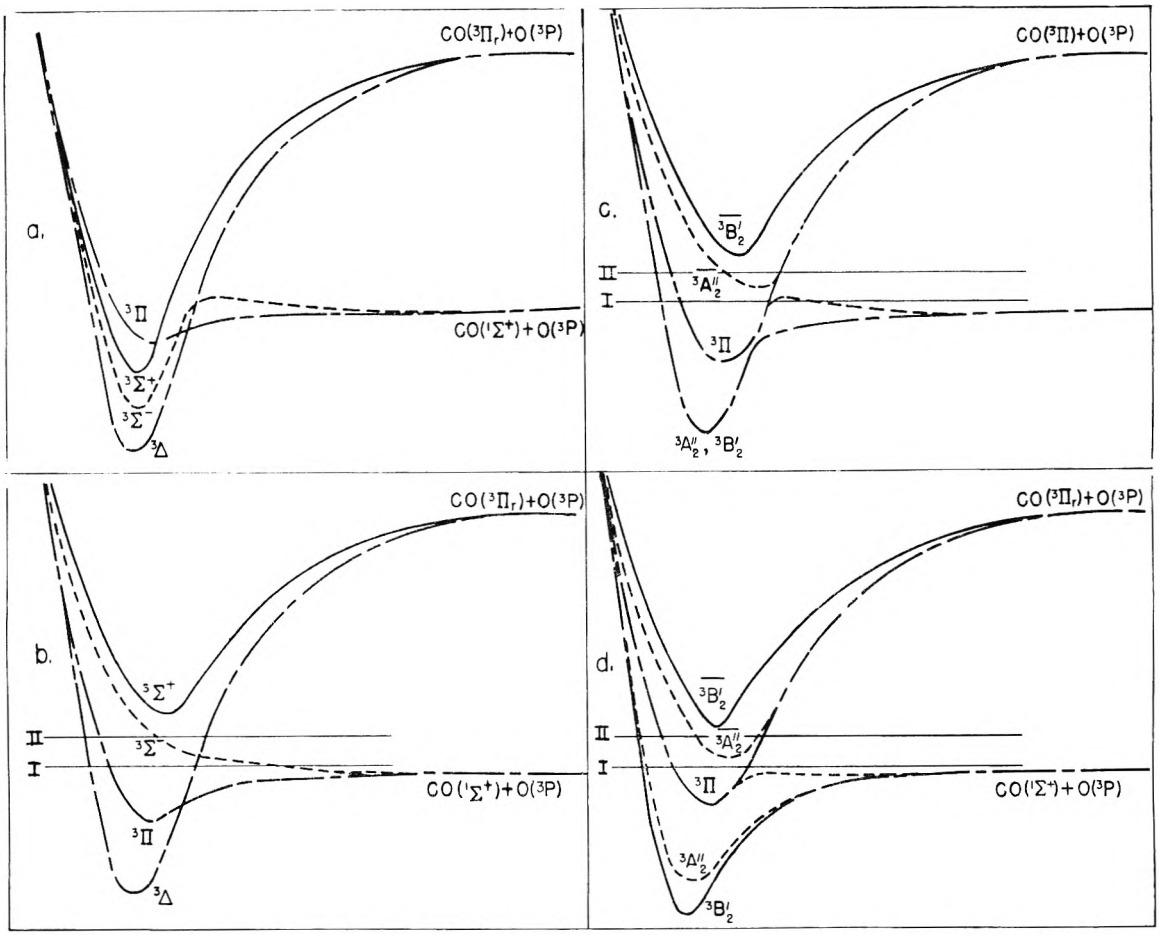

Fig. 2.—Cross section of the potential surfaces for the carbon monoxide–oxygen collision: (a) linear collision with $^3\Delta$, $^3\Sigma^-$ and $^3\Sigma^+$ below $^3\Pi$; (b) linear collision with only $^3\Delta$ below $^3\Pi$; (c) non-linear collision ($\theta \sim 160°$) corresponding to (b); (d) non-linear collision ($\theta \sim 140°$) corresponding to (b); ——, symmetric to plane of collision; ------, antisymmetric to plane of collision; — — —, both antisymmetric and symmetric which for simplicity are not split. The term symbols in (c) and (d) refer to the equilibrium molecular configuration in the notation of Walsh[12] with ′ and ″ added to indicate symmetric and antisymmetric with respect to the plane.

There remains one further point with respect to the qualitative behavior of the surfaces, that is, the order of the molecular states. If it is assumed that the order is dominated by the electronic configuration, we should expect, in order of increasing energy, the terms to be $^3\Delta$, $^3\Sigma^-$, $^3\Sigma^+$, $^3\Pi$. Since we expect the $^3\Pi$ to be bound, this order requires that there be four binding surfaces in an interval which is probably considerably less than 100 kcal. On the other hand, if the electronic interaction energies were the order of the energy difference between the $\bar{\pi}_u$ and $\bar{\sigma}_g$ orbitals, the $^3\Pi$ term may lie below one or both of the $^3\Sigma$ terms of the $(\pi_g)^3(\bar{\pi}_u)$ configuration. The two extreme cases are illustrated in Figs. 2a and b.

In the figure only those energies in the neighborhood of and below the ground state of the reactants are of interest. At higher energies the additional molecular terms are expected to introduce complications which are not shown. In anticipation of our consideration of non-linear collisions, terms symmetric to the plane of collision are distinguished from antisymmetric terms. As pointed out above, this is the only symmetry element of significance with respect to the collision.

On the basis of the correlation diagram of Mulliken,[16] the members of the $(\pi_g)^3(\bar{\pi}_u)$ configuration would be above the $^3\Pi$, thus making the $^3\Sigma^-$ extremely repulsive. In either of the cases of Fig. 2, curves which correlate for a non-linear collision cross. The surfaces for both cases have been studied with similar results. The simpler of the two cases (Fig. 2b) is discussed below.

For an angle somewhat different from 180°, we expect interaction between the surfaces of the same symmetry with respect to reflection across the plane of the collision. For relative velocities of the reactants sufficiently small, this interaction may be represented by the non-crossing of the surfaces for non-linear collisions (Figs. 2c and d). Walsh[12] has estimated all of the low-lying surfaces to have their minima for $180° \geq \theta \geq 135°$. For angles smaller than the angle of the minima, the surfaces are expected to become repulsive. This repulsive character for angles considerably different from 180° tends to accelerate the reacting systems toward the 180° configuration, thus increasing the probability that the reacting system will come into that region near 180° where there is the greatest interaction between the surfaces (Fig. 2c).

In the polyatomic molecules, the crossing of the system from one to another in the region of strong interaction between these surfaces has been dis-

cussed by Teller.[13] The probability that the system crosses from one surface to the next is dependent on the velocity of the system and the strength and geometrical properties of the interaction. How these results apply in the case of the surfaces which we consider here may be seen qualitatively by considering some particular cases.

Let us consider two energies of the reacting system designated by I and II (Fig. 2). Consider Fig. 2b, a system with either of these energies which has a turning point at the repulsive wall of the $^3\Delta$ will also turn at the attractive wall of the $^3\Delta$ curve; a system with energy II which turns at the repulsive wall of the $^3\Sigma^-$ will dissociate along this curve; and a system with energy I which turns at the repulsive wall of the $^3\Pi$ will dissociate along this curve. These conclusions follow from there being no interaction between these curves for a linear collision.

In Fig. 2d, the angle has been chosen such that the interaction between the indicated surfaces is small. For order of magnitude considerations, θ may be considered to be in the neighborhood of 140°. For this case, an antisymmetric system with energy II which turns at the repulsive $^3\bar{A}_2''$ wall will most probably dissociate, and a system which turns at the repulsive wall of the $^3\bar{A}_2''$ will most probably turn at the attractive wall of the $^3\bar{A}_2''$. A symmetric system with energy I which turns at the repulsive $^3B_2'$ wall will most probably dissociate; whereas, if it turns at the repulsive $^3\Pi$ wall, it will most probably turn at the attractive $^3\Pi$ wall.

In Fig. 2c, where the angle is intermediate between that of b and d, say 160°, behavior intermediate between that of b and d is expected. Thus a system approaching the repulsive wall from great distance along the antisymmetric extension of the $^3\Pi$ with energy II would, with a certain probability, be reflected at the repulsive wall of the $^3\bar{A}_2''$, and upon returning to the attractive $^3\bar{A}_2''$ wall, would be reflected again with a certain probability, and thus undergo the multiple reflections of a bound system. A similar situation holds for an approach along the $^3B_2'$ surface with energy I, where there is the possibility of multiple reflections at the walls of the $^3\Pi$ surface.

This very qualitative analysis is, of course, extremely simplified. In particular, the effect of transferring energy to the neglected CO bond at the repulsive walls may affect further crossings of the potential curves at their repulsive walls. This energy transfer, in the case of systems with low initial kinetic energy, would reduce the energy in the part of the system shown to a point where dissociation was not possible. At some later time in the normal course of the molecular vibrations when the energy was returned to the part of the system which we have considered, the angle could be changed to some more favorable angle for either dissociation or binding. In the case of the spacings of the surfaces shown in Fig. 2a, the effect of energy transfer in inducing crossings should be considerably more important than in the case which we have discussed.

The effect of the repulsion for small values of θ increases the probability that the colliding system will pass through that section of the surfaces where crossing from one surface to another can occur most readily. It appears probable, therefore, that the bimolecular collision of CO and O should be effective in producing excited triplet states of the CO_2 molecule with sufficient lifetimes to be of kinetic significance. It further appears that the CO_2^* of reaction (1) is not a single molecular state, but a small number of states. These states would have different lifetimes. The energies of activation required for forming these states from ground state CO and O will also be different. It is possible for certain of these states to have energies higher than the ground states of the dissociated reactants. In the case of Fig. 2a, this situation is obtainable from higher electronic configurations than the two which have never been considered.

THE CONFIGURATION OF POLYMER MOLECULES: POLYSTYRENE IN CYCLOHEXANE[1]

BY W. R. KRIGBAUM AND D. K. CARPENTER

Contribution from the Department of Chemistry, Duke University, Durham, North Carolina

Received May 27, 1955

In order to test Flory's postulate that the effective hydrodynamic radius of a polymer molecule is proportional to some average linear dimension of the molecule, light scattering and viscosity measurements were performed for a polystyrene fraction ($<M>_w = 3.2 \times 10^6$) in cyclohexane at five temperatures. The 25° interval studied includes the Flory Θ temperature. The observed dependence of $<\bar{R}^2>_z$ upon A_2 is in approximate agreement with the recent treatment of Zimm, Stockmayer and Fixman. When the Flory postulate is tested by plotting $[\eta]$ against $<\bar{R}^2>_z^{1/2}$ using a log-log scale, the points fall on a line of slope 2.2, instead of 3.0 as anticipated. As A_2 increases from zero, Φ values calculated from these data decrease by 25%, with the most rapid decrease occurring in the vicinity of $A_2 = 0$. Thurmond and Zimm first called attention to the possibility of a decrease in Φ with increasing solvent power. Examination of data in the literature provides further confirmation of this variation of Φ with A_2.

Two important quantities required for the characterization of a polymer are the molecular weight and the average molecular configuration in dilute solution, as expressed by the RMS displacement length, $(\bar{L}^2)^{1/2}$, or the RMS radius of gyration, $(\bar{R}^2)^{1/2}$. Light scattering allows direct determination of both M and R^2. If the data are plotted by the Zimm method,[2] the weight average molecular weight, $<M>_w$, and the z-average mean square radius of gyration, $<\bar{R}^2>_z$, can be obtained by constructing the "limiting tangent."

Hydrodynamic properties offer a second possible approach to polymer characterization. The hydrodynamic treatments[3] of Kirkwood and Riseman, and Debye and Bueche, assume that the polymer chain obeys random flight statistics (*i.e.*, that $\bar{L}^2 \sim M$), and introduce a permeation factor which, in effect, results in a hydrodynamic radius (*cf.* equation 1 below) which increases with M more rapidly than does $(\bar{L}^2)^{1/2}$. Flory[4] has proposed alteration of these treatments to account for the effect of excluded volume on the average molecular configuration. In particular, he has proposed the following modifications: (a) that the permeation factors in the KR and DB treatments are at their asymptotic limits for flexible chain polymers over the molecular weight range of interest, (b) that the effective hydrodynamic radius is approximately proportional to some average linear dimension of the polymer coil, such as $(\bar{L}^2)^{1/2}$ or $(\bar{R}^2)^{1/2}$ and (c) that $(\bar{L}^2)^{1/2}$ or $(\bar{R}^2)^{1/2}$ is in general expanded over the corresponding dimension for the unperturbed configuration by a factor α which increases with M due to excluded volume effects.

When these proposed modifications are tested experimentally, it is found from intrinsic viscosity measurements[5] at the Flory Θ temperature that $[\eta]_\Theta \sim M^{1/2}$, indicating that the hydrodynamic factors in the KR and DB treatments are indeed constant (postulate a) for flexible chain polymers down to surprisingly low molecular weights. There is also sufficient evidence[6,7] to indicate that the average molecular configuration is expanded in thermodynamically good solvents by a factor which increases with M (postulate c), at least throughout the observable molecular weight range.

There remains the question of how accurately the proposed proportionality between the hydrodynamic radius and $(\bar{L}^2)^{1/2}$ or $(\bar{R}^2)^{1/2}$ (postulate b) is obeyed. For intrinsic viscosity this has been stated[4] as

$$[\eta] \sim \mathfrak{R}_H^3/M \quad (1)$$

$$[\eta] = 6^{3/2}\Phi(\bar{R}^2)^{3/2}/M \quad (2)$$

where $\mathfrak{R}_H$ is the effective hydrodynamic radius and Φ is a constant for any polymer–solvent pair, independent of temperature and the polymer molecular weight. The proposed constancy of Φ may be tested in various ways. For example, one may select a given polymer-solvent pair and test a series of fractions differing in molecular weight, or employ different polymer-solvent pairs, or examine a single polymer fraction in a variety of solvents, or in a poor solvent at various temperatures in the vicinity of the Flory Θ temperature. Considerable evidence has accumulated[6,8–11] to indicate that Φ is approximately constant (*i.e.*, that $\mathfrak{R}_H$ is at least approximately proportional to $(\bar{R}^2)^{1/2}$). The data of Thurmond and Zimm[12] are an exception to the above generalization. They report a higher Φ value for a given polymer fraction in a solvent-precipitant mixture than that observed in a single good solvent, this effect becoming more pronounced if the polymer is branched.

The effect of varying solvent power upon Φ is examined in the present paper by light scattering and viscosity measurements on a single polystyrene

(1) (a) This investigation was supported by the Allegany Ballistics Laboratory, an establishment owned by the United States Navy and operated by Hercules Powder Company, under Contract NOrd 10431. (b) Presented before the Division of Polymer Chemistry at the 127th meeting of the American Chemical Society, Cincinnati, Ohio, April 4, 1955.

(2) B. H. Zimm, *J. Chem. Phys.*, **16**, 1093, 1099 (1948).

(3a) J. G. Kirkwood and J. Riseman, *ibid.*, **16**, 565 (1948).

(3b) P. Debye and A. M. Bueche, *ibid.*, **16**, 573 (1948).

(4) P. J. Flory, *ibid.*, **17**, 303 (1949); P. J. Flory and T. G. Fox, *J. Am. Chem. Soc.*, **73**, 1904 (1951).

(5) W. R. Krigbaum, L. Mandelkern and P. J. Flory, *J. Polymer Sci.*, **9**, 381 (1952).

(6) H. J. Cantow and G. V. Schulz, *Z. physik. Chem.*, [N.F.] (Frankfurt), **2**, 117 (1954).

(7) A. R. Shultz, *J. Am. Chem. Soc.*, **76**, 3422 (1954).

(8) (a) H. J. Cantow and O. Bodmann, *Z. physik. Chem.*, [N.F.] (Frankfurt), **3**, 65 (1955); (b) G. V. Schulz, J. J. Cantow and G. Meyerhoff, *J. Polymer Sci.*, **10**, 79 (1953).

(9) J. Bischoff and V. Desreux, *ibid.*, **10**, 437 (1953).

(10) T. G. Fox and L. Mandelkern, *J. Chem. Phys.*, **21**, 187 (1953).

(11) S. Newman, W. R. Krigbaum, C. Laugier and P. J. Flory, *J. Polymer Sci.*, **14**, 451 (1954).

(12) C. D. Thurmond and B. H. Zimm, *ibid.*, **8**, 477 (1952).

fraction of high molecular weight in cyclohexane. These measurements cover a 25° temperature range which includes the Flory Θ temperature, which is 307.6 ± 0.2°K. according to osmotic pressure[13] and precipitation temperature[14] measurements. This procedure possesses the advantage that the ratio of Φ values at two temperatures can be deduced without resorting to correction[11] of the observed averages, $<M>_w$ and $<\bar{R}^2>_z$, to number averages.

Experimental

Materials.—A polystyrene sample of high molecular weight was prepared by slow thermal polymerization at room temperature. This was subjected to an initial fractionation, and the center cut was further fractionated from a 0.08% benzene solution. The sample employed, HB2-3, was obtained by combining the two middle fractions. Reagent grade cyclohexane was dried over sodium and distilled before use. Precautions were taken to exclude water from both the solvent and the solutions. The concentrations of all but the most dilute solutions were determined by dry weights. Those of the most dilute solutions were determined from known dilution factors.

Intrinsic Viscosity.—The viscosity measurements were performed using a Ubbelohde viscometer calibrated for kinetic energy corrections. The flow time for water was 276 sec. at 20°. Values of (η_{sp}/c) and $(\ln \eta_{rel})/c$ were simultaneously extrapolated to zero concentration to obtain the intrinsic viscosity, $[\eta]$, for each temperature. In view of previous measurements,[15] rate of shear corrections were presumed to be negligible in this poor solvent.

Light Scattering.—The light scattering instrument is similar to that developed by Debye,[16] and will be described in detail in a forthcoming publication. Each solution to be investigated was centrifuged at 20,000 *g* for 1.5 hours to remove dust, and then transferred to a conical scattering cell fitted with a ground glass stopper. This cell was positioned reproducibly inside a cylindrical cell filled with solvent, which bore two side arms. One of these admitted the beam through an optically flat face, while the other formed a horn which trapped the transmitted beam. The outside of the cylindrical cell was painted black, except for the flat entrance face and the side through which the scattering was observed. The cylindrical cell was surrounded by a tightly fitting double-walled metal jacket through which oil was circulated from one of a series of constant temperature baths. The temperature inside the cylindrical cell was determined by means of a four junction copper–constantan thermocouple inserted through the top of the jacket and immersed in the solvent. The temperature could be controlled to within 0.05° over long periods of time, and the variation was considerably less during the period of observation. A set of measurements at five temperatures was performed for each solution before refilling the cell. Intensities were observed over the angular range 45–130°, using vertically polarized incident light and a color filter inserted near the receiver which transmitted the 4358 Å. mercury line. The reduced intensities, I_v, are reported in Rayleigh ratio units. The primary standard of intensity was a 0.5% toluene solution of the "Cornell Standard" polystyrene, having for its excess scattering a Rayleigh's ratio $\mathbf{R}_v = 4.20 \times 10^{-4}$ cm.$^{-1}$ at 4358 Å., which corresponds to an "apparent turbidity," $(16\pi/3)\,\mathbf{R}_u$, of 3.50×10^{-3} cm.$^{-1}$. The volume correction was negligible, and no depolarization correction was applied. The n^2 refractive index correction[17] was employed.

Refractive index differences were measured using a Brice–Speiser differential refractometer calibrated with sucrose solutions, taking for the latter $dn/dc = 0.145$ at 30° and 4358 Å. Measurements for polystyrene–cyclohexane covering the temperature range 33.8–41.9° yielded $dn/dc = 0.183$ at 4358 Å. and 0.173 at 5460 Å. No temperature dependence was detected within this 8° interval. The value 0.173 at 5460 Å. may be compared with 0.179 at 40° calculated by Outer, Carr and Zimm[18] using the Gladstone–Dale relation.

Results

A. Treatment of Experimental Data.—Angular intensity measurements were obtained for six concentrations of the polystyrene fraction in cyclohexane at five temperatures ranging from 32.5 to 55°. From these data $(c/I_v)_{\substack{c=0,\\ \theta=0}}$, $<\bar{R}^2>_z$ and the virial coefficient A_2 were evaluated for each temperature. For each solution, $(1/I_v)$ was plotted against $\sin^2(\theta/2)$, as illustrated in Fig. 1. The intercept of the curve for each temperature yielded values for $(1/I_v)_{\theta=0}$. Since the actual temperature of measurement for each solution varied from the nominal value by a few tenths of a degree in some cases, for each of seven angles (including 0°) $(1/I_v)$ was plotted against T, the smoothed curves for each solution providing values of $(1/I_v)$ in terms of θ and T. From these curves values of $(c/I_v)_\theta$ were determined for each nominal temperature, taking into account the effect of temperature on concentration, and these were plotted against concentration. The resulting intercepts, $(c/I_v)_{c=0}$, were then plotted against $\sin^2(\theta/2)$, and limiting tangents were calculated according to the Zimm method.[2] As shown in Fig. 2, $(c/I_v)_{c=0}^{CORR}$ was linear when the heterogeneity parameter, h,[19] was assigned the value 4, corresponding to $<M>_w/<M>_n = 1.25$ and $<M>_z/<M>_w = 1.20$. Values for $(c/I_v)_{\substack{c=0\\ \theta=0}}$

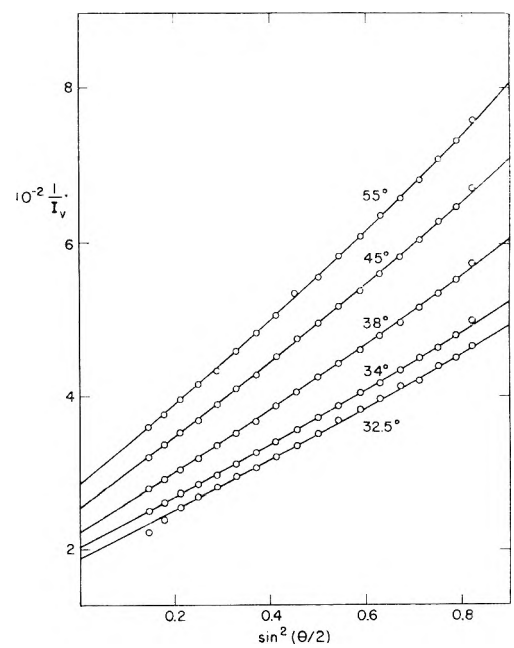

Fig. 1.—Reciprocal intensities plotted against $\sin^2(\theta/2)$ for the solution having $c = 1.104 \times 10^{-3}$ g./cm.^{3} at 35°. The centigrade temperature is indicated for each set of points.

(13) W. R. Krigbaum, *J. Am. Chem. Soc.*, **76**, 3758 (1954).

(14) A. R. Shultz and P. J. Flory, *ibid.*, **74**, 4760 (1952).

(15) W. R. Krigbaum and P. J. Flory, *J. Polymer Sci.*, **11**, 37 (1953).

(16) P. J. Flory, "Principles of Polymer Chemistry," Cornell University Press, Ithaca, N. Y., 1953, p. 284.

(17) J. J. Hermans and S. Levinson, *J. Opt. Soc. Am.*, **41**, 460 (1951).

(18) P. Outer, C. I. Carr and B. H. Zimm, *J. Chem. Phys.*, **18**, 830 (1950).

(19) To avoid confusion, the parameter characterizing the molecular weight heterogeneity is designated by h rather than z, as in ref. 2.

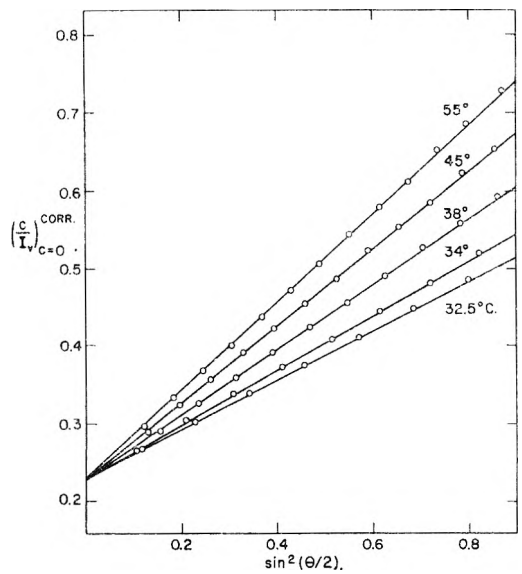

Fig. 2.—$(c/I_v)^{CORR}_{c=0}$ values for various temperatures plotted against $\sin^2(\theta/2)$. $(c/I)^{CORR}_{c=0}$ was calculated according to the procedure of Zimm,[2] setting $h = 4$.

and $\langle\overline{R^2}\rangle_z$ appearing in columns two and four of Table I were obtained from the intercepts and slopes of the curves shown in Fig. 2. Finally, values of $(c/I_v)_{\theta=0}$ deduced from the intercepts of the plots illustrated in Fig. 1 were extrapolated to zero concentration according to the procedure of Fox, Flory and Bueche,[20] but employing values for the factor g relating the third and second coefficients calculated according to the treatment of Stockmayer and Casassa.[21] Values so obtained for the osmotic second coefficient, A_2, appear in column three of Table I. Values for $(c/I_v)_{c=0,\theta=0}$ obtained in this way were practically identical ($\pm 1\%$) with those in column two. Since the factor g was always small, the linear plot of $(c/I_v)_{\theta=c}$ against c shown in Fig. 3 led to approximately the same values for the intercepts and second coefficients as those obtained from the more accurate treatments described above.

TABLE I

PARAMETERS FOR POLYSTYRENE HB2-3 IN CYCLOHEXANE

T, °K.	$(c/I_v)_{c=0,\theta=0}$	10^4A_2[a]	$\langle\overline{R^2}\rangle_z^{1/2}$ (Å.)	$[\eta]$[b]	$10^{-21}\Phi$
305.7	0.230	−0.153	494	1.06	2.6
307.2	.229	− .084	518	1.22	2.6
311.2	.227	.113	576	1.47	2.3
318.2	.230	.312	625	1.78	2.2
328.2	.232	.538	665	2.10	2.0
333.2	...	...	(690)	2.25	(2.0)

[a] A_2 in cm.³ mole/g.². [b] $[\eta]$ in deciliters/g.

B. $\langle M\rangle_w$, Θ, ψ_1 and $\overline{L_0^2}/M$.—Values for $(c/I_v)_{c=0,\theta=0}$ found in the second column of Table I are seen to be in close agreement. The reciprocal of the molecular weight is given by $K_v(C_n'/C_n)(c/I_v)_{c=0,\theta=0}$, where K_v is the usual constant and C_n and C_n' are the refraction corrections for the solution and standard, respectively. Following Hermans and Levinson,[17] we set $C_n = n^2$ and $C_n' = n'^2$, n and n' being the refractive indices of cyclohexane and toluene, respectively. Since (K_v/C_n) is dependent on temperature only through (dn/dc), and the temperature coefficient of the latter was observed to be negligible, we set $K_v(C_n'/C_n) = 13.6 \times 10^{-7}$. The average of the $(c/I_v)_{c=0,\theta=0}$ values found in column two thus yields $\langle M\rangle_w = 3.20 \times 10^6$.

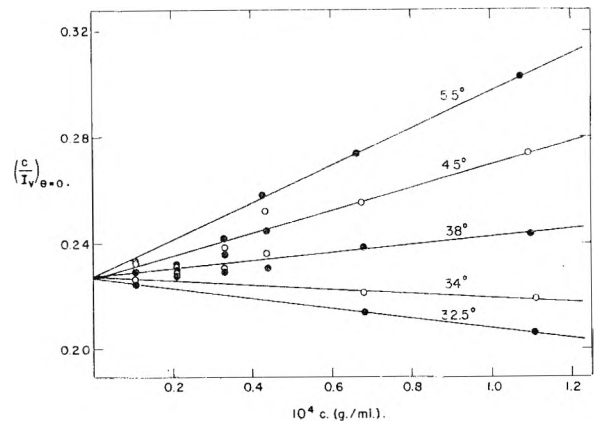

Fig. 3.—$(c/I_v)_{\theta=0}$ for five temperatures plotted against concentration.

Turning to the second virial coefficient, values of A_2 found in the third column of Table I appear plotted against the absolute temperature in Fig. 4. The Flory Θ temperature (at which $A_2 = 0$) is found to lie between 307.6–308.6°K. Taking as the best value Θ = 308.4°K., values for $\psi_1F(X)$ were de-

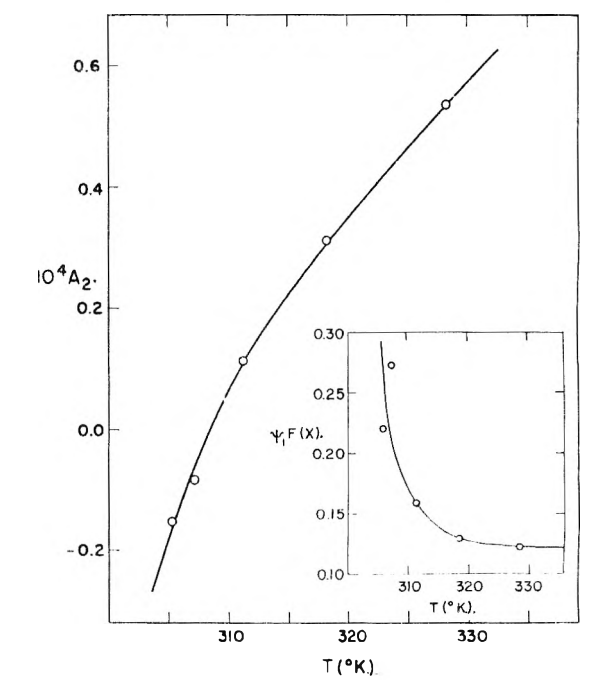

Fig. 4.—Values of the second virial coefficient for polystyrene–cyclohexane plotted against the absolute temperature. The insert shows $\psi_1F(X)$ products as a function of absolute temperature.

(20) T. G. Fox, P. J. Flory and A. M. Bueche, *J. Am. Chem. Soc.*, **73**, 285 (1951).

(21) W. H. Stockmayer and E. F. Casassa, *J. Chem. Phys.*, **20**, 1560 (1952).

duced by a procedure described elsewhere,[13] making use of the relationship

$$A_2 = (\bar{v}^2/V_1)(1 - \Theta/T)\psi_1 F(X) \qquad (3)$$

where $\bar{v}$ and V_1 are the partial specific volume of polymer and the molar volume of solvent, respectively. These values for $\psi_1 F(X)$ appear plotted against the absolute temperature in the insert to Fig. 4. Since $F(X) = 1$ at $T = \Theta$, this plot yields for the entropy parameter $\psi_1 = 0.19 \pm 0.05$.

Intrinsic viscosities for five temperatures ranging from 32.4 to 60° are given in column five of Table I. Values for $[\eta]_\Theta$ at temperature T were calculated from the relation[4]

$$\frac{[\eta]_{\Theta=T_1}}{[\eta]_{\Theta=T_2}} = \frac{K_{T_1}}{K_{T_2}} \qquad (5)$$

where $K_T = [\eta]_{\Theta=T}/M^{1/2}$ is assumed to vary linearly between 8.2×10^{-4} at 307°K. and 7.5×10^{-4} at 343°K.[22] The ratios $[\eta]_T/[\eta]_{\Theta=T}$ then yield values for the cube of the expansion factor α at temperature T. The intrinsic viscosity data were plotted in the form suggested by Fox and Flory,[4] (K_T/K_0) $(\alpha^5 - \alpha^3)/M^{1/2}$ *vs.* $1/T$, to obtain $\psi_1 = 0.14$ and $\Theta = 307.4$°K.

Values of Θ and ψ_1 for polystyrene–cyclohexane deduced from the present measurements are compared in Table II with corresponding values taken from the literature.[13,14,18,23,24]

TABLE II

THERMODYNAMIC PARAMETERS FOR POLYSTYRENE–CYCLOHEXANE

Measurement	Ref.	Θ	ψ_1
Light scattering	This work	307.6–308.6	0.19
	18	307.5–308.9	...
Osmotic pressure	13	307.6	0.36
Precipitation temp.	14	307.2	1.06
Intrinsic viscosity	This work	307.4	0.14
	23	307.2	0.13
	24	307.6	0.14

The Θ temperatures obtained from the present light scattering and viscosity measurements stand in good agreement with the literature values. The discrepancy between values for the entropy parameter ψ_1 as determined by the last three methods listed in Table II has been noted heretofore.[13] The ψ_1 values deduced from intrinsic viscosity could be nearly doubled by employing the modified value, C_M', suggested by Stockmayer.[25] One would expect light scattering and osmotic pressure to lead to the same value for ψ_1. The value deduced from the present light scattering measurements is therefore surprisingly low; however, this discrepancy may simply reflect the experimental error. Light scattering is not as precise as osmotic pressure for the determination of the thermodynamic parameters, both because temperature control is more difficult to maintain and because of the required extrapolation of the scattering data to zero angle. On the other hand, it supplements the osmotic method by extending the range of molecular weights which can be studied.

(22) See ref. 16, p. 615.
(23) T. G. Fox and P. J. Flory, *J. Am. Chem. Soc.*, **73**, 1915 (1951).
(24) A. R. Shultz and P. J. Flory, *J. Polymer Sci.*, **15**, 231 (1955).
(25) W. H. Stockmayer, *ibid.*, **15**, 595 (1955).

Taking $\Theta = 308.4$°K., we find for fraction HB2-3 in the absence of long range interferences $\langle\overline{R_0^2}\rangle_z^{1/2} = 5.37 \times 10^{-6}$ cm., which corresponds to $\langle\overline{L_0^2}\rangle_z^{1/2} = 13.2 \times 10^{-6}$ cm. The ratio $\overline{L_0^2}/M$, independent of heterogeneity, can be calculated from $\langle\overline{L_0^2}\rangle_z/\langle M\rangle_w$, if the molecular weight heterogeneity of the sample can be estimated. Assignment of $h = 4$ leads to $\overline{L_0^2}/M = 0.45 \times 10^{-16}$ for polystyrene at 35°. This is compared in Table III with $\overline{L_0^2}/M$ ratios for polystyrene taken from the literature. Values for the heterogeneity parameter h shown in parentheses represent our estimates. As would be expected in the absence of long range interferences, the $\overline{L_0^2}/M$ values found in column five show no systematic trend with molecular weight.

TABLE III

$\overline{L_0^2}/M$ FOR POLYSTYRENE AT 25–35°

Ref.	$10^{-6}\langle M\rangle_w$	h	$10^{16}(\langle\overline{L_0^2}\rangle_z/\langle M\rangle_w)$	$10^{16}(\overline{L_0^2}/M)$
18	1.61	(10)	0.56	0.52
26	1.00	(10)	.50	.46
	1.75	(10)	.49	.45
	2.30	(10)	.55	.50
	5.00	(10)	.47	.44
27	0.372	7.7	.57	.51
	1.07	7	.58	.51
	1.55	1.11	.75	.51
	2.80	7	.57	.50
Present work	3.20	4	.54	.45
			Av.	0.49

C. Dependence of $\langle\overline{R^2}\rangle_z$ upon A_2.—Zimm, Stockmayer and Fixman[28] note that several treatments of the excluded volume effect for a chain of N flexible elements of length a lead to the relationship

$$\overline{L^2} = Na^2[1 + 4z/3 + \ldots] \qquad (6)$$

They obtain a corresponding relation for the mean square radius of gyration

$$\overline{R^2} = (Na^2/6)[1 + 134z/105 + \ldots] \qquad (7)$$

where $z = (3/2\pi\ Na^2)^{3/2}\beta N^2$, β being the volume excluded to a pair of elements. In the single contact approximation employed by Zimm,[29] the excluded volume β is directly related to the second virial coefficient

$$A_2 = \mathbf{N}\beta/2M_0^2 \qquad (8)$$

where $\mathbf{N}$ is the Avogadro number and M_0 is the molecular weight of a flexible element. Although this expression for A_2 is strictly valid only at $A_2 = 0$, it should nevertheless furnish a reasonable approximation for small values of the second virial coefficient. Combination of eq. 7 and 8 yields

$$\overline{R^2} = \overline{R_0^2}[1 + 0.0572(M/\overline{R_0^2})^{3/2}(A_2/\mathbf{N})M^{1/2} + \ldots] \qquad (9)$$

We require the corresponding expression for $\langle\overline{R^2}\rangle_z$ for a heterogeneous polymer. Representing the molecular size distribution by[2,19]

(26) F. D. Kunst, *Rec. trav. chim.*, **69**, 125 (1950); Thesis, Faculty of Science, University of Paris, 1949.
(27) J. Oth and V. Desreux, *Bull. soc. chim. Belges*, **63**, 285 (1954).
(28) B. H. Zimm, W. H. Stockmayer and M. Fixman, *J. Chem. Phys.*, **21**, 1716 (1953).
(29) B. H. Zimm, *ibid.*, **14**, 164 (1946).

$$f(N) = \frac{y^{h+1}}{h!} N^h e^{-yN} \quad (10)$$

where

$$y = (h + 2)/\langle N\rangle_z = (h + 1)/\langle N\rangle_w \quad (11)$$

there is obtained

$$\langle\overline{R^2}\rangle_z = \langle\overline{R_0^2}\rangle_z \left[1 + \frac{(h + 2)^{3/2}}{(h + 1)^2} \frac{\Gamma(h + 3.5)}{\Gamma(h + 3)} Q(\langle M\rangle_w)^{1/2} A_2 + \ldots\right] \quad (12)$$

where

$$Q = \left(\frac{134}{105}\right)\left(\frac{1}{4\pi^{3/2}}\right)\left(\frac{\langle M\rangle_w}{\langle\overline{R_0^2}\rangle_z}\right)^{3/2}\left(\frac{1}{N}\right) \quad (13)$$

Substituting the values $\langle\overline{R_0^2}\rangle_z/\langle M\rangle_w = 9.02 \times 10^{-18}$ and $h = 4$ into eq. 12 and 13, one finds

$$\langle\overline{R^2}\rangle_z = \langle\overline{R_0^2}\rangle_z[1 + 0.92 \times 10^4 A_2 + \ldots] \quad (14)$$

which predicts an initial linear dependence of $\langle\overline{R^2}\rangle_z$ and A_2. The data appear plotted in this manner in Fig. 5. The slope in the vicinity of $A_2 = 0$ is 1.15×10^4, which is to be compared with the theoretical value, 0.92×10^4. This difference may arise from an underestimation of the heterogeneity of the polymer sample.

The filled circles in Fig. 5 represent the intrinsic viscosity values taken from Table I plotted against A_2. The data conform to a linear relationship, as found empirically by Oth and Desreux,[27] although we are not aware of any theoretical basis for this relationship.

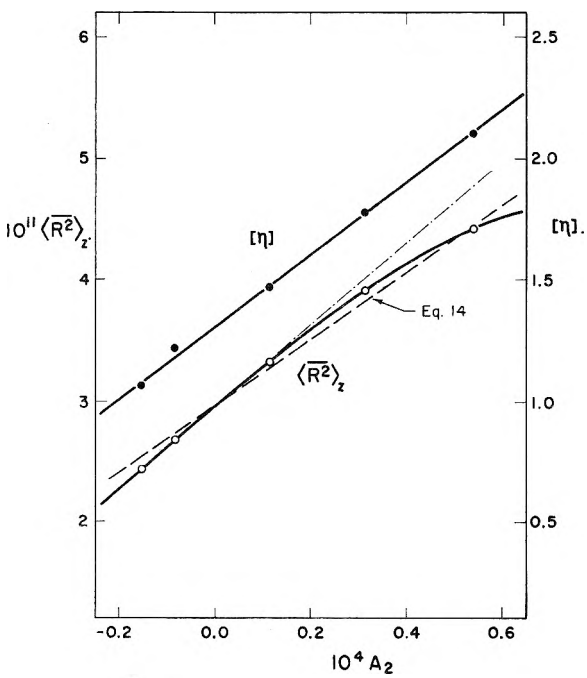

Fig. 5.—$\langle\overline{R^2}\rangle_z$ (cm.^{2}) and intrinsic viscosity (deciliter/g.) for polystyrene HB2-3 in cyclohexane plotted against A_2 (cm.^{3} mole g.$^{-2}$). The theoretical dependence of $\langle\overline{R^2}\rangle_z$ as given by eq. 14 is represented by the dashed line. The filled circles represent $[\eta]$ plotted against A_2, using the ordinate at the right.

D. Variation of Φ with A_2.—We next wish to test the postulate that the hydrodynamic radius is proportional to some average linear dimension of the polymer coil, such as $(\overline{L^2})^{1/2}$ or $(\overline{R^2})^{1/2}$. Since $[\eta]_\Theta$ measurements[5,15] indicate that the permeation factor reaches its asymptotic limit at much lower molecular weights, we would expect the intrinsic viscosities for the various temperatures to be proportional to $(\overline{R^2})^{3/2}$. Figure 6 shows the intrinsic viscosities plotted against $\langle\overline{R^2}\rangle_z^{1/2}$, using a log-log scale. A linear relationship is obtained, but

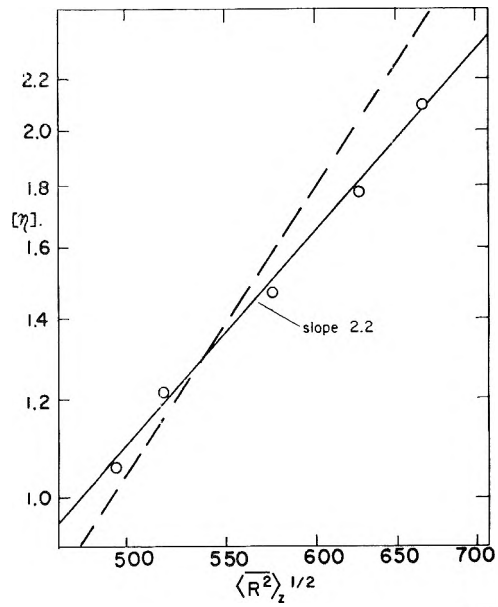

Fig. 6.—Intrinsic viscosities plotted against $\langle\overline{R^2}\rangle_z^{1/2}$ (Å.), using log–log plot. The observed slope is 2.2, while the slope of the dashed theoretical line is 3.0.

the slope is 2.2 instead of 3.0 as anticipated. This suggests that as the excluded volume increases, the hydrodynamic radius increases less rapidly than $\langle\overline{R^2}\rangle_z^{1/2}$. From eq. 6 and 7

$$\overline{L^2} = 6\overline{R^2}[1 + 0.0572z + \ldots] \quad (15)$$

thus, the relationship $\overline{L^2} = 6\overline{R^2}$ holds only for a random flight displacement distribution. If $\overline{L^2}$ and $\overline{R^2}$ increase with excluded volume at different rates, it is perhaps not surprising that the concomitant increase in the hydrodynamic radius is not strictly proportional to either of these quantities.

Before undertaking a more direct test of equation 2, the effect thereon of both polymer heterogeneity and excluded volume must be examined. Newman, *et al.*,[11] have shown that for heterogeneous polymers, the number averages of both $(\overline{R^2})^{3/2}$ and M are required. Thus, for a heterogeneous polymer equation 2 becomes[11]

$$[\eta] = (6^{3/2}/q)\Phi(\langle\overline{R^2}\rangle_z)^{3/2}/\langle M\rangle_w \quad (16)$$

where

$$q = \frac{(\langle\overline{R^2}\rangle_z)^{3/2}\langle M\rangle_n}{\langle(\overline{R^2})^{3/2}\rangle_n\langle M\rangle_w} \quad (17)$$

Newman, *et al.*, neglect the small variation of the expansion factor α with molecular weight in deriving their expression for q. Shultz[7] has taken the excluded volume effect into account by setting $\overline{R_i^2} \sim M_i^{1+2\epsilon}$. Alternatively, we may make use of eq. 7, 8 and 10 to obtain a relation for q in terms of A_2

$$q = q_0\left[1 + \left(\frac{3}{2}\right)\frac{(h + 2)^{3/2}}{(h + 1)^2}\left\{\frac{\Gamma(h + 3.5)}{\Gamma(h + 3)} - \frac{\Gamma(h + 2)}{\Gamma(h + 1.5)}\right\} Q(\langle M\rangle_w)^{1/2} A_2 + \ldots\right] \quad (18)$$

where

$$q_0 = \frac{(h+2)^{3/2}}{(h+1)^2} - \frac{\Gamma(h+2)}{\Gamma(h+1.5)} \qquad (19)$$

Substituting $\langle\overline{R_0^2}\rangle_z/\langle M\rangle_w = 9.02 \times 10^{-18}$ and $h = 4$ into eq. 13, 18 and 19 results in

$$q = 1.35[1 + 0.163 \times 10^4 A_2 + \ldots] \qquad (20)$$

In view of the limitations of the single contact approximations, we may expect the dependence of q upon A_2 as predicted by equation 20 to be valid only for small values of A_2. Evidently the dependence upon A_2 is negligible in the vicinity of $T = \Theta$, which is equivalent to the statement that ϵ in the formula of Shultz[7] is nearly zero under these conditions. We have employed $q = 1.35$ to deduce the Φ values appearing in the last column of Table I. Since the magnitude of q_0 depends to some extent upon the form of the assumed distribution function, and since the limiting tangent method is rather insensitive to the choice of h, the absolute magnitudes of these Φ values appearing in Table I may be in error by $\pm 15\%$; however, the ratios of Φ values at two temperatures should be independent of this correction. The Φ values shown in Table I appear plotted against the absolute temperature in Fig. 7. As would be expected from Fig. 6, Φ decreases with increasing temperature (or increasing solvent power). This decrease amounts to 25%, and appears to be beyond the experimental error (15% for $(\langle R^2\rangle_z)^{3/2}$ and 2% for $[\eta]$).

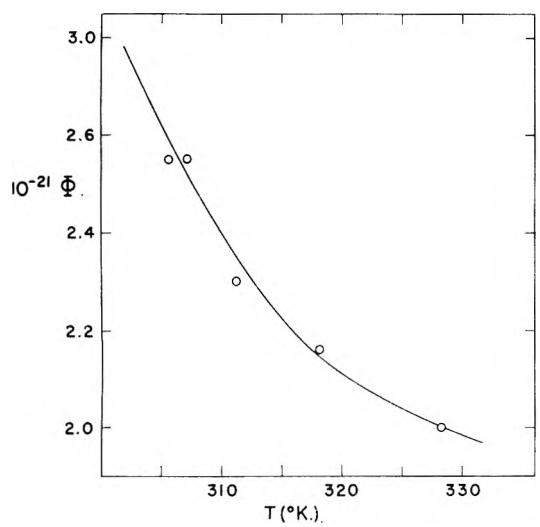

Fig. 7.—Φ values for polystyrene HB2-3 in cyclohexane plotted against absolute temperature.

This behavior suggests examining the dependence of Φ upon A_2 for other data in the literature. We require values of Φ and A_2 for one polymer fraction in a series of solvents. Unfortunately, the Φ values reported by various workers are not strictly comparable; the correction to number average has seldom been applied, and in at least one case the "low" value for Rayleigh's ratio has been used in the absolute calibration. However, since we are only interested in relative values, the following procedure was adopted. A plot of the reported Φ values for each system was smoothed, and each Φ value for that system was multiplied by the factor required to reduce the smoothed Φ at $A_2 = 0$ to a common value, arbitrarily chosen as 2.5×10^{21} to agree with the value found in Fig. 7. The Φ values so obtained for a variety of systems[11,18,26,30] appear plotted against A_2 in Fig. 8. Although once again the absolute magnitudes are not correct, the 30% decrease shown by the smoothed curve appears to be significant.

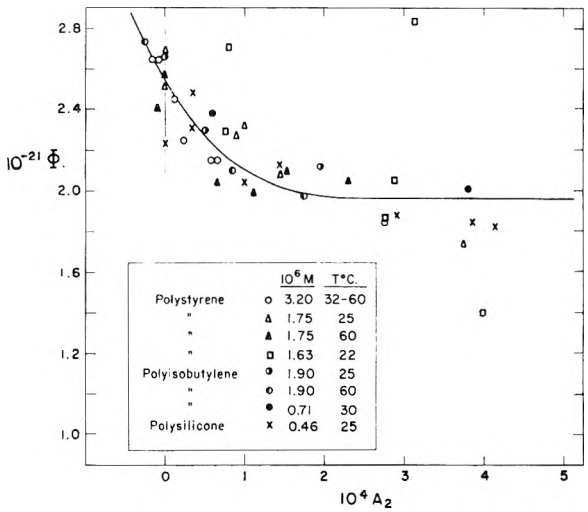

Fig. 8.—Φ values, calculated as described in the text for a variety of polymer–solvent systems,[11,18,26,30] plotted against A_2.

Several comments should be made concerning Fig. 8. Since Φ changes most rapidly in the vicinity of $A_2 = 0$, only by extending the measurements to $T = \Theta$ does the trend clearly exceed experimental error. The use of solvent—non-solvent mixtures offers the simplest means of covering a wide range of A_2 values. In compiling Φ values, Fox and Flory noted[23] an upward trend with increasing non-solvent composition; however, this trend may have been ascribed to peculiarities in the light scattering behavior of systems involving mixed solvents. Secondly, attempts to detect a variation in Φ by examining different polymer samples in various solvents, or examining a range of molecular weights for a given polymer–solvent pair, are apt to fail because of the additional errors which accumulate in the determination of the molecular weights and q factors for the various polymers.

The data of Newman, *et al.*,[11] show that Φ is approximately constant for a wide variety of polymer–solvent systems, but do not constitute a very sensitive test for the reasons mentioned above. Φ values calculated from these data for polyacrylic acid fractions in dioxane, but without the q correction, are very nearly constant. If one assumes that the fractions of higher molecular weight are more polydisperse, then the corrected Φ values would increase with decreasing A_2, in accordance with the trend shown in Fig. 8. Their values for polyisobutylene F-4 in two solvents appear as filled circles in Fig. 8 (no attempt was made to correct these two points to $\Phi = 2.5 \times 10^{21}$ at $A_2 = 0$). Although these values follow the trend of the curve, the difference (2.26 and 2.43 $\times 10^{21}$) is small because the poorer solvent was still rather far removed from the Θ condition. The same may

(30) F. P. Price and J. P. Bianchi, *J. Polymer Sci.*, **15**, 355 (1955).

be said of the data of Cantow and Bodmann.[8a] Price and Bianchi[30] calculate Φ values for a poly(dimethylsiloxane) fraction using the $<M>_w$ values observed in the mixed solvents. They state that Φ showed no trend with A_2, even when calculated using a constant $<M>_w$ value. However, values calculated in this way appear as crosses in Fig. 8. These points show a considerable variation with A_2, and only the experimental value at $A_2 = 0$ departs significantly from the smoothed curve. The Φ values reported for polystyrene by Thurmond and Zimm[12] decrease much more rapidly with A_2, both for linear and for branched fractions, than the trend represented by the smoothed curve in Fig. 8.

Not all of the data examined followed the trend exhibited in Fig. 8. In particular, the data of Oth and Desreux[27] for polystyrene in butanone–methanol mixtures indicate a constant Φ over a considerable range of A_2 values, including $A_2 = 0$.

It is difficult to ascribe the downward trend of the Φ values exhibited in Fig. 8 to any known source of error. If the viscosities were corrected to zero rate of shear, and if the dependence of q upon A_2 were taken into account, both of these factors would raise the Φ values for large A_2, but neither could compensate for the sharp decrease observed in the vicnity of $T = \Theta$. Benoit and Doty[31] imply that it may not be possible to deduce the true initial slope from a Zimm plot if $<\overline{L^2}>_z^{1/2} >$ 1000 Å. The variation of Φ observed in the present measurements might be rationalized in this way, since for this sample $<\overline{L^2}>_z^{1/2}$ is beyond the stated limiting value; however, the fact that the same molecular weight was obtained at all temperatures renders this possibility remote. Certainly such an explanation is not applicable to all the data appearing in Fig. 8.

Discussion

The KR and DB hydrodynamic treatments[3] directly or indirectly assume that the molecular configuration is that of a random flight chain. Flory[4] has proposed modification of this result to account for the expansion of the average displacement length due to long range interferences. His proposal effectively retains the *form* of the displacement distribution, but expands it by a scale factor. Recent treatments[32,33] of the excluded volume effect indicate that the form of the displacement distribution is in fact altered when the excluded volume is other than zero. Since treatments of the segment density invariably employ the assumption of random flight statistics, there is at present no way to assess the effect of such a distortion upon the hydrodynamic radius. Stockmayer and Fixman[34] have applied the KR treatment to random flight chains having over-all segment distributions modified by branching. They conclude that the hydrodynamic radius is less sensitive to changes in the segment distribution than is $(\overline{R^2})^{1/2}$. If it is assumed that the hydrodynamic radius is likewise relatively insensitive to changes in the segment distribution arising from excluded volume effects, this would offer an explanation for the observed variation of Φ with A_2.

Concerning the calculation of polymer dimensions from hydrodynamic measurements, it appears from the foregoing that $(\overline{R^2})^{1/2}$ for polymers in good solvents can be calculated from intrinsic viscosities through use of equation 2, employing the limiting value of Φ for A_2 large. If the polymer is heterogeneous, equation 2 in conjunction with $<M>_n$ yields $<(\overline{R^2})^{3/2}>_n$.[11] Unfortunately, the limiting value of Φ is not well defined at the present time. The value $\Phi = 2.1 \times 10^{21}$ cited by Fox and Flory[23,35] represents an average for both good and poor solvents. On the other hand, this may be compensated for by the fact that no heterogeneity corrections were applied in these calculations. Only near the Θ condition is a higher value of Φ indicated. The appropriate value of Φ could be estimated from Fig. 8, once the limiting value of Φ has been ascertained. Of course, the correct value of Φ corresponding to any other A_2 would serve as well in calibrating the ordinate scale of Fig. 8. The effect of this variation of Φ upon the calculated values of $(\overline{R^2})^{1/2}$ is actually not too serious, since $(R^2)^{1/2}$ varies as $\Phi^{1/3}$.

(31) H. Benoit, *J. Polymer Sci.*, **11**, 507 (1953); H. Benoit, A. M. Holtzer and P. Doty, THIS JOURNAL, **58**, 635 (1954).

(32) H. M. James, *J. Chem. Phys.*, **21**, 1628 (1953).

(33) W. R. Krigbaum, *ibid.*, **23**, in press (1955).

(34) W. Stockmayer and M. Fixman, *Ann. N. Y. Acad. Sci.*, **57**, 334 (1953).

(35) T. G. Fox and P. J. Flory, *J. Am. Chem. Soc.*, **73**, 1909 (1951).

PHYSICAL PROPERTIES OF 14 AMERICAN PETROLEUM INSTITUTE RESEARCH HYDROCARBONS, C_9 TO C_{15}[1]

BY DAVID L. CAMIN AND FREDERICK D. ROSSINI

Petroleum Research Laboratory, Carnegie Institute of Technology, Pittsburgh, Pennsylvania

Received June 10, 1955

For *n*-undecane, *n*-trideeane, *n*-tetradecane, *n*-pentadecane, 1-tridecene, 1-tetradecene, 1-pentadecene, 1-methylnaphthalene, *cis*-decahydronaphthalene, *trans*-decahydronaphthalene, *cis*-hexahydroindan and *trans*-hexahydroindan, highly purified hydrocarbons of the American Petroleum Institute (API) Research series, the following properties were measured: densities at 20, 25 and 30°, refractive indices at seven wave lengths at 20, 25 and 30°; and boiling points and vapor pressures from 40 to 790 mm. For naphthalene and 2-methylnaphthalene, also of the API Research series, boiling points and vapor pressures from 40 to 770 mm., were measured. The data on refractive indices were correlated by means of modified Cauchy and Hartmann equations, and values of the constants are given for each compound, to permit precise evaluation of the refractive index as a function of wave length. The data on vapor pressures were correlated with the Antoine equation and values of the three constants are given for each compound. Also included are calculated values of the specific dispersions, $(n_F - n_C)/d$ and $(n_g - n_D)/d$.

Introduction

The American Petroleum Institute Research Project 6 has so far reported data on the densities, refractive indices, and boiling points and vapor pressures for 81 different API Research hydrocarbons.[2-8] In this paper are reported similar data for an additional 14 API Research hydrocarbons.

Compounds Measured

These API Research hydrocarbons were made available by the American Petroleum Institute through the American Petroleum Institute Research Project 44 at the Carnegie Institute of Technology. The samples were purified by the American Petroleum Institute Research Project 6 from material supplied by the following laboratories: *n*-undecane, *n*-tetradecane, 1-tetradecene, 1-methylnaphthalene, 2-methylnaphthalene, *cis*-decahydronaphthalene and *trans*-decahydronaphthalene, by the American Petroleum Institute Research Project 6, Carnegie Institute of Technology, Pittsburgh, Pennsylvania; *n*-tridecane, 1-tridecene, *n*-pentadecane and 1-pentadecene, by the American Petroleum Institute Research Project 42, Pennsylvania State University, University Park, Pennsylvania; *cis*-hexahydroindan and *trans*-hexahydroindan, by the American Petroleum Institute Research Project 45, Ohio State University, Columbus, Ohio; and naphthalene by the American Cyanamid Company, Bound Brook, New Jersey. The purification and determination of purity and freezing point of these compounds, have been or are being reported in other papers.[9,10] The purity of the samples measured was as follows, in mole per cent.[9,10]: *n*-undecane, 99.97 ± 0.03; *n*-tridecane, 99.92 ± 0.06; *n*-tetradecane, 99.93 ± 0.06; *n*-pentadecane, 99.93 ± 0.05; 1-tridecene, 99.85 ± 0.09; 1-tetradecene, 99.73 ± 0.13; 1-pentadecene, 99.89 ± 0.05; naphthalene, 99.96 ± 0.03; 1-methylnaphthalene, 99.98 ± 0.02; 2-methylnaphthalene, 99.92 ± 0.06; *cis*-decahydronaphthalene, 99.93 ± 0.05; *trans*-decahydronaphthalene, 99.97 ± 0.03; *cis*-

TABLE I

VALUES OF DENSITY

Compound	Formula	Density,[a] g./ml. 20°	25°	30°	Temp. coefficient of density at 25°, g./ml. °C.
n-Undecane	$C_{11}H_{24}$	0.74024	0.73652	0.73284	0.000740
n-Tridecane	$C_{13}H_{28}$	.75622	.75270	.74907	.000715
n-Tetradecane	$C_{14}H_{30}$	.76275	.75917	.75566	.000709
n-Pentadecane	$C_{15}H_{32}$	.76830	.76488	.76140	.000690
1-Tridecene	$C_{13}H_{26}$	.76527	.76168	.75801	.000726
1-Tetradecene	$C_{14}H_{28}$	.77127	.76767	.76416	.000711
1-Pentadecene	$C_{15}H_{30}$	.77641	.77290	.76939	.000702
1-Methylnaphthalene	$C_{11}H_{10}$	1.02031	1.01664	1.01304	.000727
cis-Decahydronaphthalene	$C_{10}H_{18}$	0.89671	0.89291	0.88911	.000760
trans-Decahydronaphthalene	$C_{10}H_{18}$	.86971	.86592	.86222	.000749
cis-Hexahydroindan	C_9H_{16}	.88445	.88031	.87623	.000822
trans-Hexahydroindan	C_9H_{16}	.86268	.85850	.85449	.000819

[a] For air-saturated material at 1 atmosphere.

(1) This investigation was performed as part of the work of the American Petroleum Institute Research Project 6 in the Petroleum Research Laboratory of the Carnegie Institute of Technology, Pittsburgh, Pennsylvania.

(2) C. B. Willingham, W. J. Taylor, J. M. Pignocco and F. D. Rossini, *J. Research Natl. Bur. Standards*, **35**, 219 (1945).

(3) A. F. Forziati and F. D. Rossini, *ibid.*, **43**, 473 (1949).

(4) A. F. Forziati, W. R. Norris and F. D. Rossini, *ibid.*, **43**, 555 (1949).

(5) A. F. Forziati, *ibid.*, **44**, 373 (1950).

(6) A. F. Forziati, D. L. Camin and F. D. Rossini, *ibid.*, **45**, 406 (1950).

(7) F. D. Rossini, B. J. Main and A. J. Streiff, "Hydrocarbons from Petroleum," Reinhold Publ. Corp., New York, N. Y., 1953.

(8) D. L. Camin, A. F. Forziati and F. D. Rossini, THIS JOURNAL, **58**, 440 (1954).

(9) A. J. Streiff, L. F. Soule, C. M. Kennedy, M. E. Janes, V. A. Sedlak, C. B. Willingham and F. D. Rossini, *J. Research Natl. Bur. Standards*, **45**, 173 (1950).

(10) A. J. Streiff, A. R. Hulme, P. A. Cowie, N. C. Krouskop and F. D. Rossini, *Anal. Chem.*, **27**, 411 (1955).

TABLE II

VALUES OF $\beta = 1/(\lambda - \lambda^*)^{1.6}$ FOR EACH OF SEVEN WAVE LENGTHS, λ, FOR THE RANGE $\lambda^* = 0.1500$ TO 0.1750

	Wave length, λ in μ						
λ	0.6678149	0.6562793	0.5892620	0.5460740	0.5015675	0.4861327	0.4358342
	$\beta = 1/(\lambda - \lambda^*)^{1.4}$						
	$\beta_{He\ (red)}$	β_C	β_{D_1, D_2}	β_e	$\beta_{He\ (blue)}$	β_F	β_g
0.150	2.866295	2.971500	3.72943	4.401056	5.325815	5.722459	7.416812
	8879	9415	1362	17838	24328	27345	41706
.151	2.875174	2.980915	3.74305	4.418904	5.350143	5.749804	7.458518
	8923	9463	1371	17955	24509	27558	42088
.152	2.884097	2.990378	3.75676	4.436859	5.374652	5.777362	7.500606
	8968	9513	1379	18074	24692	27773	42477
.153	2.893065	2.999891	3.77055	4.454933	5.399344	5.805135	7.543083
	9014	9562	1387	18194	24877	27992	42869
.154	2.902079	3.009453	3.78442	4.473127	5.424221	5.833127	7.585952
	9060	9611	1395	18315	25064	28211	43266
.155	2.911139	3.019064	3.79837	4.491442	5.449285	5.861338	7.629218
	9106	9661	1404	18436	25252	28432	43667
.156	2.920245	3.028725	3.81241	4.509878	5.474537	5.889770	7.672885
	9153	9712	1412	18560	25443	28658	44075
.157	2.929398	3.038437	3.82653	4.528438	5.499980	5.918428	7.716960
	9199	9762	1421	18684	25636	28884	44489
.158	2.938597	3.048199	3.84074	4.547122	5.525616	5.947312	7.761449
	9246	9814	1429	18810	25830	29115	44907
.159	2.947843	3.058013	3.85503	4.565932	5.551446	5.976427	7.806356
	9294	9865	1438	18937	26028	29347	45331
.160	2.957137	3.067878	3.86941	4.584869	5.577474	6.005774	7.851687
	9341	9917	1446	19065	26226	29582	45759
.161	2.966478	3.077795	3.88387	4.603934	5.603700	6.035356	7.897446
	9389	9969	1456	19195	26427	29819	46194
.162	2.975867	3.087764	3.89843	4.623129	5.630127	6.065175	7.943640
	9438	10021	1464	19326	26631	30060	46636
.163	2.985305	3.097785	3.91307	4.642455	5.656758	6.095235	7.990276
	9486	10075	1473	19457	26835	30303	47082
.164	2.994791	3.107860	3.92780	4.661912	5.683593	6.125538	8.037358
	9535	10128	1482	19590	27044	30549	47536
.165	3.004326	3.117988	3.94262	4.681502	5.710637	6.156087	8.084894
	9586	10181	1491	19723	27253	30796	47993
.166	3.013912	3.128169	3.95753	4.701225	5.737890	6.186883	8.132887
	9636	10236	1501	19858	27465	31048	48457
.167	3.023548	3.138405	3.97254	4.721083	5.765355	6.217931	8.181344
	9684	10290	1510	19995	27679	31301	48930
.168	3.033232	3.148695	3.98764	4.741078	5.793034	6.249232	8.230274
	9735	10345	1519	20133	27896	31559	48407
.169	3.042967	3.159040	4.00283	4.761211	5.820930	6.280791	8.279681
	9784	10401	1529	20273	28115	31819	49891
.170	3.052751	3.169441	4.01812	4.781484	5.849045	6.312610	8.329572
	9828	10456	1538	20413	28335	32081	50379
.171	3.062579	3.179897	4.03350	4.801897	5.877380	6.344691	8.379951
	9879	10513	1548	20556	28559	32346	50877
.172	3.072458	3.190410	4.04898	4.822453	5.905939	6.377037	8.430828
	9932	10569	1558	20698	28786	32616	51381
.173	3.082390	3.200979	4.06456	4.843151	5.934725	6.409653	8.482209
	9985	10626	1567	20844	29014	32888	51892
.174	3.092375	3.211605	4.08023	4.863995	5.963739	6.442541	9.534101
	10040	10684	1577	20990	29246	33163	52411
.175	3.102415	3.222289	4.09600	4.884985	5.992985	6.475704	8.586512

hexahydroindan, 99.95 ± 0.02; *trans*-hexahydroindan, 99.71 ± 0.11. It is believed that in each case the impurity was of such nature and present in such small amount that the properties measured were not affected beyond the indicated limits of uncertainty.

Measurements Made

The measurements of density were made at 20, 25 and 30°, with a density balance previously described.[11] The experimental values of density are given in Table I. Individual measurements were reproducible within 0.00003 g./ml. The accuracy of the tabulated values is estimated to be ±0.00005 to ±0.00010 g./ml.

The refractive index was measured by means of the apparatus and procedure previously described.[5] The calculations and correlations were similarly

(11) A. F. Forziati, B. J. Mair and F. D. Rossini, *J. Research Natl. Bur. Standards*, **35**, 513 (1945).

TABLE III

VALUES OF $\gamma = (\beta_{0.43583} - \beta_{0.65628})/(\beta_{0.43583} - \beta_{0.54607})$, FOR VALUES OF λ^* FROM 0.140 TO 0.175 μ

Intervals of λ^*	λ^* 0.14000	0.15000	0.16000	0.1700
	$\gamma = (\beta_{0.43583} - \beta_{0.65628})/(\beta_{0.43583} - \beta_{0.54607})$			
0.000	1.483368	1.474034	1.464363	1.454341
	920	951	986	1022
.001	1.482448	1.473083	1.463377	1.453319
	923	955	989	1026
.002	1.481525	1.472128	1.462388	1.452293
	926	959	992	1030
.003	1.480599	1.471169	1.461396	1.451263
	929	961	997	1033
.004	1.479670	1.470208	1.460399	1.450230
	932	965	1000	1038
.005	1.478738	1.469243	1.459399	1.449192
	935	969	1004	
.006	1.477803	1.468274	1.458395	
	937	973	1008	
.007	1.476866	1.467301	1.457387	
	940	975	1012	
.008	1.475926	1.466326	1.456375	
	945	980	1015	
.009	1.474981	1.465346	1.455360	
	947	983	1019	

made as described previously, wherein the data obtained were correlated by means of the Hartmann equation as modified by Tilton and Gurewitz.[12]

$$n_\lambda = n_\infty + C/(\lambda - \lambda^*)^{1.6}$$

The constants in the equation were adjusted by means of a modification of the interpolation method of Gurewitz and Tilton.[12] The following abbreviations were used

$$\beta = 1/(\lambda - \lambda^*)^{1.6} \quad (1)$$

$$\gamma = (\beta_{0.43583} - \beta_{0.65628})/(\beta_{0.43583} - \beta_{0.54607}) \quad (2)$$

To facilitate the calculations, values of β and γ were calculated over certain ranges. Table II of this report gives values of β at each of the seven wave lengths for values of λ^* from 0.1500 to 0.1750 μ. Table III of this report gives values of γ for values of λ^* from 0.140 to 0.175 μ. These tables

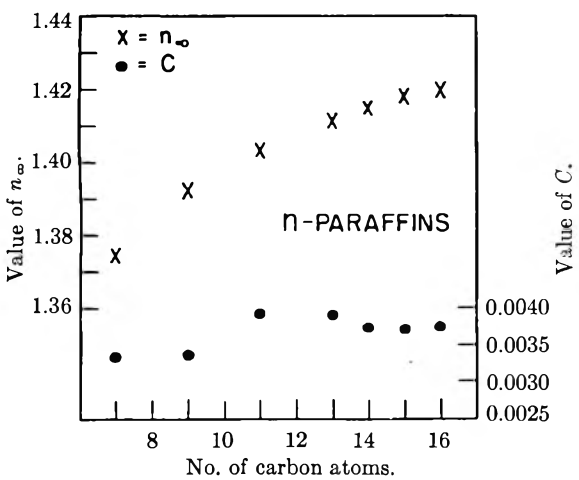

Fig. 1.—Plot of the constants n_∞ and C of the modified Hartmann equation for refractive index for the normal paraffin hydrocarbons.

(12) L. W. Tilton and Helen L. Gurewitz, *Natl. Bur. Standards*, unpublished.

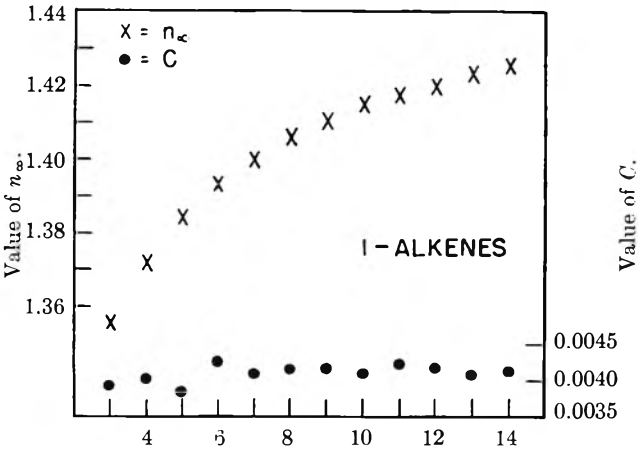

Fig. 2.—Plot of constants n_∞ and C of the modified Hartmann equation for refractive index for the monoölefin hydrocarbons (1-alkenes).

are extensions of Tables II and III, respectively, of a previous report.[5]

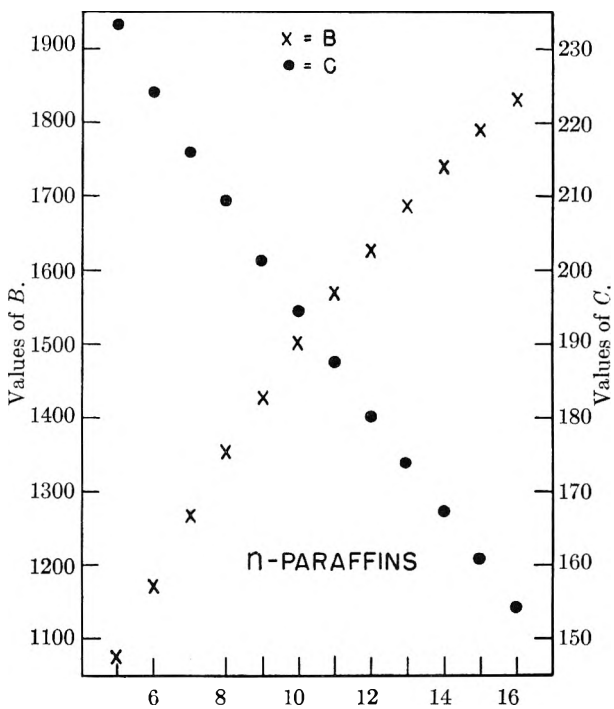

Fig. 3.—Plot of the constants B and C of the Antoine equation for vapor pressure for the normal paraffin hydrocarbons.

The value of γ was determined from the relation

$$\gamma = (n_{0.43583} - n_{0.65628})/(n_{0.43583} - n_{0.54607}) \quad (3)$$

Using Table III, the corresponding value of λ^* was interpolated. Further interpolation in Table II yielded values for β for each of the seven wave lengths used. The constant C was then readily computed from the equation

$$C = (n_{0.43583} - n_{0.65628})/(\beta_{0.43583} - \beta_{0.65628}) \quad (4)$$

The Hartmann equation was written as

$$n_\lambda = n_\infty + C\beta_\lambda \quad (5)$$

The remaining unknown constant, n_∞, was easily

TABLE IV

VALUES OF REFRACTIVE INDEX

Compd.	Formula	Temp., °C.	Refractive index: Wave length in Ångström units, spectral line: 6678.1 He_{red}	6562.8 H_C	5892.6 Na_D	5460.7 Hg_e	5015.7 He_{blue}	4861.3 H_F	4358.3 Hg_g
n-Undecane	$C_{11}H_{24}$	20	1.41483	1.41513	1.41725	1.41906	1.42144	1.42244	1.42647
		25	1.41266	1.41296	1.41507	1.41687	1.41924	1.42023	1.42424
		30	1.41049	1.41079	1.41289	1.41468	1.41704	1.41801	1.42201
n-Tridecane	$C_{13}H_{28}$	20	1.42314	1.42345	1.42560	1.42744	1.42987	1.43088	1.43501
		25	1.42100	1.42131	1.42346	1.42530	1.42773	1.42874	1.43287
		30	1.41886	1.41917	1.42132	1.42316	1.42559	1.42660	1.43073
n-Tetradecane	$C_{14}H_{30}$	20	1.42644	1.42676	1.42892	1.43078	1.43324	1.43427	1.43849
		25	1.42439	1.42470	1.42685	1.42870	1.43115	1.43217	1.43637
		30	1.42234	1.42264	1.42478	1.42662	1.42906	1.43007	1.43425
n-Pentadecane	$C_{15}H_{32}$	20	1.42940	1.42971	1.43188	1.43375	1.43623	1.43726	1.44153
		25	1.42732	1.42736	1.42979	1.43165	1.43412	1.43515	1.43940
		30	1.42524	1.42555	1.42770	1.42955	1.43201	1.43304	1.43727
1-Tridecene	$C_{13}H_{26}$	20	1.43060	1.43094	1.43336	1.43544	1.43820	1.43936	1.44409
		25	1.42843	1.42877	1.43118	1.43325	1.43599	1.43714	1.44185
		30	1.42626	1.42660	1.42900	1.43106	1.43378	1.43492	1.43961
1-Tetradecene	$C_{14}H_{28}$	20	1.43354	1.43388	1.43631	1.43839	1.44116	1.44232	1.44707
		25	1.43140	1.43174	1.43415	1.43622	1.43897	1.44012	1.44484
		30	1.42926	1.42960	1.43199	1.43405	1.43678	1.43792	1.44261
1-Pentadecene	$C_{15}H_{30}$	20	1.43607	1.43642	1.43883	1.44089	1.44365	1.44481	1.44957
		25	1.43395	1.43429	1.43669	1.43875	1.44150	1.44265	1.44739
		30	1.43183	1.43216	1.43455	1.43661	1.43935	1.44049	1.44521
1-Methylnaphthalene	$C_{11}H_{10}$	20	1.60828	1.60940	1.61755	1.62488	1.63513	1.63958	
		25	1.60592	1.60703	1.61512	1.62240	1.63259	1.63701	1.65627
		30	1.60360	1.60471	1.61278	1.62005	1.63022	1.63463	1.65386
cis-Decahydronaphthalene	$C_{10}H_{18}$	20	1.47819	1.47853	1.48098	1.48309	1.48950	1.48707	1.49189
		25	1.47601	1.47635	1.47878	1.48087	1.48365	1.48481	1.48959
		30	1.47383	1.47417	1.47658	1.47865	1.48140	1.48255	1.48729
trans-Decahydronaphthalene	$C_{10}H_{18}$	20	1.46654	1.46688	1.46932	1.47141	1.47420	1.47535	1.48011
		25	1.46438	1.46472	1.46715	1.46923	1.47200	1.47315	1.47789
		30	1.46222	1.46256	1.46498	1.46705	1.46980	1.47095	1.47567
cis-Hexahydroindan	C_9H_{16}	20	1.46932	1.46968	1.47210	1.47417	1.47690	1.47803	1.48265
		25	1.46700	1.46735	1.46976	1.47182	1.47453	1.47566	1.48025
		30	1.46468	1.46502	1.46742	1.46947	1.47216	1.47329	1.47785
trans-Hexahydoindan	C_9H_{16}	20	1.46092	1.46126	1.46363	1.46567	1.46839	1.46953	1.47419
		25	1.45860	1.45893	1.46130	1.46333	1.46604	1.46717	1.47182
		30	1.45628	1.45660	1.45897	1.46099	1.46369	1.46481	1.46945

TABLE V

VALUES OF THE CONSTANTS OF THE MODIFIED CAUCHY EQUATION

Compound	Formula	Constants in the equation $\Delta n = a + b/\lambda^2$: $a \times 10^3$ 20 to 25°	$a \times 10^3$ 25 to 30°	$b \times 10^3$ 20 to 25°	$b \times 10^3$ 25 to 30°	$\rho \times 10^5$ 20 to 25°	$\rho \times 10^5$ 25 to 30°
n-Undecane	$C_{11}H_{24}$	2.120	2.120	0.0202	0.0202	6.92	5.72
n-Tridecane	$C_{13}H_{28}$	2.135	2.135	.0011	.0011	3.84	4.00
n-Tetradecane	$C_{14}H_{30}$	2.004	2.004	.0224	.0224	3.68	3.32
n-Pentadecane	$C_{15}H_{32}$	2.049	2.049	.0146	.0146	3.64	4 36
1-Tridecene	$C_{13}H_{26}$	2.110	2.110	.0249	.0249	2.17	2.20
1-Tetradecene	$C_{14}H_{28}$	2.074	2.074	.0295	.0295	5.39	5.13
1-Pentadecene	$C_{15}H_{30}$	2.087	2.087	.0167	.0167	4.91	4.84
1-Methylnaphthalene	$C_{11}H_{10}$	2.126	2.245	.1043	.0311	2.45	4.09
cis-Decahydronaphthalene	$C_{10}H_{18}$	2.084	2.084	.0410	.0410	9.15	9.48
trans-Decahydronaphthalene	$C_{10}H_{18}$	2.115	2.115	.0203	.0203	3.98	4.31
cis-Hexahydroindan	C_9H_{16}	2.272	2.272	.0234	.0234	6.80	6.41
trans-Hexahydroindan	C_9H_{16}	2.288	2.288	.0158	.0158	8.84	3 89

computed by inserting the observed values of the refractive index at $\lambda = 0.65628, 0.54607$ and 0.43583 μ, the numerical value of C, and appropriate values of β_λ, successively into the above equation and solving three times for n_∞. Table IV gives the values of refractive index at 7 wave lengths at 20, 25 and 30°. Table V gives the values of the constants of the modified Cauchy equation. Table VI gives the values of the constants of the modified Hartmann equation. The last columns of Tables

TABLE VI

VALUES OF THE CONSTANTS OF THE MODIFIED HARTMANN EQUATION

Compound	Formula	Constants in the eq. $n_\lambda = n_\infty + C/(\lambda - \lambda^*)^{1.6}$ at 25° n_∞	C	λ^*	ρ
n-Undecane	$C_{11}H_{24}$	1.40337	0.003932	0.08352	2.98
n-Tridecane	$C_{13}H_{28}$	1.41162	.003921	.08803	0.85
n-Tetradecane	$C_{14}H_{30}$	1.41515	.003788	.09516	1.46
n-Pentadecane	$C_{15}H_{32}$	1.41811	.003738	.09870	0.85
1-Tridecene	$C_{13}H_{26}$	1.41809	.004227	.09590	1.00
1-Tetradecene	$C_{14}H_{28}$	1.42110	.004193	.09743	2.00
1-Pentadecene	$C_{15}H_{30}$	1.42381	.004079	.10182	2.07
1-Methylnaphthalene	$C_{11}H_{10}$	1.57686	.009503	.17054	7.13
cis-Decahydronaphthalene	$C_{10}H_{18}$	1.46566	.004193	.09915	2.00
trans-Decahydronaphthalene	$C_{10}H_{18}$	1.45398	.004251	.09609	1.51
cis-Hexahydroindan	C_9H_{16}	1.45639	.004487	.08389	1.57
trans-Hexahydroindan	C_9H_{16}	1.44853	.004079	.09926	1.79

TABLE VII

CALCULATED VALUES OF THE SPECIFIC DISPERSION

Temp., °C.	$10^4(n_F - n_C)/d$	$10^4(n_g - n_D)/d$	$10^4(n_F - n_C)/d$	$10^4(n_g - n_D)/d$	$10^4(n_F - n_C)/d$	$10^4(n_g - n_D)/d$
	n-Undecane		*n*-Tridecane		*n*-Tetradecane	
20	98.75	124.55	98.25	124.43	98.46	125.47
25	98.71	124.50	98.71	125.02	98.40	125.40
30	98.52	124.46	99.19	125.62	98.32	125.32
	n-Pentadecane		1-Tridecene		1-Tetradecene	
20	98.27	125.60	110.03	140.21	109.43	139.51
25	98.32	125.64	109.89	140.08	109.16	139.25
30	98.37	125.69	109.76	139.97	108.88	138.98
	1-Pentadecene		1-Methylnaphthalene		*cis*-Decahydronaphthalene	
20	108.06	138.33	295.79		95.24	121.67
25	108.16	138.44	294.89	404.76	94.75	121.06
30	108.27	138.55	295.35	405.51	94.25	120.46
	trans-Decahydronaphthalene		*cis*-Hexahydroindan		*trans*-Hexahydroindan	
20	97.39	124.06	94.41	119.28	95.86	122.41
25	97.35	124.03	94.40	119.16	94.98	122.54
30	97.31	123.98	94.38	119.03	96.08	122.65

V and VI give the root mean square values of the deviations of the observed from the calculated points. Individual measurements were reproducible within ±0.00002 to ±0.00003. The accuracy of the tabulated values is estimated to be ±0.00005 to ±0.00008.

Table VII gives the values of the specific dispersions, $10^4(n_F - n_C)/d$ and $10^4(n_g - n_D)/d$, calculated from the values of refractive index in Table IV and of density in Table I.

The measurements and calculations of vapor pressures and boiling points were made as previously described,[2,4,6,8] with the samples being introduced into the apparatus without contact with the air of the atmosphere.[6]

Table VIII gives the experimental data on the temperature and pressures of the liquid–vapor equilibrium for the compounds measured. Using the experimental data and the method of least squares, calculations were made to yield constants for the Antoine equation for vapor pressure

$$\log_{10} P = A - B/(C + t) \qquad (6)$$

Table IX gives the values of the three constants of the Antoine equation, the normal boiling point at 760 mm., the pressure coefficient of the boiling point at 760 mm., and the range of measurement in pressure and in temperature. The last column of Table IX gives the root mean-square value of the ratios of the deviations of the observed points from

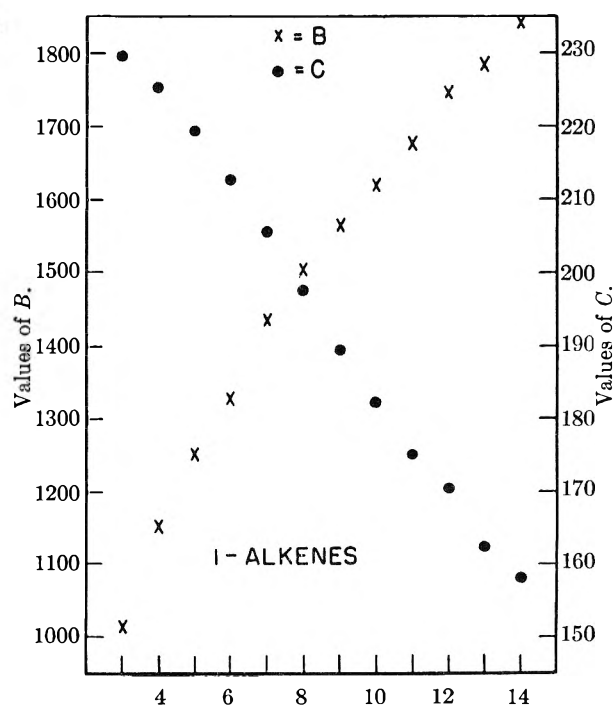

Fig. 4.—Plot of the constants B and C of the Antoine equation for vapor pressure for the monoölefin hydrocarbons (1-alkenes).

the Antoine equation to the expected standard deviation. Individual measurements of boiling points were reproducible within ±0.002 to ±0.003°. The accuracy of the tabulated values of the normal boiling point is estimated to be ±0.008 to ±0.015°.

TABLE VIII

EXPERIMENTAL DATA ON THE TEMPERATURES AND PRESSURES OF THE LIQUID–VAPOR EQUILIBRIUM

t, °C.	*P*, mm.	*t*, °C.	*P*, mm.	*t*, °C.	*P*, mm.
n-Undecane		*n*-Tridecane		*n*-Tetradecane	
197.272	786.23				
196.511	771.68	236.065	771.28	254.165	771.44
195.794	758.17	235.316	757.97	253.401	758.02
195.242	747.91				
194.595	736.05	234.052	735.86	252.104	735.86
188.431	630.45	227.524	630.35	245.408	630.36
179.802	503.12	218.367	503.00	236.013	503.00
171.724	403.38	209.788	403.29		
164.039	322.76	201.634	323.69	218.840	323.71
156.841	261.22				
150.437	214.14	187.176	214.10	204.019	214.11
143.585	171.68				
138.713	145.87	174.699	145.63	191.234	145.64
132.757	118.79				
127.467	98.29	162.749	98.10		
122.607	82.16	157.603	82.01	173.637	81.97
118.963	71.54				
115.522	62.53	150.011	62.45	165.911	62.44
110.962	52.16	145.160	51.99		
104.458	41.55	139.300	41.48	154.860	41.49
n-Pentadecane		1-Tridecene		1-Tetradecene	
				251.750	771.36
270.499	758.08	232.663	758.08	250.984	758.09
269.164	735.86	231.393	735.83	249.689	735.82
262.310	630.36	224.865	630.35	242.996	630.35
252.703	503.00				
		207.152	403.30	224.822	403.31
235.150	323.72	198.998	323.78	216.455	323.78
219.982	214.11	184.559	214.16	201.642	214.15
206.886	145.64			188.869	145.81
		160.170	98.22		
188.905	81.96				
180.919	62.44	147.442	62.44	163.516	62.44
		142.603	51.91	158.464	51.91
169.686	41.49				
1-Pentadecene		Naphthalene		1-Methylnaphthalene	
		218.638	772.00	245.326	770.74
268.273	758.10	217.848	758.40	244.555	757.79
		217.237	748.03	243.949	747.48
266.940	735.79	216.539	736.00	243.177	735.67
260.094	630.35			236.243	630.25
250.494	503.04	200.471	503.08	226.498	502.97
241.504	403.34	191.702	403.34	217.375	403.25
232.940	323.78	183.336	323.72	208.677	323.74
		175.526	261.16	200.536	261.26
		168.540	214.14	193.280	214.08
		161.104	171.60	185.505	171.62
		155.766	145.78	179.971	145.83
		143.930	98.26	167.212	98.17
		138.677	82.12	161.689	82.07
		134.548	71.53	157.539	71.33
		130.836	62.54	153.600	62.36
173.613	51.91	126.325	52.12		
				142.140	41.43

2-Methylnaphthalene		*cis*-Decahydronaphthalene		*trans*-Decahydronaphthalene	
241.760	772.03	196.376	770.52	187.867	770.55
240.957	758.42	195.635	757.57	187.140	757.60
240.336	748.07	195.055	747.50	186.563	747.55
239.613	736.00	194.370	735.66	185.885	735.67
		187.823	630.29	179.395	630.29
223.026	503.21	178.629	503.05	170.297	503.06
213.963	403.40	170.056	403.33	161.801	403.33
205.329	323.75	161.885	323.76	153.719	323.75
197.234	261.17	154.245	261.15	146.156	261.15
190.033	214.15	147.456	214.11	139.441	214.13
182.322	171.63	140.176	171.62	132.255	171.62
176.722	145.76	135.021	145.76	127.140	145.77
		128.731	118.71	120.918	118.72
164.155	98.26	123.132	98.17	115.358	98.15
158.689	82.07	118.004	82.08	110.316	82.10
154.576	71.55	114.152	71.43	106.500	71.42
150.665	62.55	110.490	62.49	102.891	62.49
145.431	52.14	105.685	52.06	98.129	52.07
139.193	41.52	99.883	41.47	92.360	41.48

cis-Hexahydroindan		*trans*-Hexahydroindan	
168.407	770.57	161.642	770.58
167.718	757.63	160.955	757.63
167.170	747.63	160.413	747.64
166.527	735.68	159.779	735.68
160.350	630.29	153.673	630.29
151.698	503.06	145.118	503.07
143.611	403.32	137.115	403.33
135.917	323.76	129.500	323.76
128.708	261.15	122.378	261.15
122.308	214.15	116.059	214.13
115.466	171.62	109.299	171.61
110.605	145.76	104.486	145.76
99.401	98.16	93.415	98.19
94.583	82.08	88.648	82.06
90.961	71.43	85.066	71.45
87.511	62.48	81.651	62.48
82.973	52.03	77.171	51.99
77.497	41.49	71.756	41.49

Discussion

In previous reports,[5,6,8] it was indicated that some correlation exists between the values of the constants n_∞ and C of the Hartmann equation and the number of carbon atoms in the normal alkyl radical for the normal paraffins and the 1-alkenes. The new data confirm and extend this correlation. Figures 1 and 2 are plots, relative to the number of carbon atoms in the normal alkyl radicals, of the values of n_∞ and C of the Hartmann equation for *n*-undecane, *n*-tridecane, *n*-tetradecane, *n*-pentadecane, 1-tridecene, 1-tetradecene and 1-pentadecene from the present investigation, plus those values previously reported for other members of these series.[5,6,8]

Also in earlier reports,[2,4,6,8] it was pointed out that some correlation exists between the values of the constants B and C of the Antoine equation for vapor pressures and the number of carbon atoms in the normal alkyl side chain for the *n*-paraffins and the 1-alkenes. The new data confirm and extend this correlation also. Figures 3 and 4 are plots, relative to the number of carbon atoms in the normal alkyl radicals, of the values of B and C of the Antoine equation for *n*-undecane, *n*-tridecane, *n*-

TABLE IX

SUMMARY OF THE RESULTS OF THE CORRELATION OF THE EXPERIMENTAL DATA WITH THE ANTOINE EQUATION FOR VAPOR PRESSURE

Compound	Formula	Constants of the Antoine equation $\log_{10}P = A - B/(C + t)$ or $t = B/(A - \log_{10}P) - C$ P in mm., t in °C. A	B	C	Normal b.p. at 760 mm., °C.	Pressure coefficient dt/dP at 760 mm., °C./mm.	Range of measurement Pressure, mm.	Temp., °C.	Measure of precision, ρ
n-Undecane	$C_{11}H_{24}$	6.97674	1572.477	188.022	195.890	0.05356	41–787	105.4–197.3	0.43
n-Tridecane	$C_{13}H_{28}$	7.00339	1689.093	174.284	235.434	.05679	52–771	145.1–236.1	1.05
n-Tetradecane	$C_{14}H_{30}$	7.01245	1739.623	167.534	253.515	.05824	62–771	165.9–254.2	1.62
n-Pentadecane	$C_{15}H_{32}$	7.02445	1789.658	161.291	270.614	.05956	41–760	169.6–270.6	1.30
1-Tridecene	$C_{13}H_{26}$	6.98563	1674.741	175.214	232.780	.05680	52–760	142.6–232.7	1.05
1-Tetradecene	$C_{14}H_{28}$	7.02005	1745.001	170.475	251.100	.05820	52–770	158.4–251.7	1.19
1-Pentadecene	$C_{15}H_{30}$	7.01555	1781.974	162.582	268.394	.05956	52–760	173.6–268.4	0.89
Naphthalene	$C_{10}H_8$	6.84577	1606.529	187.227	217.955	.05840	52–772	126.3–218.6	6.36
1-Methylnaphthalene	$C_{11}H_{10}$	7.03592	1826.948	195.002	244.685	.06047	41–771	142.1–245.4	1.58
2-Methylnaphthalene	$C_{11}H_{10}$	7.06850	1840.268	198.395	241.052	.05997	41–772	139.1–241.8	2.32
cis-Decahydronaphthalene	$C_{10}H_{18}$	6.87529	1594.460	203.392	195.774	.05710	41–771	99.8–196.4	0.66
trans-Decahydronaphthalene	$C_{10}H_{18}$	6.85681	1564.683	206.259	187.273	.05656	41–770	92.3–187.9	.51
cis-Hexahydroindan	C_9H_{16}	6.86932	1498.076	207.752	167.846	.05381	41–771	77.4–168.5	.73
trans-Hexahydroindan	C_9H_{16}	6.85971	1474.620	209.527	161.083	.05323	40–771	71.7–161.7	.81

tetradecane, *n*-pentadecane, 1-tridecene, 1-tetradecene and 1-pentadecene from the present investigation, plus those values previously reported for other members of these series.[2,4,6,8]

The foregoing correlations may be used, by appropriate interpolation or extrapolation, to obtain values for those compounds not yet actually measured.

NOTES

THE SOLUBILITY OF $UO_2HPO_4 \cdot 4H_2O$ IN PERCHLORIC ACID SOLUTIONS

BY JAMES M. SCHREYER AND C. F. BAES, JR.

Contribution from Oak Ridge National Laboratory, Carbide and Carbon Chemical Company, Oak Ridge, Tenn.

Received March 4, 1955

I. Introduction.—In a previous report,[1] the solubility behavior of three uranium(VI) orthophosphates, $(UO_2)_3(PO_4)_2 \cdot 6H_2O$, $UO_2HPO_4 \cdot 4H_2O$ and $UO_2(H_2PO_4)_2 \cdot 3H_2O$, in phosphoric acid solutions at 25° was described.

Little information is available on complex ion formation in the uranium(VI) orthophosphate system. G. R. Leader[2] has reported that solubility measurements of $UO_2HPO_4 \cdot 4H_2O$ in HNO_3 and H_3PO_4 indicate $UO_2H_2PO_4^+$ is formed in solutions of moderate phosphoric acid concentrations and that, in excess of phosphoric acid, higher complexes are formed. Baes, Schreyer and Lesser[3] reported a spectrophotometric investigation of uranium(VI) orthophosphate solutions using the method of continuous variation which indicated the presence of complex species in which the ratio of PO_4^{-3}/UO_2^{++} is unity. From additional spectrophotometric measurements,[4] Baes has estimated formation quotients for 1:1 and 2:1, phosphate to uranium, complexes which are consistent with spectrophotometric results at 0.001 and 0.04 *M* uranium(VI) concentrations. This indicates that polynuclear complex formation was not appreciable. While the present results involve higher uranium levels, it will be assumed that only mononuclear uranium complexes are formed.

In the following investigation, solubility measurements of $UO_2HPO_4 \cdot 4H_2O$ have been extended to perchloric acid solution in order to study complex ion formation in a non-complexing solvent. Solubilities have been determined as a function of the phosphate, uranium(VI) and hydrogen ion concentrations. Measurements have been confined to fairly concentrated solutions, and since the control of ionic strength is of doubtful value in such solutions, these studies were not limited to constant ionic strength except in the measurements of acidity dependence of solubility.

II. Experimental

A. Solubility of $UO_2HPO_4 \cdot 4H_2O$ at Constant Acidity.—The solubility of $UO_2HPO_4 \cdot 4H_2O$ was measured in two series of 1 *M* perchloric acid solutions at 25°; the first series contained 0–0.5 *M* U(VI) before equilibration while the second initially contained 0–3.1 *M* phosphate. The preparation of $UO_2HPO_4 \cdot 4H_2O$ and the apparatus employed have been described previously.[1]

Various experiments covering the entire range of compositions indicated that equilibrium was established in less than three days. To ensure equilibrium in all the measurements, the samples were shaken from 11 to 21 days.

The mother liquors were sampled by means of calibrated pipets or pycnometers depending on the viscosity of the solutions. They were analyzed for uranium and phosphate

(1) J. M. Schreyer and C. F. Baes, Jr., *J. Am. Chem. Soc.*, **76**, 354 (1954).

(2) G. R. Leader, CN-2195, Chemistry Division, Clinton Laboratories, 1944.

(3) C. F. Baes, Jr., J. M. Schreyer and J. M. Lesser, ORNL-1577, Oak Ridge National Laboratory, June 1953.

(4) To be submitted for publication.

by the methods previously reported[1] and for perchlorate by the method of Loebich.[5]

Wet residue analyses confirmed the 1:1 ratio of uranium(VI) to phosphate in the equilibrium solids over the entire range of concentrations studied. A few dry solids were obtained by washing the filtered solids with water and acetone and drying in air for 12 hours. These solids were identified as $UO_2HPO_4 \cdot 4H_2O$ by microscopic and X-ray diffraction analyses.

In performing these controlled acidity solubility measurements, estimation was made of the acidity effect of the dissolution process assuming the formation of $UO_2H_2PO_4^+$. Where the resulting final acidities differed appreciably from one molar, a correction was made on the solubility results. These corrections were small.

The solubility data are represented by curve I of Fig. 1. In the regions of excess uranium(VI) or excess phosphate, the solubilities of $UO_2HPO_4 \cdot 4H_2O$ are equal to the total phosphate or total uranium concentrations, respectively.

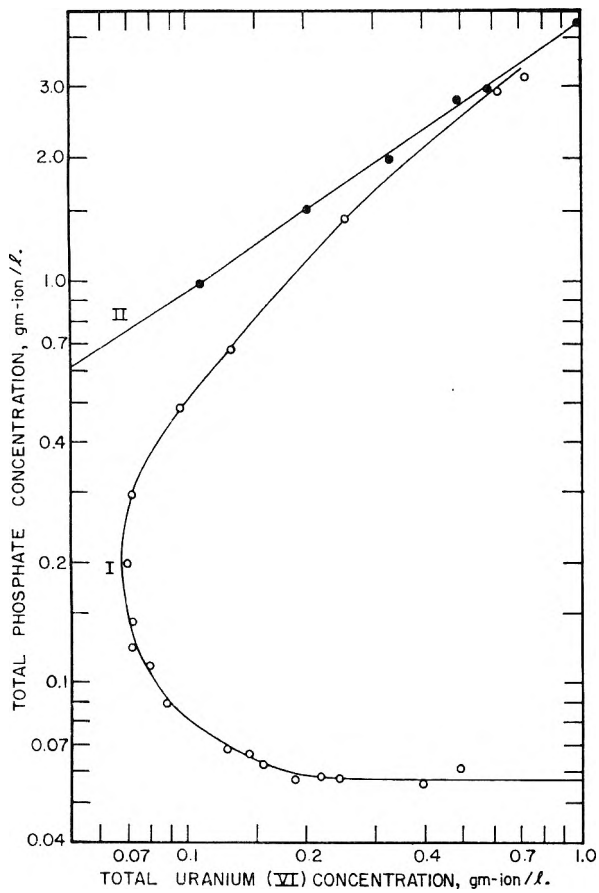

Fig. 1.—The solubility behavior of $UO_2HPO_4 \cdot 4H_2O$: I, solubilities in 1 *M* $HClO_4$ containing excess uranium(VI) perchlorate or phosphoric acid: II, solubilities in phosphoric acid.[1]

The dissolution reaction for $UO_2HPO_4 \cdot 4H_2O$ in acid solution to form uncomplexed uranium(VI) ion may be written

$$UO_2HPO_4 \cdot 4H_2O + 2H^+ \rightleftharpoons UO_2^{++} + H_3PO_4 + 4H_2O \quad (1)$$

The dissolution of the salt to form a 1:1 complex may be written

$$UO_2HPO_4 \cdot 4H_2O + (x-1)H^+ \rightleftharpoons UO_2H_xPO_4^{+(x-1)} + 4H_2O \quad (2)$$

Thus, in saturated solutions, assuming constant activity coefficients, eq. 2 shows that the total concentration of all 1:1 complexes will be constant at constant acidity. If such complexes are the only ones which are appreciably abundant in excess uranium(VI) perchlorate, the salt solubility *S* is given by the sum of the free phosphoric acid and the complex

$$S = [H_3PO_4] + [UO_2H_xPO_4^{+(x-1)}] \quad (3)$$

neglecting the small dissociation of phosphoric acid. According to eq. 1, increasing the U(VI) concentration will decrease the free phosphoric acid concentration, and from eq. 3 the solubility (equal to the total phosphate concn.) will reach a constant limiting value where all the phosphate in solution is complexed. It is evident from curve I of Fig. 1 that this is approximately the case.

In a similar manner, eq. 1 indicates that in excess phosphate the solubility (equal to the U(VI) concn.) should also approach a constant limiting value if only 1:1 complexes are present. The increasing solubility in excess phosphoric acid, curve I of Fig. 1, indicates the formation of complexes in which the phosphate to uranium(VI) ratio is greater than unity.

Some of the previously reported solubilities of $UO_2HPO_4 \cdot 4H_2O$ in pure phosphoric acid[1] have been plotted in curve II of Fig. 1 permitting a comparison with 1 *M* perchloric acid data. The two solubility curves converge in excess phosphoric acid, indicating that the principal dissolution reaction is independent of acidity and, therefore, that the complex species in solution above 0.3 *M* total phosphate are neutral.[6] Such complex species would be formed as follows

$$UO_2HPO_4 \cdot 4H_2O + (n-1)H_3PO_4 \rightleftharpoons UO_2(H_2PO_4)_2(H_3PO_4)_{n-2} + 4H_2O \quad (4)$$

This lack of acidity dependence in excess phosphoric acid is supported by a comparison of *p*H measurements of pure phosphoric acid solutions and of saturated solutions of $UO_2HPO_4 \cdot 4H_2O$ in phosphoric acid shown in Fig. 2. The *p*H measurements were made using a Beckman Model G meter with a glass electrode. The dashed curves in Fig. 2 represent the calculated *p*H if one mole of hydrogen ion is consumed (curve I) or liberated (curve II) per mole of salt dissolved.[8]

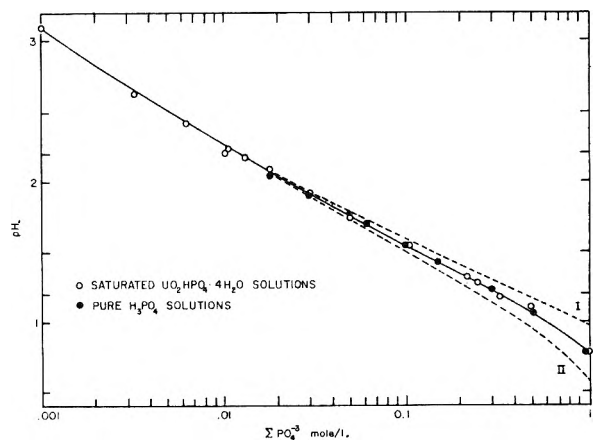

Fig. 2.—*p*H of phosphoric acid solutions.

(5) F. J. Welcher, "Organic Analytical Reagents," Vol. III, D. Van Nostrand Co., Inc., New York, N. Y., 1947, p. 144.

(6) If the solubility of $UO_2HPO_4 \cdot 4H_2O$ in phosphoric acid is due entirely to the $UO_2(H_2PO_4)_2$ complex, the solubility curve on a log-log plot should have a slope of +1. The slope of the log-log solubility curve of $UO_2HPO_4 \cdot 4H_2O$ in phosphoric acid[1] increased from +1 at 0.014 *M* total phosphate to +1.53 at 1 *M*, indicating the presence of at least one higher complex, *e.g.*, $UO_2(H_2PO_4)_2 \cdot H_3PO_4$, in higher phosphoric acid concentrations. These solubility data have been quantitatively interpreted in terms of these two neutral complexes and the 1:1 complex.[7]

(7) C. F. Baes, Jr., and J. M. Schreyer, ORNL-1579, Oak Ridge National Laboratory, July, 1953.

(8) The dashed curves were estimated as follows. From each measured *p*H for pure phosphoric acid solutions, a value for the first acid constant was calculated using $K_1 = [H^+]^2/(\text{total phosphate} - [H^+])$, for which *p*H was taken to be $-\log_{10}[H^+]$. These empirical K_1 values were used to estimate the equilibrium hydrogen ion concentration expected upon the addition and removal of *S* moles of hydrogen ion (where $S = UO_2HPO_4 \cdot 4H_2O$ solubility). The negative logarithms of these $[H^+]$ values were used in Fig. 2. It is believed that activity and liquid junction effects are accordingly minimized sufficiently to permit a reasonable estimate of this *p*H effect.

B. Acidity Dependence of $UO_2HPO_4 \cdot 4H_2O$ Solubility.—Since the acidity dependence of solubility might be useful in establishing the formulas of the 1:1 complex species in acid solutions, the solubility of $UO_2HPO_4 \cdot 4H_2O$ was determined in 0.1 to 1 *M* perchloric acid solutions. The ionic strength was controlled at approximately 1.15 *M* by adding calculated amounts of sodium perchlorate. The correction for the acidity effect of the dissolution reaction was applied in the same manner as in the 1 *M* perchloric acid measurements.

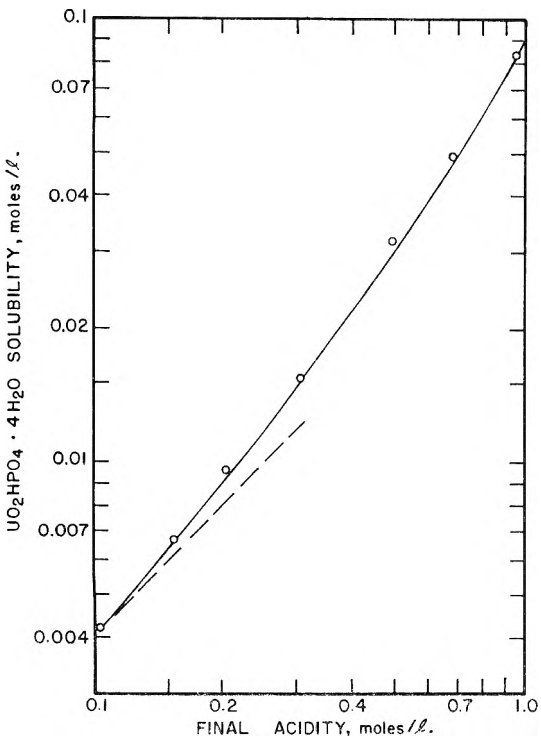

Fig. 3.—The acidity dependence of $UO_2HPO_4 \cdot 4H_2O$ solubility in $HClO_4$, μ = 1.15.

These solubility data are shown in a log-log plot in Fig. 3. The deviation from unit slope indicates an acidity dependence greater than that suggested by the equilibrium

$$UO_2HPO_4 \cdot 4H_2O + H^+ \rightleftarrows UO_2H_2PO_4^+ + 4H_2O \quad (5)$$

along with eq. 1. If activity coefficients are constant in these measurements, it is suggested that the following equilibrium in addition to eq. 1 and 5 should also be considered.

$$UO_2HPO_4 \cdot 4H_2O + 2H^+ \rightleftarrows UO_2H_3PO_4^{++} + 4H_2O \quad (6)$$

STRUCTURE OF STEARATE MONOLAYERS IN THE REGION Le-G

BY JOHN P. RYAN AND J. W. SHEPARD

Contribution No. 98 from the Central Research Department, Minnesota Mining & Manufacturing Company, St. Paul 1, Minnesota.

Received March 12, 1955

At very large molecular areas, monolayers of long chain acids on aqueous substrates seem to exhibit a behavior in accord with the perfect gas law $FA = kT$, where F is the force (dynes/cm.), A is the molecular area, k is the Boltzmann constant of a three-dimensional gas and T is the absolute temperature. As the area is decreased, the two-dimensional gas becomes imperfect. At temperatures between 20 and 40°, the pressure becomes constant at an area of about 200 Å.^{2} per molecule and remains constant as the area is decreased to about 30 Å.^{2} per molecule. Between these limits the film is heterogeneous and Harkins[1] has designated this region as the Le-G region. Some workers have postulated that the monolayers in this region consist of small islands of liquid expanded phase in a sea of the gaseous phase. Harkins and Fischer[2] have demonstrated the heterogeneity of this type of film by surveying the surface with an electrode which measures surface potential. For gaseous films, the surface potential is generally less than five millivolts. If there are islands or continents, the surface potential will be much higher since it increases with the mean number of film molecules under the electrode surface. For palmitic acid films at 22° and 48 Å.^{2} molecular area, Harkins and Fischer found surface potential values which varied from 35 to 330 millivolts when they surveyed the surface. Above 28 Å.^{2} molecular area, stearic acid behaved similarly. Condensed films of stearic acid are quite coherent and the surface potential is lowered only slightly when the pressure is reduced. If time is given for two-dimensional evaporation to take place, the surface potential will reduce to a few millivolts at extremely low pressures.

Recently Ries and Kimball[3] reported the presence of islands in monolayer films of *n*-hexatriacontanoic acid using an electron microscopic technique. We have also been studying this phenomenon using C-14 tagged calcium stearate. Tagged stearate monolayers were deposited on aluminum slides at a low film pressure (42 Å.^{2} molecular area) and about 30° using the technique of Blodgett.[4] The molec-

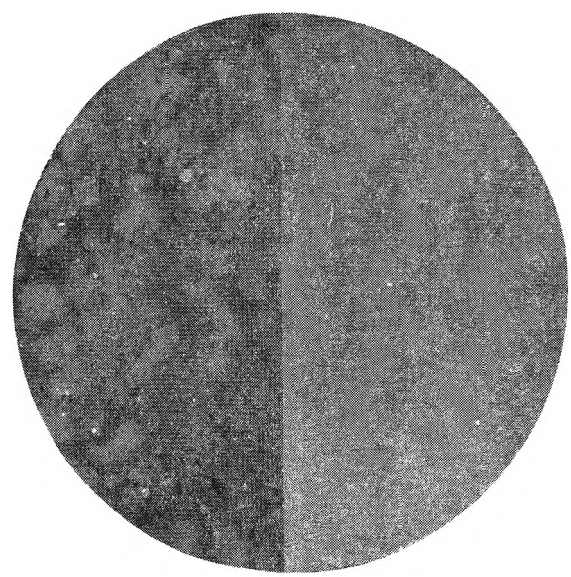

a b

Fig. 1a.—Autoradiograph of a stearate monolayer deposited on aluminum at low pressure. The light areas are islands of liquid expanded phase surrounded by gaseous phase (×3).

Fig. 1b.—Autoradiograph of a condensed stearate monolayer deposited on aluminum (×3).

(1) W. D. Harkins, "The Physical Chemistry of Surface Films," Reinhold Publ. Corp., New York, N. Y., 1952.

(2) W. D. Harkins and E. K. Fischer, *J. Chem. Phys.*, **1**, 852 (1933).

(3) H. E. Ries, Jr., and W. A. Kimball, THIS JOURNAL, **59**, 94 (1955).

(4) K. B. Blodgett, *J. Am. Chem. Soc.*, **56**, 495 (1934); **57**, 1007 (1935).

ular area of 42 Å.^{2} was calculated from the measured activity of the deposited, condensed stearate monolayer (20.5 Å.^{2} molecular area). Autoradiographs[5] of the film deposited at low pressure establish the presence of islands of liquid expanded phase surrounded by areas of gaseous phase (Fig. 1a). These results show that the Le-G region is a two-phase region.[6] The light areas represent high levels of activity and, consequently, greater concentrations of tagged stearate than the surrounding darker areas. For comparison an autoradiograph of a condensed monolayer of tagged calcium stearate deposited on aluminum is also shown (Fig. 1b).

These results show the value of this technique for studying phase changes in monolayer films.

(5) "No Screen" X-ray plates used.

(6) No change takes place in the stearate film as it is lifted out of the water by the aluminum slide. See Langmuir, *Trans. Faraday Soc.*, **15**, 62 (1920); K. B. Blodgett, *J. Am. Chem. Soc.*, **56**, 495 (1934); **57**, 1007 (1935).

THE TERNARY SYSTEM *n*-PROPYL ALCOHOL, TOLUENE AND WATER AT 25°[1]

By Elton M. Baker

Contribution from the Radiation Laboratory, University of California, Berkeley 4, Cal.

Received July 1, 1955

Liquid scintillation counting of tritium water may require a toluene–alcohol–water mixture with the alcohol acting as a consolute liquid between the water and toluene.

Other workers[2] have used methanol and ethanol as the alcohol, but the detecting efficiency of the phosphor solvent has been very low due to the light-quenching properties of the alcohol.

Since toluene is one of the more efficient solvents for phosphors used in scintillation counting of tritium in water, it seemed feasible to study a system containing another alcohol which would show greater solubility in the hydrocarbon phase. It was believed that *n*-propyl alcohol, which is miscible in all proportions in both toluene and water and which has a higher dielectric constant and greater hydrogen-bonding character than other alcohols studied, might prove to be a suitable alcohol since it should be possible to have a higher weight per cent. of toluene in solution and result in less quenching of the energy transfer process by the alcohol.

In order to select a practical and completely miscible mixture of liquids to be used as a solvent system for phosphors for liquid scintillation counting of tritiated water, it was desirable to obtain solubility data for the ternary system containing *n*-propyl alcohol, toluene and water.

Washburn, *et al.*,[3-5] have studied toluene–water systems with various alcohols as the consolute liquid, but *n*-propyl alcohol was not included with the alcohols reported.

(1) The work described in this paper was sponsored by the U. S. Atomic Energy Commission.

(2) F. N. Hayes and R. G. Gould, *Science*, **117**, 480 (1953).

(3) E. R. Washburn and L. S. Masin, *J. Am. Chem. Soc.*, **59**, 2076 (1937).

(4) E. R. Washburn and A. E. Beguin, *ibid.*, **61**, 1694 (1939).

(5) E. R. Washburn and A. E. Beguin, *ibid.*, **62**, 579 (1940).

Materials.—Water was distilled from alkaline potassium permanganate and collected while hot and stored immediately. Eastman Kodak Co. grade *n*-propyl alcohol was distilled over calcium chloride; only the middle fraction was used. Its specific gravity was d^{25}_4 0.7999 ± 0.0002 while its index of refraction $n^{25}D$ was 1.3854 ± 0.0001.

Toluene of "Analytical Reagent" grade was dried over sodium and fractionally distilled. This liquid had a specific gravity d^{25}_4 0.8593 ± 0.0002 and an index of refraction $n^{25}D$ 1.3325 ± 0.0001. These values check closely with those recorded in the "International Critical Tables."

Experimental and Discussion

A calibrated 10-ml. pycnometer was used to determine the specific gravity and an Abbe refractometer was used to determine the refractive index. A constant temperature bath at 25.0 ± 0.1° was used to control the temperature of all liquids.

Weighed portions of *n*-propyl alcohol and toluene in ground glass stoppered flasks were brought to 25° in the constant temperature bath. Water was added from a calibrated buret in small quantities with shaking and allowing the temperature of the solution to return to 25° before further additions of water. After the end-point (milky translucency, due to separation of a second phase) was reached, the mixture was left in the bath for 30 min. before the specific gravity and refractive index were determined.

A large-scale curve was plotted from the data of Table I which shows the variation of refractive index with the percentage of each component in the saturated solutions. The scale was such that 1 mm. represented 0.2% of the compo-

Table I

Solubilities, Refractive Indices and Specific Gravities for the Ternary System, Toluene, *n*-Propyl Alcohol and Water at 25°

Toluene, wt. %	*n*-Propyl alcohol, wt. %	Refractive index	Specific gravity
91.016	8.493	1.4815	0.8537
88.978	10.297	1.4789	.8530
85.784	13.190	1.4750	.8516
79.913	18.300	1.4672	.8493
71.136	25.906	1.4572	.8468
65.742	30.104	1.4518	.8455
58.484	36.001	1.4431	.8446
47.442	44.089	1.4322	.8441
41.460	47.820	1.4238	.8450
29.663	54.526	1.4091	.8494
18.299	56.596	1.3938	.8536
11.697	53.954	1.3829	.8773
4.573	42.525	1.3684	.9128
1.855	30.295	1.3578	.9420
0.609	22.653	1.3519	.9601
0.444	20.969	1.3505	.9637

Table II

Refractive Indices and Composition of Conjugate Solutions at 25°

Toluene phase			Water phase		
Alcohol, %	Toluene, %	Refractive index	Alcohol, %	Toluene, %	Refractive index
2.45	97.50	1.4890	8.20	91.30	1.3393
7.20	92.30	1.4829	11.80	87.75	1.3428
11.85	87.15	1.4771	14.00	85.50	1.3444
20.50	77.30	1.4656	14.70	84.90	1.3458
25.20	71.90	1.4590	15.50	84.00	1.3465
30.80	65.00	1.4509	15.90	83.85	1.3468
38.90	54.45	1.4386	17.70	82.02	1.3466
48.35	40.70	1.4225	19.10	80.55	1.3489
50.15	37.60	1.4190	19.30	80.30	1.3482
55.90	25.20	1.4041	22.20	77.25	1.3510
56.65	17.50	1.3936	22.40	77.00	1.3513

nent and 0.0004 in refractive index. This curve was used in determining the composition of the conjugate solutions formed when alcohol in insufficient amounts to bring about homogeneity was added to two liquid-phase mixtures of toluene and water. After equilibrium was reached at 25°, samples were removed from each of the layers, for determination of the refractive index. The composition of each phase with the refractive index is given in Table II. A plot of the data from Table II is given on the equilateral triangle of Fig. 1. The tie lines were obtained from the

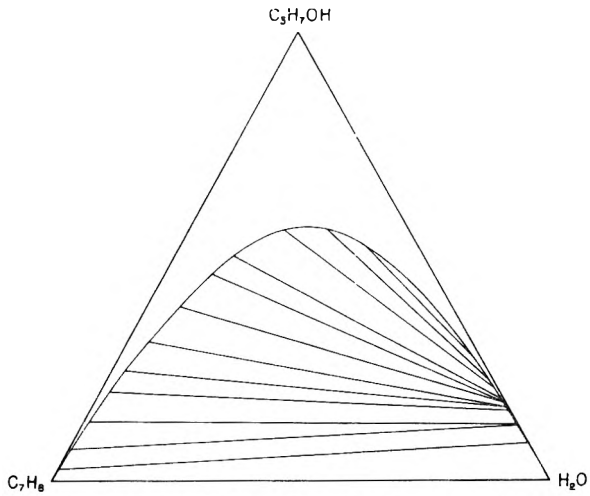

Fig. 1.—Ternary solubility diagram for *n*-propyl alcohol, toluene and water.

analysis of the conjugate mixtures. The position of the plait point on the right-hand side of the diagram indicates an increase in solubility of alcohol in the toluene as the concentration of the alcohol is increased. A plot of the distribution of alcohol between the two phases shows a lack of constancy but increases in toluene as the concentration increases. The change in distribution of alcohol in the organic and water layers is compared with those of other alcohols in Fig. 2.

When the solubility curves for the *n*-propyl alcohol–toluene–water system are compared with those for the system containing methanol, ethanol and isopropyl alcohol, it is observed that methanol is less efficient and isopropyl alcohol is most efficient in bringing about miscibility in water–toluene systems.

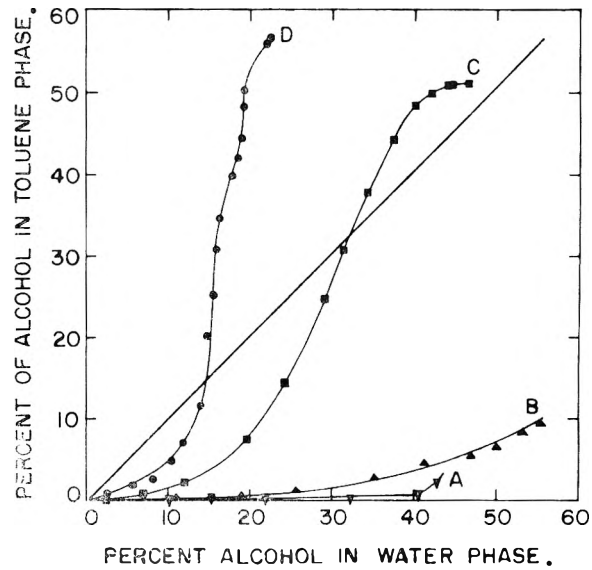

Fig. 2.—Distribution of alcohols between conjugate solutions of water and toluene: A, methanol[3–5]; B, ethanol[3–5]; C, isopropyl alcohol[3–5]; D, *n*-propyl alcohol.

As the amounts of alcohols are increased in the system, there is an increasing proportion of alcohol found in the toluene layer; *n*-propyl alcohol increases most rapidly and next to it comes isopropyl alcohol. It is observed that as the *n*-propyl alcohol is increased in the system the slope of the tie lines, Fig. 1, changes from a positive slope to a horizontal line and, finally, to a negative slope as the toluene phase dissolves an increased proportionate amount of the alcohol than is found in the water phase. This is true only when *n*-propyl or isopropyl alcohol is used as the consolute liquid.

From the curve in Fig. 1, the compositions of various miscible mixtures may be selected for a suitable phosphor solvent mixture containing tritiated water.

Acknowledgment.—The author wishes to thank Misses Esther Jacobson and Patricia Smith for their capable assistance with several of the measurements necessary in this work.

COMMUNICATION TO THE EDITOR

A MOLECULAR DYNAMIC THEORY OF CHROMATOGRAPHY

Sir:

It is interesting to note the resemblance of the results obtained in the "Molecular dynamic theory of chromatography" [J. Calvin Giddings and Henry Eyring, THIS JOURNAL, **59**, 416 (1955)] to those of a theory based on a transfer coefficient. Such a theory has been applied by many authors[1] to the heating or cooling of a porous bed by a current of gas. The basic equations are

$$-\frac{\partial T_1}{\partial Y} = T_1 - T_2 = +\frac{\partial T_2}{\partial Z} \qquad (1a,b)$$

where T_1 = temperature of gas, T_2 = temperature of solid, Y = length in dimensionless units, Z = time in dimensionless units.

In the case usually studied, the bed is initially at a constant temperature, say $T = 0$, and gas is introduced at another temperature, say $T = T_0$, so that the initial and boundary conditions read

$$Y = 0 \qquad T_1 = T_0 \qquad (2a)$$

$$Z = 0 \qquad T_2 = 0 \qquad (2b)$$

The solid *at the bed entrance* is heated from $T_2 = 0$ to $T_2 = T_0$ with a gas constantly at $T_1 = T_0$ so that in view of equation (1b)

$$(T_2)_{Y=0} = T_0(1 - e^{-Z}) \qquad (3)$$

Likewise, the first element of gas introduced at $T_1 = T_0$ will constantly meet cold solid ($T_2 = 0$), so that (1a) gives

$$(T_1)_{Z=0} = T_0 e^{-Y} \qquad (4)$$

Similar exponential decay is observed by Giddings and Eyring upon desorption from initially filled or adsorption on empty surfaces, with rate constants K_1' and k_1, so that the calculations should merge when

$$Z = k_1' t \qquad (5)$$

$$Y = k_1 t_0 \quad (t_0 = \text{time of passage of fluid}) \qquad (6)$$

The well-known solutions of (1) and (2) are

$$\frac{T_1}{T_0} = e^{-Y}\int_0^Z e^{-u} I_0(2\sqrt{Yu})du + e^{-Y-Z} I_0(2\sqrt{YZ}) \qquad (7)$$

and

$$\frac{T_2}{T_0} = e^{-Y}\int_0^Z e^{-u} I_0(2\sqrt{Yu})du \qquad (8)$$

The results for the introduction of a peak of solute are found differentiating T_1 and T_2 according to time. $\partial T_2/\partial t$ is most conveniently found by the use of (1b) while deriving $(T_1 - T_2)$ from (7) and (8). This yields Giddings and Eyring's equation (9). $\partial T_1/\partial t$ is found by differentiating (7). This gives Giddings and Eyring's equation (5).

Giddings and Eyring have assumed the solute to start either in the liquid, their eq. (5), or in the solid, their eq. (9), but always observed it in the final liquid.

In the present derivation the heat is always introduced with the inlet gas, but it is observed at the end in either the gas, eq. (7), or the solid, eq. (8).

Giddings and Eyring's eq. (5) and the derivative of our eq. (7) are thus applicable to strictly identical cases.

From the identity of their eq. (9) with the derivative of our eq. (8) one concludes that for the result it is immaterial whether the "extra" transfer is at inlet or end.

N. V. DE BATAAFSCHE PETROLEUM MAATSCHAPPIJ
(ROYAL DUTCH/SHELL GROUP)
THE HAGUE, HOLLAND A. KLINKENBERG

RECEIVED OCTOBER 10, 1955

(1) Anzelius (1926); Schuman, Furnas, Nusselt and others; for a review see A. Klinkenberg, *Ind. Eng. Chem.*, **46**, 2285 (1954).

Number 14 in
Advances in Chemistry Series

edited by the staff of
Industrial and Engineering Chemistry

NOMENCLATURE FOR TERPENE HYDROCARBONS

A system of nomenclature for terpene hydrocarbons (including sections on information to aid in the reading of terpene literature) which was prepared by Mildred W. Grafflin. It has been accepted by the Nomenclature Committee of the American Chemical Society's Division of Organic Chemistry and approved by the ACS on recommendation of its general Nomenclature, Spelling and Pronunciation Committee. Accepted by the IUPAC. 109 pages.

paper bound—$3.00

order from:

Special Publications Dept.
American Chemical Society
1155 Sixteenth Street, N. W.
Washington 6, D. C.

A challenging opportunity for

SCIENTISTS

- **physicists**
- **mathematicians**
- **physical chemists**
- **experimental psychologists**

to apply creative, scientific methods to vital problems in military operations research. To above-average scientists seeking above-average rewards, we can offer:

- **a secure future**
- **freedom to think in a virgin field**
- **growth potential**
- **important results**

Openings are filling rapidly. Send us your resume *now.*

Address: Mr. R. A. Langevin
TECHNICAL OPERATIONS INC.
777 14th Street, N.W.
Washington 5, D. C.

Literature Resources for Chemical Process Industries

Designed To Help Both The *New* And The *Experienced* Searcher Of Literature Find What He Wants

Discusses various information sources with 13 articles on market research, 7 on resins and plastics, 6 on textile chemistry, 10 on the food industry, 10 on petroleum, and 13 on general topics, plus 34 pages of index.

order from:

Special Publications Department
American Chemical Society
1155 Sixteenth Street, N.W.
Washington 6, D.C.

Number 10 in
Advances in Chemistry Series

edited by the staff of
Industrial and Engineering Chemistry

582 pages—paper bound—$6.50 per copy

WILEY BOOKS

SMALL-ANGLE SCATTERING OF X-RAYS

By André Guinier, University of Paris, and Gérard Fournet, École Supérieure de Physique et Chimie, Paris; translated by Christopher B. Walker, University of Chicago. A clear, logical review of the entire field, covering theory, experimental procedures, and applications. Emphasis is placed on the differences which exist between small-angle scattering and the more familiar techniques of ordinary x-ray diffraction. Experimental equipment is described in sufficient detail to enable you to build the typical devices in your own laboratory. Ample material is provided on the type of problem that can be solved by small-angle scattering techniques, and there is a full bibliography. 1955. 268 pages. Probably $7.50.

RESONANCE IN ORGANIC CHEMISTRY

By George Willard Wheland, University of Chicago. This is the only current work to deal explicitly with resonance theory in chemistry. It differs from the conventional treatment of organic chemistry in its concern with the application of quantum mechanical methods to problems of molecular structure. At the same time its approach to quantum theory is uniformly chemical and, particularly, organic chemical. 1955. Approx. 820 pages. Probably $12.00.

ELEMENTARY THEORY OF NUCLEAR SHELL STRUCTURE

By Maria Goeppert Mayer, University of Chicago, and J. Hans D. Jensen, University of Heidelberg. The two research scientists who have been mainly responsible for the development of the nuclear shell structure theory, discuss in this book a wide variety of nuclear data from the viewpoint of the single, unified theory. A publication in Wiley's Structure of Matter Series, Maria Goeppert Mayer, Advisory Editor. *1955. 269 pages. $7.75.*

INTRODUCTORY NUCLEAR PHYSICS, Second Edition

By David Halliday, University of Pittsburgh. This revision of the standard introduction to the subject offers a balanced account of the fundamentals of the whole field of nuclear physics. Among the notable additions in the new edition is a chapter on the elements of wave mechanics and the inclusion of a number of fundamental formula derivations. *1955. 493 pages. $7.50.*

ELEMENTARY CRYSTALLOGRAPHY

By M. J. Buerger, Massachusetts Institute of Technology. An introduction to the fundamental geometrical features of crystals. *Ready in December.*

Order your on-approval copies today.

JOHN WILEY & SONS, Inc. **440 Fourth Ave., New York 16, N. Y.**